REVIEW ARTICLE

van der Waals forces in density functional theory: a review of the vdW-DF method

IOP Publishing Reports on Progress in Physics
Rep. Prog. Phys. **78** (2015) 066501 (41pp) doi:10.1088/0034-4885/78/6/066501

Review Article

van der Waals forces in density functional theory: a review of the vdW-DF method

Kristian Berland[1,5], Valentino R Cooper[2], Kyuho Lee[3,4], Elsebeth Schröder[5], T Thonhauser[6], Per Hyldgaard[5] and Bengt I Lundqvist[7]

[1] Centre for Materials Science and Nanotechnology, SMN, University of Oslo, NO-0318 Oslo, Norway
[2] Materials Science and Technology Division, Oak Ridge National Laboratory, Oak Ridge, TN 37831-6114, USA
[3] Molecular Foundry, Lawrence Berkeley National Laboratory, Berkeley, CA 94720, USA
[4] Department of Chemical and Biomolecular Engineering, University of California, Berkeley, CA 94720, USA
[5] Microtechnology and Nanoscience, MC2, Chalmers University of Technology, SE-412 96 Göteborg, Sweden
[6] Department of Physics, Wake Forest University, Winston-Salem, NC 27109, USA
[7] Department of Applied Physics, Chalmers University of Technology, SE-412 96 Göteborg, Sweden

E-mail: kristian.berland@smn.uio.no

Received 29 April 2014, revised 20 December 2014
Accepted for publication 14 January 2015
Published 15 May 2015

Invited by Mei-Yin Chou

Abstract

A density functional theory (DFT) that accounts for van der Waals (vdW) interactions in condensed matter, materials physics, chemistry, and biology is reviewed. The insights that led to the construction of the Rutgers–Chalmers van der Waals density functional (vdW-DF) are presented with the aim of giving a historical perspective, while also emphasizing more recent efforts which have sought to improve its accuracy. In addition to technical details, we discuss a range of recent applications that illustrate the necessity of including dispersion interactions in DFT. This review highlights the value of the vdW-DF method as a general-purpose method, not only for dispersion bound systems, but also in densely packed systems where these types of interactions are traditionally thought to be negligible.

Keywords: van der Waals forces, London dispersion interaction, sparse matter, density functional theory, physisorption, molecular crystals, intramolecular forces

(Some figures may appear in colour only in the online journal)

1. Introduction

The field of van der Waals (vdW) interactions has grown enormously since its infancy [1]. This is particularly true when considering how such forces can be included within electronic structure methods. As such it is not possible to cover the entire field in a single review paper. This review focuses on the history, development and application of one specific approach for including dispersion interactions within the framework of density functional theory (DFT); the van der Waals density functional (vdW-DF). For reviews on other methods and approaches we direct the reader to references [2–10].

Identified in 1873, there is a force that today attracts more interest than ever. It was first introduced in a doctoral thesis by Johannes Diderik van der Waals 'on the continuity of the gaseous and liquid state' at Leiden University [11]. The existence of the vdW force [12] is today well established. It is present everywhere, but its variation from one environment

to another and its complex manifestations still pose challenging questions nearly one hundred years after van der Waals was awarded the Nobel Prize in physics. These questions are relevant for such varied systems as soft matter, surfaces, and DNA, and in phenomena as different as supramolecular binding, surface reactions, and the dynamic properties of water. Long-standing observations together with a flow of improved experiments challenge existing theories, and a general theoretical framework that can describe small molecules as well as extended systems is needed.

The vdW interaction is a true quantum phenomenon [13, 14]. Asymptotic models and interpretations, such as those setting the interactions of point particles with separation R and molecules at a distance z outside a surface as R^{-6} [13, 15] and z^{-3} [16], respectively, and the fact that the multitude of such power laws for this microscopic force [17] depends on the microscopic shapes, were given early. Today's challenges might concern more subtle observations, such as detailed analyses of diffractive scattering of H_2 and D_2 off single-crystal surfaces or the properties of DNA and liquid water.

In physical-chemistry terminology the term vdW includes the following forces between molecules: (i) two permanent dipoles (Keesom force), (ii) a permanent dipole and a corresponding induced dipole (Debye force), and (iii) two instantaneously induced dipoles (London dispersion force) [13, 15]. In the condensed-matter community, typically just the latter, which has a nonclassical origin, is referred to as the vdW force.

A proper theory for atoms and molecules should account for all forces at play, including covalent bonds, hydrogen bonds, and electrostatic interactions, because they are all relevant in typical materials and systems. DFT [18–21] is such a general framework for bonding and structure. vdW interactions emanate from dynamic electron correlations, causing a net attraction between fragments of electrons in many-electron systems. Like all non-relativistic electronic effects, the vdW interactions are present in the exact DFT functional [1]. Proper inclusion of vdW interactions in DFT calculations requires that the total energy functional depends on the electron density $n(\boldsymbol{r})$ in a manner that reflects both the long-ranged and medium-ranged nature of vdW interactions. The usual implementation of DFT involves the solution of the Kohn–Sham equations [19], which are one-electron Schrödinger equations in the presence of an effective one-electron self-consistent potential $V_{\rm eff}(\mathbf{r})$. This potential is the sum of the Coulomb potential from the density $n(\boldsymbol{r})$, the external potential—typically the Coulomb potential of the cores—and the functional derivative of the exchange-correlation density (xc) functional $E_{\rm xc}$ $[n(\mathbf{r})]$, which describes many-particle effects. The latter is universal and can in principle be derived from a diagrammatic expansion in many-body perturbation theory. This functional is often evaluated in the local-density approximation (LDA) [19, 20, 22–24] or extensions thereof, such as the generalized-gradient approximation (GGA) [25–27]. With the LDA and GGA, DFT is successful in a broad range of applications [20, 21].

From a technology perspective, the significance of LDA, e.g. for semiconductor physics and thus the development of electronics, cannot be overestimated [28]. The timing of the Nobel Prize for DFT to Kohn closely followed that of its breakthrough in chemistry—a breakthrough that is linked to its ability in the GGA [25–27] to accurately describe covalent bonds.

Until the start of this century, the route to extend the DFT approximations to long-range forces has at best been a vision. By construction, LDA and GGA neglect the long-range, nonlocal correlations that give rise to the vdW forces. There are still many papers with claims like 'vdW accounted for by LDA'. Such statements are wrong from a formal perspective and it is easy to give counterexamples in applications [29, 30].

Being a correlation effect, vdW interactions are included in $E_{\rm xc}[n(\mathbf{r})]$ [1]. In practice, however, approximate forms of $E_{\rm xc}$ have to be found. Studies of interacting inert atoms, molecules, and surfaces, with analysis of the polarizabilities of the participating species [31, 32], give the well-known asymptotic R^{-6} form of London for atomic and molecular dimers [13, 15, 33, 34], the Lennard-Jones z^{-3} law for a neutral molecule on a surface [16], and the d^{-2} interaction law [35, 36] for pairs of solids. There are also studies [37–39] showing that the frequency-dependent polarizabilities, to a good approximation, can be described by a one-pole formula, with one frequency characterizing each atom or molecule. Studies like these can be helpful in the search for an approximate $E_{\rm xc}$ that includes vdW forces. In the literature, an extensive knowledge of density fluctuations in general [40] and the role of plasmons in particular [37–39] has been developed. An important tool in this context is the 'adiabatic connection formula', which connects $E_{\rm xc}$ and the density–density correlation function [24, 41, 42].

The field of vdW interactions in DFT was practically absent before around 1990, but picked up at the end of the previous century, grew immensely during the first decade of the present one, and increased exponentially thereafter. Overall, there are now several kinds of approaches to the theme, 'Use investments in traditional DFT and add an account for vdW interactions'. Several of these are based on calculating atom-based pair potentials [43–51], some of those also with the inclusion of advanced screening mechanisms [50–53]. This review emphasizes one orthodox, that is, a first-principles DFT treatment [29, 54–63] of the long-to-medium-ranged forces between fragments across regions with low densities, the Rutgers–Chalmers vdW-DF method which includes vdW forces by using a nonlocal exchange-correlation functional. Inspired by this functional, there are also other nonlocal density functionals such as those proposed by Vydrov and Van Voorhis [64, 65].

There are already several review papers on vdW interactions in electron systems. In addition to our own 2005 [61] and 2009 reviews [66], we can list the reviews [2–8] and perspective papers [9, 10]. Considering the significant impact of the Rutgers–Chalmers vdW-DF on the field, we believe a review article that thoroughly covers this method—from its prehistory to the successive developments from the early 90s [1] and the broader activity in the long-standing Rutgers–Chalmers collaboration and the current status of vdW-DF—is in order. Together with Langreth[8], the authors of this review have

[8] David C Langreth passed away, 27 May 2011.

worked within this collaboration. Other methods, particularly those closely related to vdW-DF, will be discussed as well. However the aim of this discussion is to put the development in context and to highlight the nature of vdW-DF. For a more complete review of the other methods, we recommend that the reader consults other review articles on the topic [2–10].

In the beginning of the program to include vdW forces in DFT, contact was established with earlier developments. Initial attempts were made with the nonlocal average density approximation (ADA) and weighted density approximation (WDA) density functionals [67], unfortunately with limited success. Next, asymptotic functionals were derived for atomic and molecular dimers [44, 53, 68, 69] in part by modifying a Rapcewicz–Ashcroft [43] concept. Similar functionals were also developed for free molecules, molecules outside of a surface [52], and for two parallel surfaces [52, 70, 71]. The 90s involved development of conceptual ideas, implementations, and adaptation of existing codes, new codes, and exchange functionals.

The new century began with the development of two complete vdW functionals, first in a two-dimensional configuration [29, 54, 58] and then in a general geometry [56, 59, 62, 63, 72]. There are applications involving the interactions of atoms [44, 59, 62, 69], molecules [69], solids [59, 62, 73–75], molecular solids [76–79], surfaces [80, 81], adsorption [80–83], graphene [55, 58, 61, 63, 73, 75, 78, 80, 84–88], metals [89, 90], oxides [74, 91, 92], polymers [93–95], nanosystems [76, 86, 94, 96–98], adsorbate interactions [97, 99–100], clusters [101], DNA [102–104], nanotubes [76], the carbon nanotube (CNT) morphology [94, 96, 98], water [105], and the list goes on.

The objective of vdW-DF is to provide within DFT an efficient method for calculations of vdW effects in all kinds of electron systems based on many-body physics and general physical laws. In this regard, the vdW-DF method differs from methods that use empirical, semi-empirical, and ad hoc assumptions for such calculations. By semi-empirical, one typically refers to methods that rely on optimization to reference systems for which data from accurate, computationally expensive methods are available. So far, we have published general nonlocal functionals in 2004 (vdW-DF; also referred to as vdW-DF1 [59]) and in 2010 (vdW-DF2 [63]). Based on physical principles, we have also developed progressively more consistent exchange functionals (i.e. vdW-DF-C09 (2010) [106] and vdW-DF-cx (2014) [107, 108]) to complement the vdW-DF1 nonlocal correlation. Together these works demonstrate that the vdW-DF method [56, 57, 59, 61–63, 72, 107–109] provides a good framework for developing successively improved functionals.

2. The beginnings

Sparse matter has strong local bonds, as well as vdW bonds, and other weak bonds. A proper description must include all. Numerous treatises ([21] is a recent one) have been devoted to the chemical or valence bond. Thus it is fair to focus on just the vdW bond here, keeping in mind the whole set of bonds present. There are many different configurations where vdW forces act between atoms or fragments of electron densities separated by empty space. Extreme voids are provided by gas-solid interfaces, which lead us to a discussion of the early surface-physics work important for functional development, with contributions from the Ashcroft group, Langreth and Vosko, and others.

2.1. Surface-physics background and experimental aspects

A typical introduction to vdW forces starts with molecule–molecule interactions. To reach the vdW-DF functional we choose a condensed-matter and surface physics perspective, as our background is in these fields.

Surface potentials can be obtained by bombarding atoms or molecules against surfaces and studying the scattering. In the early days, studies on metals were lagging behind those on, for instance, ionic crystals. On metal single crystals, diffraction spots are much weaker. This reflects the much weaker corrugation of close-packed metal surfaces [110] than of, e.g. an ionic crystal, like LiF(1 0 0) [111]. In the 70s, experimental techniques improved, and metal surfaces started to drive the development [110]. On the theory side, jellium and smooth surfaces were studied.

In the early 90s, the stage for describing the physisorption on metal surfaces using the jellium model was set by the Zaremba–Kohn (ZK) theory [112, 113]. The ZK theory provides key concepts, such as repulsive walls, vdW attraction, induced surface charges, and dynamic image or vdW planes. It also provides a semi-quantitative framework for analysing accurate experimental results. This is the 'traditional picture' of physisorption, where the interaction potential $V(z)$ between a metal surface and an inert adparticle at a separation z apart is approximated by a superposition [16, 17, 113, 114],

$$V(z) = V_R(z) + V_{\mathrm{vdW}}(z)\,. \tag{1}$$

The short-range Pauli repulsion, $V_R(z)$, is due to the overlap between orbital tails of the metal conduction electrons and the closed-shell electrons of the adparticle. In the Lennard-Jones potential [16] it was expressed either as R^{-12} or an exponential, as in

$$V_R(z) = V_{RO}\exp(-\alpha z)\,, \tag{2}$$

where the constants V_{RO} and α determine the strength and the range of the repulsive potential. There are schemes to calculate $V_R(z)$ from the shifts of the one-electron energies of the metal induced by the adparticle, for instance calculated with perturbation theory, where the adparticle can be described with pseudopotentials and the metal surface in a jellium model. As the local density of metal-electron states decays exponentially away from the surface, the exponential form of the repulsive wall (2) follows.

The long-range vdW attraction, $V_{\mathrm{vdW}}(z)$, arises from adsorbate-substrate electron correlations. A common approximate form is

$$V_{\mathrm{vdW}}(z) = -\frac{C_{\mathrm{vdW}}}{(z - z_{\mathrm{vdW}})^3} f\big(2k_c(z - z_{\mathrm{vdW}})\big)\,, \tag{3}$$

where z_{vdW} is the dynamic image-plane location [112]. The magnitude of the asymptote, C_{vdW}, and the position of the vdW

plane, z_{vdW}, depend on the dielectric properties of the metal substrate and the polarizability of the adsorbate [112, 115]. The function $f(x)$ saturates the vdW term at atomic-scale separations. In some accounts it has the form $f(x) = 1 - (1 + x + x^2/2)\exp(-x)$. This saturation lacks a rigorous prescription, which leaves a level of arbitrariness for $V_{vdW}(z)$. These empirical saturation functions, like those in [17, 114, 116, 117], resemble the damping functions used in semi-empirical DFT descriptions of dispersive interactions [49].

The development of experimental techniques often makes once canonized theoretical results appear insufficient. An example is given by gas-surface scattering, in particular diffractive scattering in the elastic backscattering mode which can exhibit resonance structures. Beams of light molecules scattered off single-crystal Cu surfaces can be used to deduce physisorption potentials. In the case of scattering of H_2 and D_2 off the Cu(111) surface [116,117], the physisorption well-depth of 30.9 meV is substantially larger than the ZK value of around 22 meV [116,117].

Inert atoms and molecules undergo no significant change in their electronic configurations when they physisorb. Even in metallic physisorption, the coupling to electronic excitations is weak, which makes the adsorption essentially electronically adiabatic [118]. The energy transfer occurs through the phonons of the solid lattice [119]. The internal molecular degrees of freedom add further details to the particle-surface interaction. Contact between theory and experiment can be established when the potential energy surface governing the gas-surface collision process is known. For well-defined impact conditions, molecular-beam-scattering experiments can provide such information and also data on energy transfer and sticking probabilities [17].

The benchmark provided by resonant elastic backscattering of light molecules, like H_2 on Cu single-crystal surfaces, is extraordinary. The data provide (i) quantum-mechanical energy eigenvalues, ϵ_i, for H_2 in the potential energy well, which are directly tied to measured intensities, (ii) the laterally averaged physisorption potential V_0, which is derived from measured data, (iii) the corrugation V_1, also derived from measured data, and (iv) the laterally averaged min-to-max variation of the rotational anisotropy V_2 [17].

Figure 1 shows the potential energy curves for H_2 on Cu(111), (100), and (110), deduced from resonant elastic backscattering experiments. These potential wells can trap H_2 [17, 116, 117]. The traditional theoretical picture of the interaction between an inert adsorbate and a metal surface [113, 114, 120] is used to deduce the potential energy curves based on the experimental energy-level values. The resulting physisorption potentials based on (1) and (3) provide a good fit. The curves in figure 1 have potential-well depths of 29.5, 31.4, and 32.3 meV and a potential minimum located at 3.50 Å outside the topmost layer of copper ion cores on Cu(111), (100), and (110), respectively [17, 116, 117].

The physisorption potential $V(z)$ (1) depends on the details of the surface electron structure, via both the electron spill out (V_R) and the centroid of fluctuations of exponentially decaying surface charges (V_{vdW}). For a given adparticle, this results in a crystal-face dependence of $V(z)$

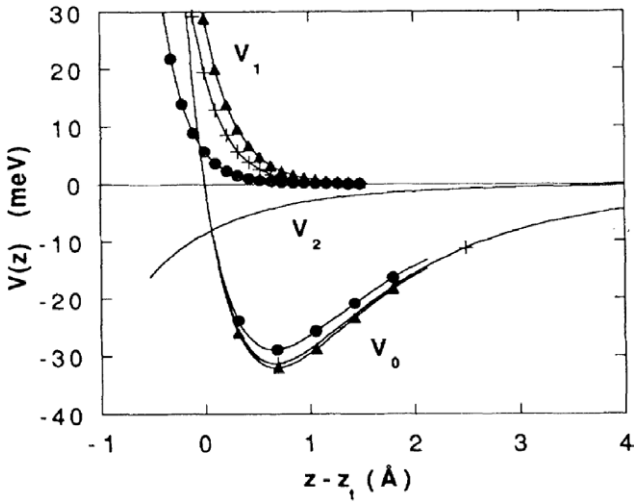

Figure 1. Physisorption interaction potentials for H_2 (D_2) on Cu(111) (circles), Cu(100) (squares) and Cu(110) (triangles) [116]. $V_0(z)$, $V_1(z)$ and $V_2(z)$ are the laterally averaged physisorption potential, the corrugation potential, and the laterally averaged min-to-max variation of the rotational anisotropy V_2 potential functions, respectively. The position z of the molecular centre of mass is given with respect to the classical turning point z_t at $\epsilon_i = 0$. Reprinted with permission from [116], © 1993 American Physical Society.

[121]. From the ZK theory one gets no strong hints about the dependence on n (**r**), needed in DFT. However, the weak dependence of the diffraction of, e.g. the He atom on metal surfaces was observed early [110]. It is explained in terms of a simple link between the scattering potential and the electron-density profile. This gives a hint for approximate DFT: the He-surface interaction energy, $E_{He}(\mathbf{r})$, can be reasonably well expressed as [122]

$$E_{He}(\mathbf{r}) \simeq E_{He}^{hom}\big(n_o(\mathbf{r})\big)\,, \tag{4}$$

where $E_{He}^{hom}(n)$ is the energy change on embedding a free He atom in a homogeneous electron gas of density n. In this case, $n_o(\mathbf{r})$ is the host electron density. On close-packed metal surfaces the electron distribution $n_o(\mathbf{r})$ is smeared out along the surface [123], resulting in weak corrugation. The crude proposal (4) might be viewed as the precursor to the effective-medium theory [124].

Figure 2 shows the calculated density profiles for the Cu(111), (100), and (110) surfaces, using DFT. It illustrates the point that the corrugations on these facets are small, but increasing when going from (111) to (100) to (110). For the scattering experiment the density contours far away from the surface, in the tails of the wavefunctions, are particularly important.

The kinematical condition for a diffraction resonance involving a surface reciprocal lattice vector **G** is

$$\epsilon_i = \epsilon_n + \frac{\hbar^2}{2m_p}(\mathbf{K}_i + \mathbf{G})^2\,, \tag{5}$$

where ϵ_n is the bound-state energy, m_p the particle mass, and ϵ_i and $\mathbf{K}_i$ the energy and wavevector components parallel to the surface of the incident beam. When the resonance condition (5) is fulfilled, weak periodic lateral corrugations greatly

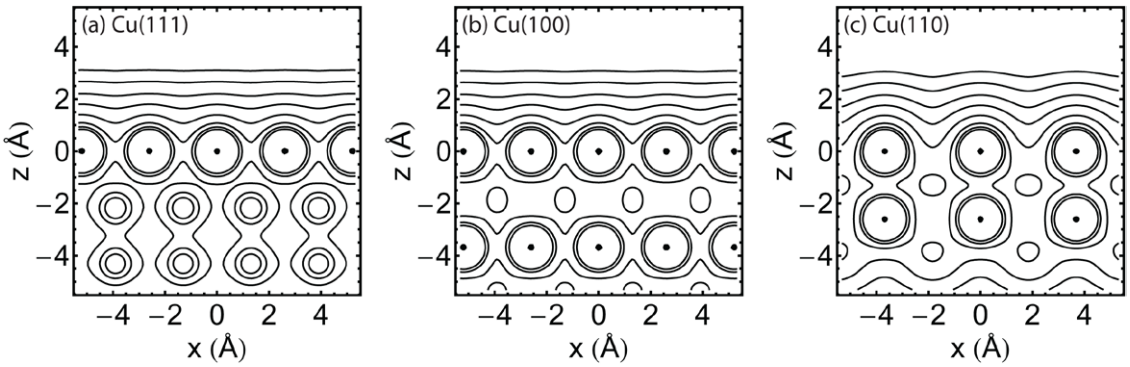

Figure 2. Electron density profiles of the clean Cu(1 1 1), (1 0 0), and (1 1 0) surfaces calculated with the vdW-DF2 functional [63]. The density contours take values in a nonlinear fashion. Reprinted with permission from [90], © 2012 Institute of Physics.

affect diffracted beam intensities. The resonances are usually observed as narrow features in the spectra of the diffracted beam intensities. This sharpness allows a number of levels to be uniquely determined. A single accurate gas-surface potential curve can then be constructed according to the Rydberg–Klein–Rees method of molecular physics [125]. Detailed mapping of the bound level spectrum and the gas-surface interaction potential by resonance scattering measurements has only been performed for hydrogen [116, 121, 126–130]. Having two isotopes, H_2 and D_2, with significantly different masses available as well as the different rotational populations of para-H_2, ortho-D_2, and the normal species, is extremely useful in data analysis.

2.2. Surface physics and theoretical aspects

To describe the excitation spectrum of electrons in the framework of noninteracting particles, Bohr and collaborators already realized [37] that a simple assumption one can make is to associate each point in the atom with a single frequency, which is a function only of the local density—a model used in particular by Lindhard and Scharff [131]. In the simplest version, one chooses the frequency equal to the classical plasma frequency

$$\omega_{\mathrm{p}} = \sqrt{4\pi n e^2 / m} \quad . \tag{6}$$

The choice of this resonance frequency is equivalent to assuming that the local response to the field is the same as that of a uniform electron gas of a density equal to the local density $n(\mathbf{r})$.

For atoms, this type of approximation has been used to calculate the response function for external electrical fields with long wavelengths [132]. For metals there are famous publications that rely on this model [37, 38]. The extensive experience in studying density fluctuations by this Copenhagen school [37, 38, 131] has influenced our thinking, in particular bringing attention to the role of plasmons [37, 38]. We call this 'the plasmon description'. It is common not only for atoms, metals, and stopping power, but also for models such as the 'Swedish electron gas' [133], and for the modelling of plasmonics [134] plasmaronics [135, 136], and transition metals [137]. There is thus a rich variety of physical systems that have nurtured the conceptual development behind the vdW-DF method. Many of these appeal to the density of electrons $n(\boldsymbol{r})$, but, like for the GGA, results that depend on the gradient of the density are of key interest. Results for inhomogeneous electron systems in general, and surfaces in particular, come into focus.

Surfaces are thus important for the development of electron-structure theory. The first descriptions of interacting electrons in condensed matter were made for the homogeneous electron gas. The many-body aspects of this model system of charged fermions were relatively successfully treated with diagrams, which emerge in perturbation theory to infinite order or with a corresponding quantum-field theory. Going beyond the homogeneous electron gas, a functional that performs well on surfaces is likely to be useful even for other classes of systems.

To account for vdW forces by DFT one considers how charge density fluctuations that are basically dynamic in nature can be accounted for with a static quantity like the density $n(\boldsymbol{r})$. This problem together with the nature and form of the vdW interaction in DFT are treated in three many-body articles from the late 80s [43, 136, 137].

vdW bonds emanate from nonlocal electron correlations. This is illustrated in early dipole-model descriptions of the interactions in noble-gas crystals [138, 139]. The electrodynamical coupling between the atomic dipoles gives a shift in the dipolar oscillator frequencies, and the sum of all these shifts gives the vdW binding energy [138, 139].

2.3. Work of the Ashcroft group, and Langreth and Vosko

A particular type of dipolar oscillations is present in noble metals. The question of effective interatomic potentials in noble metals arising from quantum fluctuations in the atom-centred d electrons can be addressed with diagrammatic perturbation theory [136]. With a philosophy of incorporating the many-body interaction between the core states from the outset, many of the cohesive properties of noble metals are found to be directly linked to fluctuation effects. Maggs and Ashcroft (MA) [136] identified large contributions to the potentials that originate in certain diagrams for the homogeneous electron gas, which had been overlooked in the linear response of homogeneous systems. These are the ones with the screened Coulomb interaction between ions and they lead to the possibility of recovering vdW forces in nonlocal

functional theories of the electron gas. The diagrams corresponding to vdW interactions between the core electrons are screened by the intervening electron gas. This screening is given by the frequency-dependent dielectric function for the homogeneous electron gas. The core density–density response function ('vertices') depends on the frequency-dependent core polarizability. To a good approximation the internal lines can be replaced with a simplified expression involving the plasma frequency (6) and wavevector q, as follows [137]:

$$4\pi\omega^2 / q^2(\omega^2 + \omega_p^2) \, . \tag{7}$$

The simplest model assumes the core fluctuations to be dominated by a single excited-state frequency, Δ, which makes the integrals over frequency straightforward, giving an approximate formula for the screened vdW interaction energy for a pair of atoms separated by r in a polarisable metal [136],

$$E_b(r) = \frac{3\Delta}{4}\frac{\alpha^2(0)}{r^6}\left(\frac{\Delta}{\Delta + \omega_p}\right)^3 . \tag{8}$$

This result relates to DFT via the Hohenberg–Kohn–Sham [18, 19] energy-response kernel $K_{xc}(q)$, a key property in the description of responses in electron systems. In a dense homogeneous electron gas it is defined by [137]

$$\delta E_{xc} = \sum_q K_{xc}(q) | \, \delta n_q \, |^2 \, , \tag{9}$$

where n_q is the electron-gas density in planewave representation. The kernel defines the static dielectric function $\epsilon(q)$ of the electron gas,

$$\epsilon(q) \; = \; 1 - (4\pi e^2 / q^2)\chi(q) \, , \tag{10}$$

$$\chi(q) \; = \; \frac{\chi_0(q)}{1 - 2K_{xc}(q)\chi_0(q)} . \tag{11}$$

Figure 3 shows diagrams corresponding to corrections to the free-electron response function $\chi_0(q)$. The approximation $K_{xc} = 0$ is the random-phase approximation (RPA) and corresponds to disregarding these higher-order diagrams. The $q = 0$ component corresponds to the LDA. The expansion

$$K_{xc}(q) = K_{xc}(0) + \frac{\pi e^2}{8k_F^4} Z(q) q^2 \tag{12}$$

defines the dimensionless quantity $Z(q)$. Here

$$K_{xc}(0) = -\frac{\pi e^2}{2k_F^2}[1 + \lambda(1 - \ln 2)] \, , \tag{13}$$

where, to sufficient accuracy [137],

$$\lambda = (\pi a_0 k_F)^{-1} = 0.521 r_s / \pi = (k_{TF} / 2k_F)^2 \, . \tag{14}$$

For $q \to 0$, diagrammatic perturbation theory has given important results to leading order in $r_s(n)$: Z (0) is a number independent of e^2 [140]; the value is Z (0) = 1.98 − 7/9. There are two types of contributions:

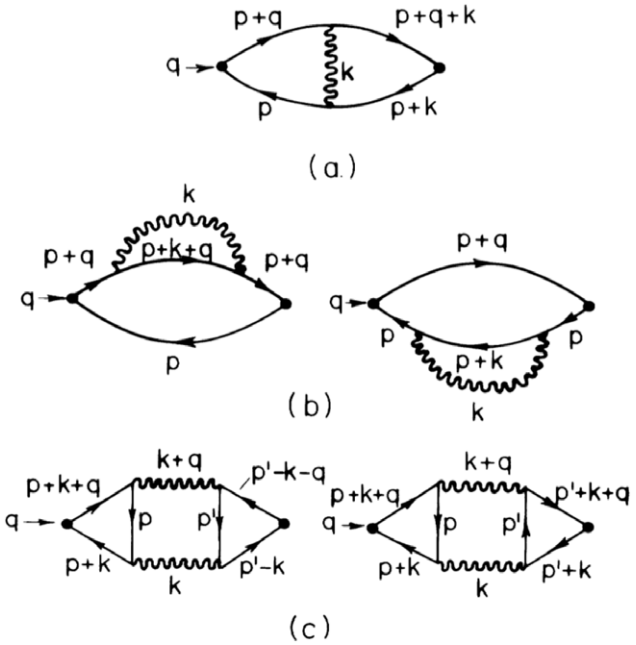

Figure 3. Diagrams for the leading order corrections to the response function χ. The wiggly lines are the screened Coulomb interaction in the random-phase approximation. Diagrams in (*a*) and (*b*) contribute to Z_x, whereas the diagrams in (*c*) contribute to Z_c. Reprinted with permission from [137], © 1987 American Physical Society.

$$Z(q) = Z_c(q) + Z_x(q) \, . \tag{15}$$

For finite q, it has been shown that the exchange part $Z_x(q)$ remains close to its zero-q value of −7/9 [137]. For small q, the correlation part is given by

$$Z_c(q) = 1.98 + 0.77\, Q \ln Q - 1.25\, Q + \ldots \, , \tag{16}$$

to within 1% for Q up to about 1, where $Q = q\sqrt{3}/k_{TF}$.

These results are relevant for DFT [137], providing input to the Langreth–Mehl functional [25] as well as indicating ways to improve it. They also provide the leading-order correction to the static Lindhard screening function [38].

Rapcewicz and Ashcroft (RA) [43] considered the coupling between fluctuations giving rise to an attractive interaction. This interaction originates in the lowest-order fluctuation term of the interacting electron gas. The corresponding diagram is similar to that of figure 3, but the two three-point functions are connected by two internal screened Coulomb lines [137].

Seeking a DFT account of vdW forces, one has to face the fact that vdW forces are linked to density fluctuations, while DFT is linked to densities. RA exploit the analogy between the correlation hole and the electron charge localized around nuclei in condensed atomic systems [43] to connect vdW forces arising from the fluctuations in the electron liquid to the electron density $n(\boldsymbol{r})$. Clearly, such a reformulation is helpful for designing nonlocal correlation functionals in DFT.

RA raise the question of 'vdW interactions from fluctuations in an otherwise static response charge' in the same way as it had been done for the atomic case. From the standard

argument for the atomic case [141] together with dimensional analysis [136], Maggs and Ashcroft [136] expected an attractive pair interaction of the form [43, 136]

$$\sim -\hbar\omega_{\rm p}\frac{r_s^6}{R^6}. \tag{17}$$

The work of RA illustrates that a plasmon picture can be used to formulate a theory of vdW forces in an electronic liquid. Thus we can benefit from decades of experience with LDA and GGA, which can also be formulated in terms of plasmons.

3. Asymptotic functionals

Traditionally, the asymptotic form at large separations has attracted the most interest. The first attempts by us and others to capture vdW behaviour in approximate forms of $E_{\rm xc}[n(\mathbf{r})]$ also concerned asymptotic functionals describing the interaction between widely separated fragments of electrons. Both local and semilocal approximations (GGAs) have the wrong asymptotic dependences on separation. To retain the vdW interactions in approximate DFT methods, there are, however, several previous ideas and results for approximate nonlocal functionals, and even for local or semilocal approximations to benefit from.

Several not so successful attempts were first made. One started from the so-called weighted-density approximation [67]. With the Gunnarsson–Jones expression for the xc hole [142], the leading term for two widely separated neutral objects becomes $-C_5R^{-5}$, whereas for a neutral point-like object outside a metal surface it goes like $-C_2z^{-2}$ [1]. In addition, the C-coefficients take unphysically high values.

A dipole–dipole type of weighted-density approximation for $E_{\rm xc}$ has also been attempted. It appeared to be able to retain the image potential ($-1/4z$) but failed to connect long- (i.e. $-R^{-6}$) and short-range parts [1].

3.1. The functional of Rapciewicz and Ashcroft

The attention of vdW-DF developers then turned to the RA work [43]. In their study of the fluctuation attraction in condensed matter, the lowest-order fluctuation term corresponds to a diagram with two three-point functions, connected by two internal screened Coulomb lines—see figure 3(*c*). The lowest order fluctuation term shown in figure 3 leads to a static vdW attraction between electrons [13, 33]. Its physical significance is greater than its formal order in perturbation theory might imply, which is related to the dynamical screening. The effective interaction between electrons at $\mathbf{r}_1$ and $\mathbf{r}_2$ is [1, 43]

$$-\frac{3}{4}\hbar\left(\frac{e^2}{m}\right)^2\times\frac{1}{[\omega_{\rm p}(\mathbf{r}_1,\mathbf{r}_2)]^3|\,\mathbf{r}_1-\mathbf{r}_2|^6}\ . \tag{18}$$

Here, the dielectric function is given by the plasmon-pole approximation for a homogeneous electron gas with an effective density given by the geometrical mean of the densities

$$n_{\rm eff}=[n^{(1)}(\mathbf{r}_1)\,n^{(1)}(\mathbf{r}_2)]^{1/2} \tag{19}$$

of the two fragments, so that the effective plasma frequency becomes

$$\omega_{\rm p}(\mathbf{r}_1,\mathbf{r}_2)=\left[\omega_{\rm p}(\mathbf{r}_1)\,\omega_{\rm p}(\mathbf{r}_2)\right]^{1/2}\ . \tag{20}$$

An approximate formula for the screened vdW interaction energy for a pair of atoms separated by r in a polarizable metal is given by (8). However, to get a density functional that is valid in both the uniform gas and separated atom limit [44] we must have a form that is viable and physically motivated in both limits, as seen in section 3.2.

3.2. Improvement by Andersson, Langreth, and Lundqvist

It is desirable that the approximate density functional is valid, viable, and physically motivated in both the uniform-gas and separated-atoms limits. Such a situation arises when we consider an effective density in the kernel $K_{\rm xc}$ defined by the expression for the exchange-correlation energy of a slightly nonuniform system [44]:

$$\delta E_{\rm xc}=\int {\rm d}^3r_1\int {\rm d}^3r_2\ K_{\rm xc}(\mathbf{r}_1,\mathbf{r}_2)\ \delta n(\mathbf{r}_1)\ \delta n(\mathbf{r}_2)\ , \tag{21}$$

as given by the real-space representation of (9). The interaction between two small but distant charge perturbations in a uniform electron gas is described through the limiting behaviour of this linear-response kernel $K_{\rm xc}$ [1]. This has implications for the effective plasmon frequency $\omega_{\rm p}$ in equation (20). In the formulation by Andersson, Langreth, and Lundqvist (ALL) [44] the effective density is

$$n_{\rm eff}=\left[\sqrt{n(\mathbf{r}_1)\,n(\mathbf{r}_2)}\left(\sqrt{n(\mathbf{r}_1)}+\sqrt{n(\mathbf{r}_2)}\right)\right]^{2/3}\ , \tag{22}$$

and the total fragment density is used instead of δn in the isolated fragment limit, following [25, 43, 143]. This gives an effective long-range interaction of the form

$$\phi(\mathbf{r}_1,\mathbf{r}_2)\to\frac{3e^4}{2m^2}\frac{1}{\omega_{\rm p}(\mathbf{r}_1)\omega_{\rm p}(\mathbf{r}_2)[\omega_{\rm p}(\mathbf{r}_1)+\omega_{\rm p}(\mathbf{r}_2)]|\,\mathbf{r}_1-\mathbf{r}_2|^6}\ , \tag{23}$$

which differs from the RA expression (18). This has the same form as the London expression for the vdW interaction between two atoms A and B at separation R, for the case where only one excitation frequency $\omega_{\rm A/B}$ is considered for each atom [12, 13],

$$E_{\rm vdW}^{\rm London}=-\frac{3e^4}{2m^2}\frac{Z_{\rm A}Z_{\rm B}}{\omega_{\rm A}\omega_{\rm B}(\omega_{\rm A}+\omega_{\rm B})}\frac{1}{R^6}\ . \tag{24}$$

The long-range interaction is related to the electric susceptibility $\chi_i(\omega)$ or polarization response of a uniform electron gas at density $n(\boldsymbol{r})$ to an external electrical field

$$E_{\rm xc}^{l-r}=-\frac{3}{\pi}\int_0^\infty {\rm d}u\int_{V_1}{\rm d}^3r_1\int_{V_2}{\rm d}^3r_2\frac{\chi_1({\rm i}u)\chi_2({\rm i}u)}{|\mathbf{r}_1-\mathbf{r}_2|^6}\ . \tag{25}$$

For two atoms, widely separated by a distance R, (25) gives $E_{\rm xc}^{l-r}=-C_6R^{-6}$, with the standard expression for C_6 in terms of the atomic polarizabilities $\alpha_i(\omega)$ [12, 144].

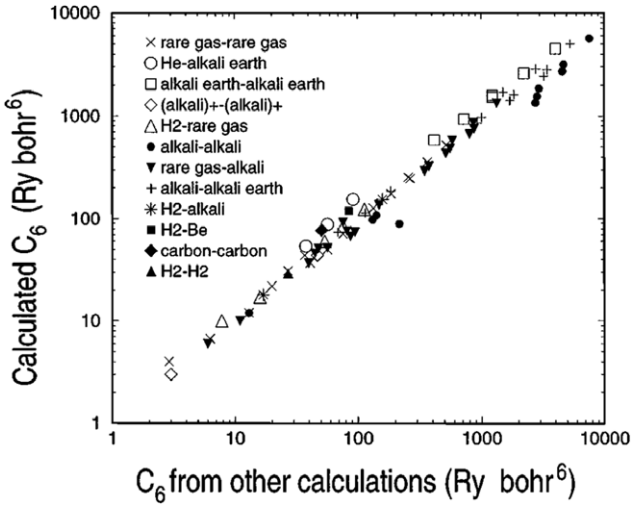

Figure 4. van der Waals coefficients C_6 (in Ry atomic units) calculated from $E_{xc}^{l-r} = -C_6 R^{-6}$ and (26) and (28), plotted against corresponding values from first-principles calculations. Reprinted with permission from [44], © 1996 American Physical Society.

The ALL theory is crude. Like RA, it contains a cutoff, specifying the spatial regions where the response to an electric field is defined to be zero. Results can be overly sensitive to the specific cutoff. Nevertheless, results based on ALL compare well with those of first-principles calculations, over wide classes of atoms and molecules [69, 145] (figure 4).

ALL also provides one of the foundations for the more general vdW-DF, which was developed nearly a decade later. It shows that a functional that is quadratic in the density works [44]. Once the interaction at large distance was understood, it took a decade before we could grasp the small-separation limit (see section 6).

The ALL functional has had multiple applications, sometimes with the addition of empirical damping functions, which will be discussed in the next chapter.

3.3. Improvement by Dobson et al

In a parallel and independent study, Dobson and Dinte [146] focused on constraint satisfaction in local and gradient susceptibility approximations in the development of a vdW density functional. They show how charge conservation and reciprocity, that is $\chi(\mathbf{r}, \mathbf{r}', iu; \lambda) = \chi(\mathbf{r}', \mathbf{r}, -iu; \lambda)$, can be built into local density or gradient approximations for density–density response functions (susceptibilities). Applying these ideas, they were able to derive a variant of the RA formula for the vdW interaction.

To describe vdW forces, an approach is introduced [147] that (i) simplifies the problem of achieving hole normalization; that is ensuring that the xc hole contains one charge unit [24], and (ii) facilitates the derivation of vdW functionals. This expression for the vdW interaction between nonoverlapping electronic systems is similar but not identical to the RA one [43]. In the denominator the geometric mean $(\omega_1\omega_2)^{1/2}$ has been replaced by an arithmetic mean giving a kernel form similar to equation (23). This makes the result less sensitive to a low-density cutoff. This choice was motivated partly by the desire to reduce the noise sensitivity compared to RA. A cutoff, for example, like that in RA, would certainly still be appropriate, because the uniform-gas-based approximation seriously overestimates the response in the outer tails of the electronic density.

The essential point, though, is that a formula for vdW asymptotic interactions has been derived by a simple local-density approach, which embodies suitable constraints. The satisfaction of charge conservation is essential, because without it equation (25) would represent the second-order Coulomb interaction between spurious nonzero charges, and would not give the correct r_{12}^{-6} interaction.

3.4. Self-consistency and the inclusion of corrections

The ALL functional [44] calculates the frequency-dependent molecular polarizability as a perturbation in the screened electric field

$$\mathbf{E}(\mathbf{r}, \omega) = \mathbf{E}_{ext}(\mathbf{r}, \omega) / \epsilon(\omega; n(\mathbf{r})) \; . \tag{26}$$

It thus uses a local-density screening account, that is a local approximation for the appropriate response functions [52]. This would be wrong for macroscopic objects, but gives surprisingly good results for atoms and molecules [44, 69].

In [52], a procedure for describing the interactions of a molecule with a surface which relies on a better account of the electrodynamics is developed. It starts from Maxwell's equations and the standard electrodynamic treatment of the electric field and the displacement vector. The factorization of the electron density proposed in ALL (26) is equivalent to assuming a local-density response to the external electric field. In the improved procedure, to get the atomic polarizability $\alpha(iu)$ and similar quantities, one uses a local relationship between the polarization $\mathbf{P}(\mathbf{r}, \omega)$ and the total electric field $\mathbf{E}(\mathbf{r}, \omega)$,

$$\mathbf{P}(\mathbf{r}, \omega) = \frac{1}{4\pi}[\epsilon(\mathbf{r}, \omega) - 1]\mathbf{E}(\mathbf{r}, \omega) \; , \tag{27}$$

and solves the Poisson equation $\nabla \cdot \mathbf{D}(\mathbf{r}, \omega) = \nabla \cdot [\epsilon(\mathbf{r}, \omega) \times \mathbf{E}(\mathbf{r}, \omega)] = 0$ in the presence of an external electric field $\mathbf{E}_{ext}(\mathbf{r}, \omega)$. In this evaluation a diagonal dielectric tensor is used:

$$\epsilon_{\alpha\beta}(\mathbf{r}, \mathbf{r}'; \omega) = \delta_{\alpha\beta} \, \delta(\mathbf{r} - \mathbf{r}') \, \epsilon(\mathbf{r}; \omega) \; , \tag{28}$$

with the standard dielectric form

$$\epsilon(\mathbf{r}; \omega) = 1 - \frac{\omega_p^2(\mathbf{r})}{\omega^2} \; . \tag{29}$$

Applications to polarizabilities and charge centroids show that these successfully describe the asymptotic physisorption of He, Be, and H_2 on jellium and of H_2 on the low-indexed facts of Al [52]. Comparison is also made with results from time-dependent LDA calculations [115] and experiment [121]. Calculated trends in the vdW coefficient and the vdW reference-plane position z_{ref} [148] signal that this reference plane depends strongly on the crystal facet. There are also applications to interactions between macroscopic bodies, in particular between two parallel surfaces [70].

With the overall goal of a general functional, the treatments of the electrodynamics need unification. A method with a proper electrodynamical account for all kinds of geometries has also been developed [53]. This development unifies several earlier treatments [44, 52, 70] used for the cases of molecular pairs, a molecule outside a surface, and parallel surfaces, respectively.

It can be noted that in the long-range limit the fully electrodynamical account performs quite well, even for the buckyball C_{60}, where standard ALL has some problems [69]. Furthermore, recent studies have been concerned with properly describing the C_{60} polarization [149, 150]. However, this was done quite well even with the fully electrodynamical account of ALL [69]. The calculated polarizabilities and vdW coefficients are in good agreement with results in the literature. This makes it possible to easily calculate these quantities for complex systems with useful accuracy [53]. Finally, we note that the approximation in ALL turns out to be in good agreement with the self-consistent account for typical molecular geometries. This was an important clue in the development of the vdW-DF for general geometries described in section 6.

4. Other methods for including vdW interactions

4.1. Brief overview of methods

Other methods have also been proposed for studies of vdW systems. Traditional DFT is a natural starting point. There are three main types of approaches: (i) explicit density functionals, (ii) DFT extended with atom-pair potentials, and (iii) perturbation theory, typically in the random-phase approximation. This review focuses on explicit density functionals with an emphasis on the path that led to the vdW-DF. Still, we briefly review other methods because the accuracy of different methods for the inclusion of vdW forces is compared in so many studies and because the contrast between these methods helps to highlight the nature of vdW-DF.

The approach of extending approximate DFT with pair-potentials has been widely used, both in jellium-type surface studies [115, 129] and in explicit electron-structure calculations [45–49, 151–154]; for a review see [155]. The force fields used have often been heavily parametrized either through fitting to experimental data sets or to calculated results using more advanced methods, although less so in the most recent forms [49].

The simplest pair potential is the London $\sim -R^{-6}$ form. In modern variants, this potential is 'dressed' with a damping function $F(R)$, which preserves the long-range behaviour of the dispersion interaction, while preventing the singularity in the dispersion term from overwhelming the repulsive term at short ranges. An early form for $F(R)$ was proposed by Brooks [156], who warned against the crudeness of the approximation. More recently, Nordlander and Harris proposed a prefactor similar to the $f(x)$ in the ZK expression (3) [114]. Starting from the ZK expression for the vdW attraction potential $V(z)$ of an atom outside a surface, they argue that introducing such a damping function amounts to introducing a wavevector cutoff k_c in a wavevector analysis [114].

For molecular complexes, from small organic molecules to large and composite systems, like sparse materials and protein-DNA complexes, traditional DFT calculations with pairwise vdW potentials are commonly used. Two well-known methods are DFT-D [46, 47, 49] and TS-vdW [48]. The idea is that strong covalent bonds are well described by traditional approximations, like the GGAs [25–27] and a pairwise atomistic correction can be used to account for the vdW forces. In these methods, there are two kinds of parameters that must be specified. The first kind are dispersion coefficients C_6, which characterize the asymptote, and the second kind are cutoff radii r_{cut}, which characterize the damping functions.

The DFT-D method has been successively refined for higher accuracy and less empiricism. In the recent DFT-D3 version [49] dispersion coefficients and cutoff radii are computed from first principles. To distinguish between dispersion coefficients of atoms in different chemical environments, the method relies on the concept of fractional coordination numbers. The DFT-D3 pairwise account of vdW forces can be tailored to different density functionals lacking such forces by adjusting two global parameters. Advantages of the method include the facts that it is simple, asymptotically exact for a gas of weakly interacting neutral atoms, and atomic forces are easy to calculate. The DFT-D3 [49] framework does allow for three-body nonadditivity terms to be included, though these are not in the standard version. Such effects have been shown to be non-negligible for large molecular systems and organic solids [157].

The TS-vdW method is also an almost parameter-free method for accounting for long-range vdW interactions. It relies on the summation of interatomic C_6R^{-6} terms that are updated for each configuration based on the electron density of a molecule or solid by scaling reference coefficients for the free atoms [48]. The mean absolute error in the C_6 coefficients is 5.5%, when compared to accurate experimental values for 1225 intermolecular pairs. The effective atomic C_6 coefficients have been shown to depend strongly on the bonding environment of an atom in a molecule [48].

Comparing huge data sets is becoming more and more common in first-principles and semiempirical calculations. The same datasets are often used in many comparative studies for semiempirical parametrization, for instance, no less than 29 different systems in [46] as early as 2004. However, these datasets are often biased towards small dispersion bound molecules. The goal is to develop a functional that crosses the boundary for what is thought to be traditional dispersion-bound complexes to covalent-bonded systems. As such, the vdW-DF philosophy has been to try to benefit from what can be deduced from basic theory. Irrespective of these differences, we acknowledge that skilful users of, for instance, the DFT-D method, regularly produce valuable results.

A different kind of approximate approach, which can be seen as going beyond a density-based xc in DFT, is to use the RPA to calculate the correlation energy. This method has become much more efficient [158], but still carries higher computational cost than DFT. Since the RPA describes the

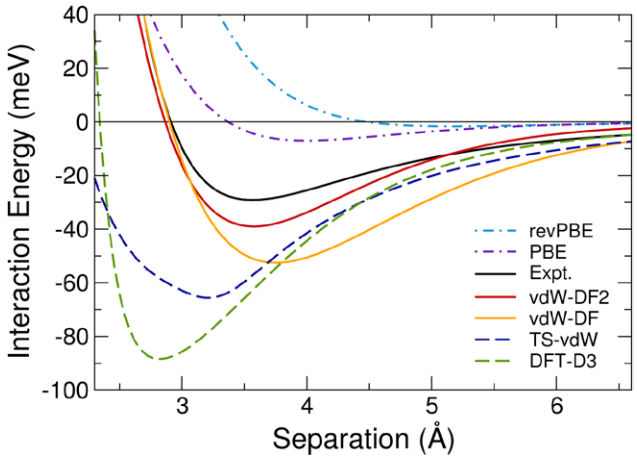

Figure 5. Comparison between experimentally determined [116] and calculated interaction energy curves for H_2 on Cu(1 1 1) using different methods. Reprinted with permission from [90], © 2012 Institute of Physics.

response in terms of single-particle orbitals, it is presumably a suitable complement to the exact exchange energy [159], particularly when comparing systems in which the number of particle-hole excitations remains unchanged [160]. The RPA correlation energy [39] incorporates a screened nonlocal exchange term and long-range dynamic correlation effects that underpin vdW bonding [159]. Several suggestions for RPA corrections exist [40]. A recent study [161] suggests a single-excitation extension for RPA calculations in inhomogeneous systems, which lowers the mean average error for noncovalent systems. RPA calculations have been used for solids [159, 162], molecular systems [163, 164], and layered materials [165].

Relatively expensive methods, such as RPA, provide a rough benchmark for methods that include vdW forces, particularly for bulk materials and larger systems where traditional quantum chemistry methods fall short. However, these methods are approximate and will themselves require extensive benchmarking to determine how accurate they are in general.

4.2. Case of H_2 on Cu(1 1 1)

The accuracy of methods that include vdW forces are often assessed based on how good the numbers are for a particular set of systems. Quantitative comparisons are a common ingredient in many recent publications in the field and there are often only small differences between the methods, with modern vdW-DF variants typically faring well. These comparisons are important, because accuracy is important, but that does not mean that these studies always provide insight into how well a method captures the physics of a problem. One can often learn more from specific case studies. This is illustrated by a comparison between modern calculated results on the interaction energy curve of H_2 on Cu(1 1 1) [89, 90] with the results of backscattering experiments detailed in section 2.1 and in figure 1. The comparison in figure 5 indicates a major shortcoming of typical pairwise atomistic corrections to DFT, namely their limited or complete inability to distinguish between bulk and surface electrons. It is important to note here that it does not suggest that such methods are inherently bad; however, it does suggest that they are not good starting points for developing general-purpose methods to handle all sorts of sparse and dense matter. As such, it serves to motivate our emphasis on nonlocal correlation functionals.

Figure 5 shows the comparison between calculated (DFT-D3 [49], TS-vdW [48], vdW-DF1, and vdW-DF2) and experimental results. vdW-DF2 gives interaction curves in good agreement with the experimental physisorption curve. vdW-DF1, exhibiting its expected overestimation of separation, is less accurate but is still in qualitative agreement with experiment. DFT-D3 on the other hand fails to predict a binding in reasonable agreement with experiment with a well depth four times deeper than experiment and significantly shorter separations. It should be noted that C_6 coefficients for every coordination number are not available for copper. However, using TS-vdW, which has built-in mechanisms to adjust the dispersion coefficients based on the density around the atoms does not resolve the issue.

H_2 on Cu(1 1 1) is a particularly difficult system, because the response of the tiny hydrogen molecule is so different from copper—a coinage metal where *d*-shell electrons also come into play. The good results of vdW-DF therefore present one of its major successes and are strongly tied to its ability to distinguish between different density regions—an ability that is very important. For many other cases, pair-potential based methods can produce numbers that are competitive with, and sometimes even better than, vdW-DF-based methods. This typically occurs for systems with a nature fairly similar to the datasets they were developed with. The failure of pair-potential based methods for the case of H_2 on Cu(1 1 1) however raises questions concerning the general transferability of such potentials, in particular to metallic systems. One can indeed question if the partitioning of vdW forces into contributions arising from specific atoms is justified for metallic systems.

4.3. Asymptotic functionals with damping functions

The ALL functional, presented in the previous chapter, has served as an important milestone on the path to vdW-DF. Others have further developed ALL along a different path, using the ALL functional to determine the dispersion coefficients for traditional DFT with force-field potentials. Some of these extensions start with an analysis of the range-separated contributions to the full xc energy [166, 167]. Sato and coworkers [168, 169] developed an approach that adds ALL to a long-range-corrected DFT [170] based on a formulation that merges GGA exchange with the Hartree–Fock description. At large separations, it includes both nonlocal exchange and correlation terms. This method has been applied to π-bonded aromatic complexes, as well as dipole–dipole and hydrogen-bonded systems [168, 169]. Gräfenstein and Cremer [6] combined GGA with an efficient evaluation of the ALL energy and force terms in a partitioning scheme. They found good agreement with coupled-cluster calculations for the benzene dimer [6].

The Silvestrelli approach is similar in nature, but evaluates the ALL term [171] for localized orbitals [20], specifically maximally localized Wannier functions [172, 173]. The idea is to describe ALL in terms of the partial electron densities of the occupied Wannier orbitals. Expanding the density in such orbitals $n = \sum_l |w_l|^2$ in each fragment, the ALL functional is used to determine asymptotic vdW interaction coefficients $C_{6,l,m}$ for every pair (l, m) that can be formed from two orbitals of different fragments. The total vdW interaction is evaluated by summing over all such pairs. An advantage of this approach is that a damping function exclusively affects contributions of inter-fragment (l, m) pairs which have overlapping densities. The approach is successful for a range of systems, including vdW solids, molecular dimers, and aromatic complexes [171, 174].

More recently, two extensions of this framework were designed [175, 176]. The first includes additional states in the Wannier representation [175] to improve orbital localization and symmetry which, for example, is relevant for describing the benzene ring. The second [176] corrects for the density overlaps that exist within fragments and replaces the ALL specification of the asymptotic vdW coefficients with the simpler London account [14]. The first step eliminates arbitrariness in the vdW description that can arise from symmetry breaking, for example in weakly bonded noble-gas dimers [175]. These extensions and adjustments of the original formulation by Silvestrelli [171] produce good agreements with the binding energies of coupled-cluster calculations for a range of organic complexes.

Finally, other approaches that rely on density dependent C_6 coefficients have also been developed and used to include vdW forces in DFT. The Tkatchenko–Scheffler method [48] mentioned earlier is a hybrid between this approach and traditional atomistic pair potentials. There are also the Vydrov–Van Voorhis [177] and the Becke–Johnson [178, 179] formulations. The Vydrov–Van Voorhis approach is a limiting case of the VV09 functional [64] (section 6.6) that is itself a fully nonlocal density functional related to the general geometry vdW-DF. The Becke–Johnson formulation, which also provides multipole corrections in terms of C_8 and C_{10} coefficients, describes the vdW interactions as an electrodynamical multipole coupling of nonisotropic exchange holes that are formed in the electron gas around the nucleus. Emphasizing the energy shifts arising with the hole coupling, the approach is linked with the RA picture [43] of vdW forces and thus related to the physical picture underpinning ALL.

5. Functionals for all distances: functional for layered systems

This chapter is devoted to our first all-space vdW functional. The first four chapters gave an introduction to (i) the nature of vdW interactions, (ii) their importance, (iii) their relevance for DFT, and (iv) early work that stimulated further development. Here, we present the early history of the vdW-DF method, with the first explicit general functionals vdW-DF (more recently termed vdW-DF0) in 2003 [29, 54–56, 58], vdW-DF1 (originally termed vdW-DF) in 2004 [59, 62], and vdW-DF2 in 2010 [63]. The vdW-DF method has the potential for developing successively improved functionals [107–109]. Their common roots allow us to present a joint introduction to these functionals. Following this introduction, we outline the derivation of vdW-DF0 and present examples of applications to illustrate its nature and its potential for future improvements.

vdW forces are often associated with asymptotic formulas and such formulas are used in many theoretical schemes. The singular behaviour that occurs at small separations has been dealt with by introducing saturation functions. However, vdW forces are important for all bonds and reactions as they originate from nonlocal correlations among electrons and are relevant in an extensive region of intermediate-sized separations. We seek to construct approximate vdW functionals with an account of sparse matter that seamlessly extend the local (LDA) and semilocal approximations (GGA) for exchange and correlation [19, 24, 27, 42, 180].

The adiabatic connection formula (ACF) [24, 41, 42] is the starting point for developing vdW-DF. The ACF provides an expression for the exchange-correlation energy $E_{\rm xc}$ in terms of a coupling-constant integration λ, as follows

$$E_{\rm xc} = -\int_0^1 {\rm d}\lambda \int_0^\infty \frac{{\rm d}u}{2\pi} {\rm Tr}\,\{\chi(\lambda, {\rm i}u)V\} - E_{\rm self}\ . \qquad (30)$$

Here, $\chi(\lambda, {\rm i}\,u)$ is the density response function or the reducible density–density correlation function in many-body theory, at a coupling strength λ with a density $n(\mathbf{r})$ set to that of the fully interacting system. $V(\mathbf{r} - \boldsymbol{r}') = 1/|\mathbf{r} - \boldsymbol{r}'|$, and $E_{\rm self}$ is the Coulomb energy of all electrons. The coupling-constant integration is computationally complex and calls for simplification and approximations.

In the vdW-DF method [54, 56–59, 61–63, 72, 107, 108], we work with the local field response function, or irreducible correlation function $\tilde{\chi}(\lambda, {\rm i}u)$, defined via a Dyson equation

$$\chi(\lambda, {\rm i}u) = \tilde{\chi}(\lambda, {\rm i}u) + \lambda\tilde{\chi}(\lambda, {\rm i}u)V\chi(\lambda, {\rm i}u)\ . \qquad (31)$$

This function provides a full description of screening in the electron gas at any given coupling constant λ. The leading order approximation for $\chi(\lambda, {\rm i}u)$, i.e. the RPA, sets $\tilde{\chi}(\lambda, {\rm i}u) = \tilde{\chi}(0, {\rm i}u)$. Since λ then acts just as a prefactor of V in the coupling-constant integration, it can be performed analytically. Higher-order correlation diagrams with internal Coulomb interactions, each proportional to λ, may have intricate λ-dependences in the irreducible correlation function $\tilde{\chi}(\lambda, {\rm i}u)$ that prohibit analytical solutions and complicate numerical ones.

Progress in the development of vdW-DF was made [54] by assuming that the coupling dependence of $\tilde{\chi}$ can be neglected when performing the λ integration (30), even beyond the RPA. Since the leading term in λ is made explicit, we approximate $\tilde{\chi}({\rm i}u)$ by a value at a characteristic coupling constant $0 < \lambda_c < 1$ and complete the integral to obtain

$$E_{\rm xc} = \int_0^\infty \frac{{\rm d}u}{2\pi} {\rm Tr}\{\ln[1 - \tilde{\chi}({\rm i}u)V]\} - E_{\rm self}\ . \qquad (32)$$

The PhD thesis of Rydberg [56, 57] mentions 'RPA-like approximations', noting that approximations beyond the RPA can also allow for an approximate evaluation of the coupling-constant integration (30). This can for instance be achieved by using a dielectric function, where the λ-dependence is absorbed into the plasmon dispersion [57].

The layered vdW-DF in its early formulation [54] and subsequent realizations [29, 55, 56, 58, 61] are based on the so-called full-potential approximation (FPA), as detailed in a later publication [61]. In this section, we further discuss the FPA together with the layered-geometry vdW-DF version. This approximation involves replacing $\tilde{\chi}_\lambda$ by $\tilde{\chi}_{\lambda=1}$, leading to equation (32). In the vdW-DF design, a model dielectric function ϵ specifying $\tilde{\chi}$ should not include nonlocal correlations [56, 57, 59, 62, 72, 109]. Reference [61] discusses spectator excitations [43] in $\tilde{\chi}(\lambda, \mathrm{i}u)$ and notes that if spectator contributions in $\tilde{\chi}_{\lambda=1}$ are discarded in the FPA, one obtains the exact vdW asymptote.

The vdW-DF method differs from RPA-based methods, which specify the response functions $\tilde{\chi}$ in terms of the single-particle orbitals without taking many-body effects into account. The vdW-DF method instead relies on a scalar model dielectric function. The continuity equation relates this model dielectric function to $\tilde{\chi}$ [54, 56, 59, 61, 62], as follows

$$\tilde{\chi} = \nabla\alpha \cdot \nabla \,, \tag{33}$$

where the scalar susceptibility α satisfies $\epsilon = 1 + 4\pi\,\alpha$. In terms of the scalar dielectric function ϵ, the formal result (32) can be written as

$$E_{\mathrm{xc}} = \int_0^\infty \frac{\mathrm{d}u}{2\pi}\,\mathrm{Tr}\left\{\ln\left(\nabla\epsilon\cdot\nabla G\right)\right\} - E_{\mathrm{self}} \,, \tag{34}$$

where $G = -V/4\pi$ denotes the Coulomb Green function. The model dielectric function ϵ is chosen to make $\tilde{\chi}$ reflect essential features of an LDA and GGA description.

For the homogeneous electron gas (HEG), equation (32) reduces to the following expression

$$E_{\mathrm{xc}}^{\mathrm{HEG}} = \int_0^\infty \frac{\mathrm{d}u}{2\pi}\,\mathrm{Tr}\{\ln[\epsilon^{\mathrm{HEG}}(\mathrm{i}u)]\} - E_{\mathrm{self}} \,, \tag{35}$$

where $\epsilon^{\mathrm{HEG}}(\mathrm{i}u)$ denotes the dielectric function of the homogeneous system. This result will be helpful when we remove short-ranged correlation effects from the full functional.

The expression for E_{xc} in the vdW-DF framework (34) can in principle be formulated as an exact relation [57, 109]. The local field response functional $\tilde{\chi}$ is then viewed as arising at a characteristic coupling-constant value $0 < \lambda_{\mathrm{char}} < 1$. The argument is that for every E_{xc} one can find a scalar dielectric function that satisfies equation (34) [56]. Such a scalar dielectric function can formally be expressed [109] in terms of

$$-\chi(\mathrm{i}u)V = 1 - \exp\left[\int_0^1 \mathrm{d}\lambda\,\chi(\lambda, \mathrm{i}u)V\right], \tag{36}$$

which provides a mean-value specification of $\chi(\mathrm{i}u)$. In principle, this expression can be used to determine the characteristic $\tilde{\chi}(\mathrm{i}u)$ of equation (32). The different vdW-DF versions thus rest on a common formally exact framework [57, 109]. The various versions differ in which approximations are made.

5.1. Development of the layered-geometry van der Waals density functional

Planar-geometry problems can be viewed as quasi-one-dimensional. Treating them as such was helpful in the formulation of the vdW-DF for layered geometries. Though its general applicability is limited, this functional is useful for key model systems such as jellium slabs and some real materials such as vdW bonded layered systems.

The first formulation of the layered vdW-DF was proposed by Rydberg, Dion, Langreth, and Lundqvist for strictly planar systems [54]. Results for the interaction between two parallel jellium slabs agree well with those of an earlier more elaborate calculation [181]. The correlation-interaction energy was found to saturate significantly with shorter separations. The study concludes: 'generalizations to three-dimensional systems are possible and (…) there should be a basis for applications to numerous physical, chemical, and biological systems, (…) such as crystals, liquids, adhesion, soft condensed matter, and scanning-force microscopy'.

The layered-geometry vdW-DF [29, 55, 58] of Rydberg, Dion, Jacobson, Schröder, Hyldgaard, Simak, Langreth, and Lundqvist can be applied to real layered systems, such as graphite, boron nitride, and molybdenum disulphide, with the breakthrough of a first predicted vdW-bond energy value of an extended system, a graphene bilayer, in 2001 [55]. In this functional, the exchange-correlation energy functional

$$E_{\mathrm{xc}}^{\mathrm{vdW-DF}}[n] = E_{\mathrm{xc}}^{0}[n] + E_{c}^{\mathrm{nl}}[n] \,, \tag{37}$$

is split into a semilocal functional part $E_{\mathrm{xc}}^{0}[n]$ and a nonlocal part $E_{c}^{\mathrm{nl}}[n]$. This splitting is retained in later versions of the functional. The full electron-density variation, including the in-sheet variations, is retained in E_{xc}^{0}, while the evaluation of the smaller nonlocal correlation E_{c}^{nl} is based on a planar average of the density. The assumption is that the vdW forces are less sensitive to the microscopic details than other terms of the DFT evaluation. As a convenient shorthand, we will denote this layered-geometry vdW-DF as vdW-DF0 in the following.

vdW-DF0 is valid at all separations. The semilocal functional E_{xc}^{0} is specified as the sum of local correlation [180] and gradient-corrected exchange given within GGA using the Zhang and Yang reparametrization [182] of PBE [27] (revPBE). This functional is chosen because it was considered to give interaction energies in close agreement with exact Hartree–Fock exchange at separations relevant for vdW bond lengths and did not exhibit appreciable binding in vdW systems [61].

A central ingredient in vdW-DF0 is a simple plasmon-pole description of the sheet response. The evaluation of the nonlocal correlation term is adapted from [54], and the laterally-averaged density $n(z)$ is used to define a characteristic $\tilde{\chi}$. The response description is in turn given by a model dielectric function based on a plasmon-pole form,

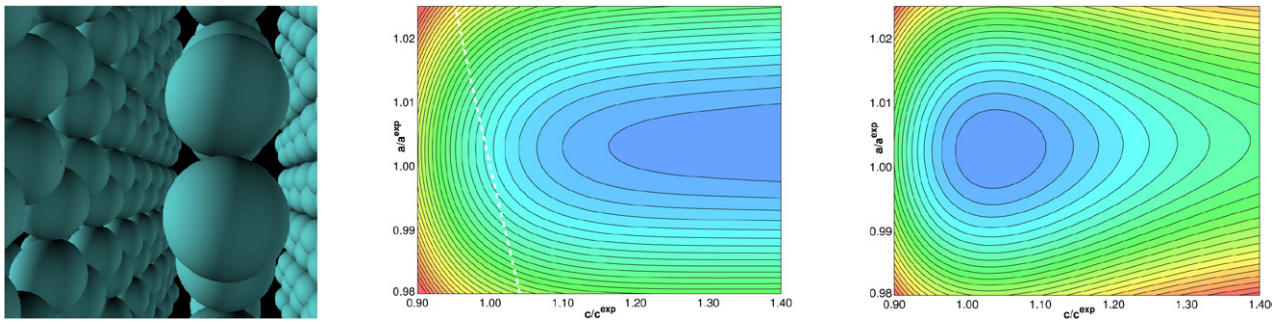

Figure 6. The role of vdW forces in graphite. The left panel shows the atomic configuration which comprises densely packed graphene sheets with large inter-sheet separations, $c_{\rm exp} \approx 3.35$ Å. A low electron density characterizes the inter-sheet regions. The nonlocal correlation acts across these regions, providing material cohesion. The middle and right panels contrast the variation of the interlayer interaction energy for our GGA (PW91 [183]) and layered-geometry vdW-DF0 [58] studies, here plotted as functions of both inplane lattice constant a and interlayer separation c, relative to the experimental values ($a^{\rm exp}$, $c^{\rm exp}$). The dashed curve in the middle panel identifies (a, c) values that are consistent with the experimentally observed unit-cell volume of graphene. The colour scale for the potential energy plots ranges from 0 (light green) to −5 eV (dark blue). Reprinted with permission from [29], © 2003 Elsevier.

$$\epsilon_k(z, \mathrm{i}u) = 1 + \frac{\omega_{\rm p}{}^2(z)}{u^2 + (m v_{\rm F}(z) q_k)^2/3 + q_k^4/4} \ . \qquad (38)$$

Here $\omega_{\rm p}{}^2(z) = 4\pi\, n(z)/m$ and $m v_{\rm F}(z) = [3\pi^2\, n(z)]^{1/3}$. The plasmon dispersion is $q_k^2 = k^2 + q_\perp^2$, where $\boldsymbol{k}$ is the in-plane wavevector. In this model, the $q_\perp^2$ value has a special purpose, as it is designed to reflect the local-field susceptibility α corresponding to the dielectric function. It is set by matching the static polarizability to that of an individual sheet as obtained in a regular DFT calculation with an external field. Since the $q_\perp^2$ reflects the full density variation, it mitigates the error of computing vdW forces from a laterally averaged density.

The dielectric function is local in the z-direction but includes in-plane dispersion. The definition (38) thus extends the form $\epsilon = \epsilon^{\rm HEG}$ used to define a plasmon propagator $S \equiv 1 - \epsilon^{-1}$, as used in early determinations of LDA correlation [22, 24, 134]. The plasmon-pole form of ϵ (38) is inspired by the models of Lindhard and Bohr [37, 38]. The construction for layered-geometry vdW-DF0 calculations can be seen as an approximation to treating $\tilde{\chi}$ in the FPA limit as $q_\perp^2$ is evaluated at the full coupling strength.

To obtain an explicit expression for the nonlocal term $E_c^{\rm nl}$ [54, 58], we need to remove the semilocal part of equation (34). The HEG result (35) suggests the following expression

$$E_{\rm xc}^0 = {\rm Re} \int_0^\infty \frac{{\rm d}u}{2\pi} {\rm Tr}\left\{\ln(\epsilon)\right\} - E_{\rm self} \ . \qquad (39)$$

In effect, we obtain an expression for the nonlocal correlation

$$E_c^{\rm nl} \equiv \int_0^\infty \frac{{\rm d}u}{2\pi} {\rm Tr}\left[\ln(\,\nabla\epsilon \cdot \nabla G\,) - \ln\epsilon\right] \ . \qquad (40)$$

The evaluation of $E_c^{\rm nl}$ proceeds by viewing equation (40) as a one-dimensional electrodynamical problem [29, 54, 56, 61]. One solves a Poisson equation

$$\frac{\rm d}{{\rm d}z}\left(\epsilon_k \frac{\rm d}{{\rm d}z}\phi_k\right) - k^2 \epsilon_k \phi_k = 0 \qquad (41)$$

to obtain the solution $\phi_k(z, \mathrm{i}u)$, given that a charged sheet is introduced at $z = 0$. One also determines the solution $\phi_{k,0}(z, \mathrm{i}u)$ for empty space, i.e. with $\epsilon = 1$. Finally, one extracts the nonlocal correlation energy per area A [54, 61]

$$E_c^{\rm nl}/A = -\lim_{L\to\infty} \int_0^\infty \frac{{\rm d}u}{2\pi} \int \frac{{\rm d}^2k}{(2\pi)^2} \ln\left(\frac{\phi_k{}'(L)}{\phi'_{k,0}(L)}\right) \ . \qquad (42)$$

A valuable feature of vdW-DF0 is that it treats the screening exactly by solving the Poisson equation. The idea of mapping the $E_c^{\rm nl}$ evaluation onto an electrodynamics problem [54, 56] could be more widely applied. One might conceive calculating the nonlocal correlation in a similar manner for other systems with high symmetry, for example, filled and hollow spheres and cylinders.

5.2. Applications of the layered functional

The major features of the vdW bond in a prototype DFT application can be illustrated with graphite. Figure 6 shows the atomic configuration with dense and sparse regions (left), binding-energy contours [29] obtained with traditional DFT in the GGA (middle), and with the layered-geometry vdW-DF0 (right) as functions of both the inplane (intra-sheet) lattice constant a and inter-sheet separation c divided by their experimental reference values ($a_{\rm exp}$, $c_{\rm exp}$). The dashed curve in the middle panel identifies (a, c) values that are consistent with the experimentally observed unit-cell volume $V_{\rm Gr}^{\rm exp}$.

In the GGA description, interlayer binding is absent except at an unphysically large separation and with minuscule binding energy, a few meV per graphene atom. An early GGA study of graphite structure found a relevant value of c only because it constrained the search to the curve specified by $V_{\rm Gr}^{\rm exp}$ [29]. The vdW-DF0 results reflect a solution to a long-standing challenge in traditional DFT: the state-of-the-art DFT, which was GGA at the time, should not rule out the existence of the most stable carbon allotrope, i.e. graphite.

With the development of the layered-geometry vdW functional, vdW-DF0, in 2001 [29, 55], we could announce 'a binding-energy value of 10.3 meV Å^{-2}' [55], which corresponds to 43 meV per atom [29] in good agreement with the experimental reference at the time of 34 meV/atom [184]. In contrast, LDA calculations yielded 20 meV [185–189] and

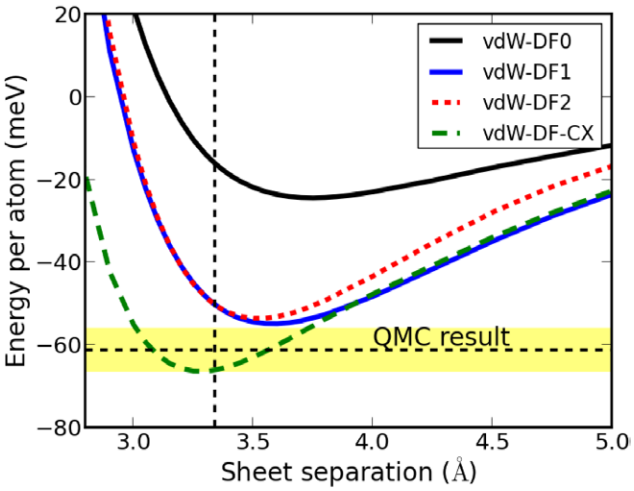

Figure 7. Comparison between the results for the interlayer binding energy of graphite obtained with the layered-geometry vdW-DF [29], later general-geometry vdW-DF functionals, and a quantum Monte Carlo (QMC) [190, 191] calculation. Here, the covalent bond length in the layer is fixed to the experimental value. The dashed vertical line indicates the experimental reference for the sheet separation. The dashed horizontal line indicates the results of QMC, with error bars indicated by the yellow region.

GGA calculations barely gave binding. The simple fact that vdW-DF had a number, a correct sign, and a reasonable magnitude spurred much enthusiasm among the developers in the field and this optimism was communicated by the title of the report 'Hard numbers for soft matter' [29]. The early vdW-DF0 applications indeed signalled the start of an era of tremendous activity by us and others.

Early applications of vdW-DF0 include the binding between two graphene sheets [29, 55, 58] and the interlayer binding in graphite, boron nitride, and molybdium disulphide, MoS_2 [29, 61]. The results were judged promising for the vdW-DF method [29]. Overall, the performance was encouraging for binding distances, binding separations, and elastic response, considering its nonempirical basis and the approximations made.

The first applications of vdW-DF0 for real materials relied on the PW91 functional to describe semilocal exchange effects, which later was replaced with revPBE to avoid spurious binding. This substitution results in smaller binding energies and larger interlayer separation distances and therefore generally reduces the agreement with experiments. The choice was nevertheless important to firmly establish the role of vdW forces in layered materials.

Figure 7 compares results of vdW-DF0 and later versions of the vdW-DF for general geometries for graphite. As a modern reference for the cohesion energy, we use QMC results [191]. Thus, we avoid experimental uncertainties and contributions from zero-point and thermal motion that are not a part of standard DFT in the Born–Oppenheimer approximation. The figure shows a successive improvement in cohesion energy and separation with the biggest step being taken when going from vdW-DF0 to vdW-DF1. The shallow binding of vdW-DF0 and the overestimation in separation can partly be attributed to the choice of exchange, as revPBE is quite repulsive in this region.

The comparison of results from different functionals in figure 7 indicates that the plasmon model of vdW-DF1 and vdW-DF2, described in section 6, is more suited for describing nonlocal correlations than that of vdW-DF0. An advantage of vdW-DF0 is its exact handling of screening, although subject to the limitations imposed by its more limited description of local-field effects.

In addition to the early progress for the layered vdW system, the vdW-DF0 has also been adapted to provide an early DFT account of polyaromatic hydrocarbons (PAHs) dimers in selected geometries [84, 192, 193]. The adaptation rests on defining an effective area per PAH molecule [193]. This step can be viewed as an analogy to deducing estimates of the graphite interlayer binding energy from the measured binding energy of increasingly larger PAH dimers [194]. This effective-area approach gives at least a qualitative account of vdW binding between PAH molecules [192, 193].

vdW-DF0 fairly well describes the cohesion in layered systems like graphite and other layered materials such as boron nitride and molybdenum disulphide. This is in spite of the fact that the nonlocal correlation term in vdW-DF0 is based on a laterally averaged density with an emphasis on a FPA representation of the local-field response $\tilde{\chi}$. Perhaps the most important aspect of the vdW-DF0 development was the strong encouragement it provided for further developments.

6. General-geometry vdW-DF

6.1. Design of general-geometry vdW-DF versions

A general-geometry vdW-DF should obey general physical laws, be physically transparent, transferable, and simple enough to allow efficient computations. Previous studies in the late 20th century taught us that (i) nonlocal correlations among the electrons are essential for describing sparse matter; (ii) vdW forces emanate from dynamic electron correlations; (iii) vdW forces relate to the static electron density $n(\boldsymbol{r})$ via, for instance, the classical plasma frequency $\omega_p = \sqrt{4\pi ne^2/m}$; and (iv) the asymptotic vdW potentials can at large separations be derived from the small wavevector ($q \to 0$) limit of the plasmon dispersion ω_q and give a reasonable magnitude and correct form for the interaction between atoms and molecules [44, 69], between neutral molecules and insulating surfaces [52], as well as between surfaces [70]. This experience was incorporated into the layered-geometry functional, vdW-DF0 [29, 54–56, 58], as was the value of a plasmon-pole description for the electron-gas dielectric function [134, 195].

The vision for a new nonlocal functional for general geometries was, and still is, that it should be a general-purpose one; able to describe all kinds of materials and molecular systems from the dense to the sparse [56, 72, 107–109]. This philosophy emphasizes binding separations in favour of the asymptote. While the asymptotic behaviour is determined by long wavelength, i.e. $q \to 0$, excitations in the polarizable medium, nonlocal correlations at shorter separations arise from many different electron–hole pair

excitations and plasmon modes. To describe vdW forces at typical binding separations, a plasmon model that covers the overall effect of many different q values is needed. To this aim, the GGA can be used as a guide, as this approximation provides an excellent account of interactions within dense matter. The plasmon model should adhere to known constraints for the electron gas [30, 57, 59, 62, 63, 107–109]. The functional should also connect seamlessly between the description at vdW binding separations and the regime of covalent bonds.

The preferred procedure used to derive the explicit vdW-DF has varied with time. In this chapter we outline a procedure, similar to the one appearing in Rydberg's thesis [57], which has been successively refined and complemented [59, 61, 62, 109]. This procedure is based on a mean-value evaluation of the integral of the dimensionless coupling constant λ, as detailed in section 5. This starting point is exact and is thus more natural for deriving the explicit functionals [57, 109] than relying on the FPA outlined in the seminal paper by Dion and coworkers [59].

To design a general geometry functional, an essential step is to define an expansion parameter for the coupling-constant averaged expression in (34) and for the nonlocal correlation (40). In this step, we use the propagator concept of many-body theory, building on simple forms like $1/(\omega - \omega_q)$. For the functional development from (40), a suitable choice is $S_{\rm xc}(iu) \equiv \ln(\epsilon(iu))$, which can be seen as an auxiliary, spatially nonlocal, polarization function [57]. This dielectric function is formally defined in terms of the coupling-constant integration of the density response function as discussed in section 5. To better understand the connection to the MA, RA, and ALL pictures of vdW interactions and nonlocal correlations [43, 44, 136] (discussed in section 3), we may instead consider $S(iu) \equiv 1 - \epsilon(iu)^{-1}$, that is $S_{\rm xc}$ to lowest order in S. Its connection to the propagator form is easily seen in the case where $\epsilon(\omega) = 1 - {\omega_{\rm p}}^2/\omega^2$.

In practice, an ansatz is made for $S_{\rm xc}$ in terms of a single-pole plasmon description that is constrained by physical laws, including charge conservation, cancellation of self-correlation, and time-reversal symmetry. The plasmons that give rise to the nonlocal correlation in vdW-DF, described in terms of the poles of the polarization function $S_{\rm xc}(iu)$, are parametrized by connecting the dielectric function to the so-called internal functional [57, 59, 63],

$$E_{\rm xc}^{\rm int} = \int_0^\infty \frac{{\rm d}u}{2\pi} {\rm Tr}\{S_{\rm xc}\} - E_{\rm self} \ , \qquad (43)$$

which describes short-range exchange and correlation effects and can be described through a semilocal exchange-correlation functional. The polarization function $S_{\rm xc}(iu)$ bears strong resemblance to the coupling-constant averaged density response function defined in (30) and is equivalent in the homogeneous electron gas limit (35). It is closely related to the plasmon propagator that describes the collective response of the electron gas. By neglecting the longitudinal projection in (34) the polarization function becomes short ranged and no effects associated with long-range vdW forces are included within this quantity. It can thus be viewed as a short-range external field response function.

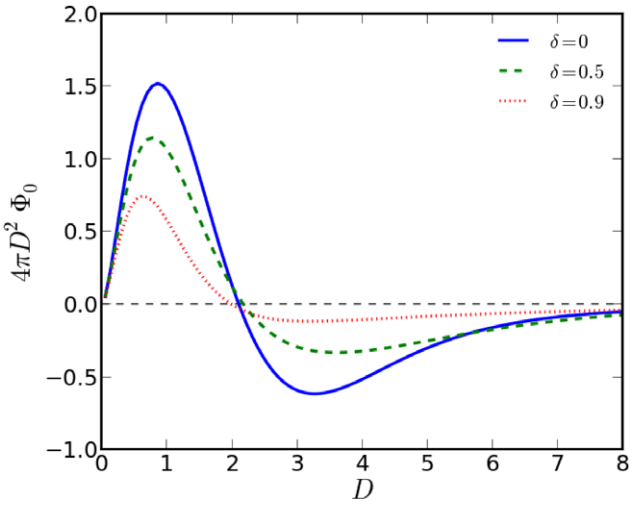

Figure 8. The kernel (in a.u.) as a function of the dimensionless separation D for three values of the asymmetry parameter δ. Figure similar to that appearing in the erratum [60].

The advantages of the nonempirical general-geometry functionals, vdW-DF1, vdW-DF2, and vdW-DF-cx include an increasingly improved consistency between the semilocal functional $E_{\rm xc}^0$ that describes the energetic contributions to the total energy arising from short-range exchange and correlation effects, and the internal functional parametrizing the plasmons [59, 62, 63]. Such consistency is related to charge conservation of the exchange-correlation hole, and improving this aspect of vdW-DF has been one driving force for successive refinements of the functional [107, 108].

6.2. Outline of derivation and approximations made

The first presentation of the general-geometry vdW-DF concept [57] was a manuscript in Rydberg's PhD thesis [56]. It contained several of the key steps required to obtain the general-geometry vdW-DF, a framework for formal improvements, and an implementation that enabled efficient computations of the nonlocal correlation energy in terms of a six-dimensional integral,

$$E_c^{\rm nl} = \frac{1}{2}\int {\rm d}^3r\ {\rm d}^3r'\ n(\mathbf{r})\ \Phi_0(\mathbf{r},\mathbf{r}')\ n(\mathbf{r}') \ . \qquad (44)$$

The formal results meant great progress, and together with [61] and [72], which include time invariance, they form the basis for the final vdW-DF1 paper [59, 60]. Just like with the layered functional, the full xc functional in vdW-DF1 is given by the sum of a semilocal part $E_{\rm xc}^0$ and the nonlocal correlation (37).

The kernel (44) describing the nonlocal correlation is shown in figure 8, expressed in terms of the dimensionless parameters D and δ. The parameter D can be viewed as an effective scaled separation between two density regions, while δ describes how different the response of these two density regions are. It is interesting that the kernel in its universal form keeps its shape in successively improved approximations.

Thus, how D and δ are scaled determines the nonlocal correlation energy, for instance, when going from vdW-DF1 to vdW-DF2.

The nonlocal correlation energy functional $E_c^{\rm nl}$ (44) is only one part of the xc-energy functional. There are also the local correlation and the semilocal exchange. A glance at vdW-DF-type functionals proposed by us [59, 63, 106, 107] and others [196–198] shows that improvements beyond vdW-DF1 have been primarily concerned with the exchange part E_x, which so far has been treated in GGA.

The original vdW-DF1 paper [59] targeted the vdW bond, which motivated using the revPBE exchange functional. When vdW-DF1 is used for other bonds, such as mixes of vdW with covalent, ionic, *d*-electrons, and hydrogen bonds, this can give results close to the mark, such as for covalent bond lengths in carbon systems [73]; in other cases, the results are further away, such as for bond lengths within coinage metals [30, 197]. Some have expressed disappointment, perhaps unfairly, considering that the vdW bond was the target. However, the overall goal of the vdW-DF is to describe general matter, and with successive refinements, as discussed in section 6.5, it is approaching that goal.

Assessing vdW methods by benchmarking against accurate quantum chemistry results for a particular set of systems is common but not enough. For instance, results for a set of molecular dimers exhibiting vdW and hydrogen bonds might not be helpful for studies of transition metals with *d*-shell electrons. This example emphasizes the value of both a broader benchmarking, including comparisons with extensive experimental data sets [89], and of designing functionals based on general criteria, such as those given by fundamental physical laws. An important example is the law of charge conservation, which is essential in many-body theory [199] and DFT. A central concept is the xc hole: the depletion of the mean density surrounding a given electron. A special case which is easy to envision is the charge depletion left behind by an electron leaving a metal surface. The failure of the gradient expansions in the density functional proposed in the original Kohn–Sham formulation of DFT [18, 19], which is inferior to the LDA, can be blamed on the violation of the charge sum rule [142]; that is, its xc hole does not integrate to unity [24]. Likewise, the success of LDA for the hydrogen atom, with its far from homogeneous electron distribution [24], is credited to compliance with the charge sum rule. In the design of general-geometry vdW-DFs, charge conservation is important. In the early work, results for the almost homogeneous electron gas were carefully selected from many-body theories honouring conserving approximations.

The derivation outlined here is close to that of the original one [57], but updated by the insights that led to the final vdW-DF1 version [59], as well as recent analysis [109]. Details for the more familiar derivation relying on the FPA-based approach [59], which uses $S = 1 - 1/\epsilon$ as an expansion parameter, can be found elsewhere [72, 200]. Since the exact expression for $S_{\rm xc}$ is not known (43), an ansatz is made in the planewave representation $S_{\rm xc}(\boldsymbol{q}, \boldsymbol{q}')$ based on four constraints: time-reversal symmetry; the *f*-sum rule, which is linked to current conservation [201]; cancellation of the self-energy; and charge conservation.

Time-reversal symmetry is built into the construction by defining $S_{\rm xc}$ as a symmetric function of a related quantity $\widetilde{S}$, as follows

$$S_{\rm xc}(\mathbf{q}, \mathbf{q}') = \frac{1}{2}[\widetilde{S}(\mathbf{q}, \mathbf{q}') + \widetilde{S}(-\mathbf{q}', -\mathbf{q})] \,. \tag{45}$$

The second constraint, the *f*-sum rule, implies that in the high-frequency ω limit, $S_{\rm xc} \to -4\pi/(m\,\omega^2) n\,(\boldsymbol{q} - \boldsymbol{q}')$ [59]. With the following form of $\widetilde{S}$, this constraint is ensured,

$$\widetilde{S}(\mathbf{q}, \mathbf{q}') = \int \mathrm{d}^3 r \mathrm{e}^{-\mathrm{i}(\mathbf{q}-\mathbf{q}')\cdot\mathbf{r}} \frac{\omega_{\rm p}^2(n(\mathbf{r}))}{[\omega + \omega_{\mathbf{q}}(\mathbf{r})][-\omega + \omega_{\mathbf{q}'}(\mathbf{r})]} \,. \tag{46}$$

Here, the classical plasmon frequency in the numerator can be viewed as an amplitude in a spectral function with poles at $-\omega_{\boldsymbol{q}}(\mathbf{r})$ and $\omega_{\boldsymbol{q}'}(\mathbf{r})$. The high-frequency limit of $S_{\rm xc}$ corresponds to the dielectric function taking on its familiar high frequency limit, $\epsilon(\omega) = 1 - \omega_{\rm p}^2/\omega^2$.

The third constraint is that the divergence in the self-energy term (43) must cancel out. This constraint requires that the dispersion ω_q crosses over to a free-electron behaviour $\omega_q \to q^2/2$ in the large q limit—a natural limit, as it reflects that fast moving electrons have no time to interact with each other. To see how this cancellation occurs, we use the specific form of $S_{\rm xc}$ to write equation (43) in the form

$$E_{\rm xc}^{\rm int} = \int \mathrm{d}^3 r \; n(\mathbf{r})\, \epsilon_{\rm xc}^{\rm int}(\mathbf{r}) \,, \tag{47}$$

with

$$\epsilon_{\rm xc}^{\rm int}(\mathbf{r}) = \int \mathrm{d}^3 q \; \epsilon_{\rm xc}^{\rm int}(\mathbf{r}, \mathbf{q}) = \pi \int \mathrm{d}^3 q \left(\frac{1}{\omega_q(\mathbf{r})} - \frac{2}{q^2} \right) , \tag{48}$$

which makes the cancellation evident. The term $\epsilon_{\rm xc}^{\rm int}(\mathbf{r})$ is identified as the xc energy density of the internal functional. This expression also provides a wavevector decomposition [42] of the internal functional for a given plasmon dispersion $\omega_{\boldsymbol{q}}$.

The fourth constraint is charge conservation. The polarization function $S_{\rm xc}$ remains bounded in the upper right quadrant of the complex-frequency plane. As a result of the longitudinal projection of ϵ, the coupling-constant averaged response function is given by $\chi = \nabla\epsilon \cdot \nabla G$. This property ensures that the expression for the full xc energy (34) is charge conserving [59, 107, 109]. The corresponding xc hole integrates to unity [108, 109]. The intricacies of the charge conservation in vdW-DF is discussed further after the full functional has been laid out.

The specific form chosen for the plasmon frequency ω_q should be simple yet capture the overall plasmon response. The following form was chosen

$$\omega_q(\mathbf{r}) = \frac{q^2}{2} \frac{1}{h(q\,/\,q_0)} \,, \tag{49}$$

with $h(y) = 1 - \exp(-\gamma\, y^2)$ and $\gamma = 4\pi/9$. The $q_0(\mathbf{r})$ parameter sets an inverse length scale and determines the plasmon dispersion in a spatial region. With the added benefit of being

simple, this form cancels out the divergence in the self-energy term and ensures a finite plasmon frequency in the $q \to 0$ limit.

The plasmon dispersion should reflect the overall response in a spatial region. This property is established by identifying the internal functional with a specific semilocal xc functional, which determines a specific value of $q_0(\mathbf{r})$ at each $\mathbf{r}$. For this step, it is helpful that the xc-energy density of the internal functional (48) can be evaluated analytically. The result,

$$\varepsilon_{\rm xc}^{\rm int}(\mathbf{r}) = -\frac{3}{4\pi} q_0(\mathbf{r}) \,, \tag{50}$$

resembles the exchange energy density of LDA: $\varepsilon_x^{\rm LDA}(n) = -(3/4\pi)\, k_{\rm F}(n)$. In fact, the homogeneous electron gas expression (35) given in the previous chapter indicates that in the homogeneous limit, it is natural to set the internal functional equal to the xc energy of the LDA. Thus, we can identify $q_0^{\rm HEG}(n) = k_{\rm F}(n)\, \varepsilon_{\rm xc}^{\rm LDA}(n)/\, \varepsilon_x^{\rm LDA}(n)$.

In extending the procedure for setting the inverse length scale $q_0(\mathbf{r})$ to inhomogeneous systems, two specific choices are made in vdW-DF1. First, the internal functional is identified as a semilocal functional that combines local correlation effects in an LDA description with GGA level exchange effects. This results in [59]

$$q_0(\mathbf{r}) \;= k_{\rm F}(\mathbf{r}) \frac{\varepsilon_x^{\rm LDA}(\mathbf{r}) F_x^{\rm int}(s) + \varepsilon_c^{\rm LDA}(\mathbf{r})}{\varepsilon_x^{\rm LDA}(\mathbf{r})} \,. \tag{51}$$

Here, $F_x^{\rm int}(s)$ is the exchange enhancement factor and depends on the reduced gradient $s(\mathbf{r}) = |\nabla\, n|/(2k_{\rm F}(\mathbf{r}) n\,(\mathbf{r}))$. Second, the Langreth–Vosko [202] form is used for the exchange enhancement factor $F_x^{\rm int}$. This enhancement form is a simple quadratic function of s [59, 137], i.e.

$$F_x^{\rm int}(s) = 1 - \left(\frac{Z_{ab}}{9}\right) s^2 \,. \tag{52}$$

Here, $Z_{ab} = -0.8491$. We postpone a discussion of why these choices were made until after we have laid out some more details of the derivation.

The close resemblance between q_0 and $k_{\rm F}$ is a consequence of a carefully chosen value for γ. This does not make γ an adjustable parameter, rather it is an arbitrary parameter in the true sense of the word. A different value of γ would result in a different scaling of q_0, but the plasmon dispersion (49) and thus the nonlocal correlation would end up the same.

Now that an ansatz for the expansion parameter $S_{\rm xc}$ has been specified, we turn to expanding the expression for the xc energy (34). Since $S_{\rm xc}$ can be formally represented by a matrix, we can use the relation $\epsilon = \exp[S_{\rm xc}]$ in the expansion of (34). The first order term is the internal functional (43). Since (43) is intended to include all xc effects except the nonlocal correlations, the second order expression is identified as the vdW-DF approximation for the nonlocal correlation,

$$E_c^{\rm nl} = \int_0^\infty \frac{{\rm d}u}{4\pi} {\rm Tr}\{S_{\rm xc}^2 - (\nabla S_{\rm xc} \cdot \nabla G)^2\} \,. \tag{53}$$

To obtain this result, one can use partial integration and $\nabla^2 G = 1$. In a planewave representation the nonlocal correlation can be written as

$$E_c^{\rm nl} = \int_0^\infty \frac{{\rm d}u}{4\pi} \int \frac{{\rm d}^3q\, {\rm d}^3q'}{(2\pi)^3 (2\pi)^3} \\ [1 - (\hat{\mathbf{q}} \cdot \hat{\mathbf{q}}')^2] S_{\rm xc}(\mathbf{q}, \mathbf{q}') S_{\rm xc}(\mathbf{q}', \mathbf{q}) \,. \tag{54}$$

By design, this expression vanishes in the homogeneous limit. Once $S_{\rm xc}$ becomes diagonal, only terms with $\boldsymbol{q}' = \boldsymbol{q}$ contribute, for which the term within the bracket vanishes. The expansion (54) implies that the popular vdW-DF versions, unlike RPA and unlike the vdW-DF framework [109], cannot account for many-body dispersion effects [51, 149, 190, 203, 204] at every length scale. The many-body dispersion effects often involve the screening impact on the lower-energy plasmons and are primarily relevant in the asymptotic-interaction regime [109, 190, 205]; however, at binding separations there are many plasmons that contribute to the nonlocal-correlation attraction [30]. As such, building upon the underlying account of the GGA response, the popular (expanded) vdW-DF versions do indeed reflect many-body dispersion effects at binding separations [109].

The nonlocal correlation in the familiar form (44), with two spatial integrals over a kernel $\Phi_0(\mathbf{r}, \mathbf{r}')$ that connects two density regions $n(\mathbf{r})$ and $n(\mathbf{r}')$, is obtained after integrating over the imaginary frequency and both planewave coordinates $\boldsymbol{q}$ and $\boldsymbol{q}'$. Of these integrals the one over u and the angular parts of $\boldsymbol{q}$ and $\boldsymbol{q}'$ can be performed analytically. This leaves us with two one-dimensional integrals over q and q', which are performed numerically. The resulting kernel can be tabulated once and for all in terms of $d = q_0(\mathbf{r})\, |\mathbf{r} - \mathbf{r}'|$ and $d' = q_0(\mathbf{r}')\, |\mathbf{r} - \mathbf{r}'|$ or related quantities such as $D = (d + d')/2$ and $\delta = (d - d')/2D$. The two spatial integrals that remain come from $S_{\rm xc}$ (46). That the kernel depends on merely two dimensionless parameters follows from the judiciously chosen ansatz for $S_{\rm xc}$ and the fact that only a single function sets the effective inverse length scale $q_0(\mathbf{r})$ that describes the plasmon dispersion.

To discuss choices in the design of vdW-DF1 and its properties, it is convenient to express the xc functional of vdW-DF as

$$E_{\rm xc}^{\rm vdW-DF}[n] = E_{\rm xc}^0[n] + E_c^{\rm nl}[n] \,, \tag{55}$$

that is, with explicit nonlocal correlation and a term with local correlation and exchange $E_{\rm xc}^0$.

In vdW-DF1, the $E_{\rm xc}^0$ is given by the sum of LDA correlation and the revPBE [182] variant of GGA exchange. Conceivably, one could consider including semilocal correlation terms within $E_{\rm xc}^0$; however, the nonlocal correlation term also has significant semilocal contributions [57] and double counting is undesirable. A strict derivation in terms of the $S_{\rm xc}$ expansion starting from equation (34) implies that $E_{\rm xc}^0[n]$ equals the internal functional $E^{\rm int}$. However, relying on the internal functional to describe the semilocal xc energy implies that one trusts the simple plasmon model in $S_{\rm xc}$ to accurately describe not only the overall plasmon response, but also the exchange energy, the biggest part of the xc energy. Given its simple form, it is natural that correction terms could arise. For one, the Langreth–Vosko expression (52) that was chosen for the internal functional to parametrize the plasmon

dispersion is a poor description in the regime of large density variations (high-s). However with correction terms, the conserving expression (34), involving a longitudinal projection of ϵ, would no longer describe the full xc energy. None of the vdW-DFs have an exact agreement between $E_{\rm xc}^{\rm int}$ and $E_{\rm xc}^{0}$ which would make them free of implicit correction terms, but there is a successively better agreement when going from vdW-DF1 to vdW-DF2 and to the newest development vdW-DF-cx [107]. The latest version is guided by the aim of using a consistent exchange choice; thus achieving this goal (32) for the most relevant density regions.

Charge conservation nevertheless remains an essential design principle for vdW-DF. The difference between $E_{\rm xc}^{\rm int}$ and $E_{\rm xc}^{0}$ only affects the short range part of the functional. Further, charge conservation is also imposed by relying on conserving approximations for $E_{\rm xc}^{0}$ and $E_{\rm xc}^{\rm int}$ separately. For $E_{\rm xc}^{0}$ the construction of the explicit form of the exchange functional can be traced to the construction of a numerical GGA that is designed by imposing conservation on the xc hole that arises in a gradient expansion [27, 143, 206, 207]. This is particularly true for the exchange functional used in vdW-DF2, the PW86r functional [207], which is fitted directly to such a numerical GGA construction.

For the internal functional, charge conservation [109] follows from the wavevector form (48). It provides an expression for the angle-averaged xc hole $n_{\rm xc}^{\rm int}(\mathbf{r},\mathbf{q}) = q^2\epsilon^{\rm int}(\mathbf{r},\mathbf{q})$ around a given $\mathbf{r}$, as expressed in momentum space. The relation follows since the spherically averaged xc hole $\bar{n}_{\rm xc}^{\rm int}(\mathbf{r},\mathbf{q})$ [24, 67] also defines a natural wavevector decomposition [42, 137, 208] for the energy per particle. Since $\omega_{\boldsymbol{q}}$ is finite in the $\boldsymbol{q}\to 0$ limit, $n_{\rm xc}^{\rm int}(\mathbf{r},0) = -1$. Thus, the integral over the xc hole in spatial coordinates gives -1, i.e. the depletion of a single electron.

Next, we discuss the choices made for the internal functional $E_{\rm xc}^{\rm int}$. Langreth, one of the vdW-DF architects, also had a central role in the developments that led to GGA with a diagram-based foundation [25, 42, 137, 202, 208]. Some of this development is reviewed in section 2.3. The diagram-based foundation means that the starting point is the terms that arise in a perturbative many-body expansion of the almost homogeneous electron gas. Such terms can be neatly visualized by Feynman diagrams, as in figure 3. vdW-DF1 uses a Langreth–Vosko (LV) [59, 62, 202] form for the exchange enhancement factor (52). The LV value of $Z_{\rm ab}$ that is used in vdW-DF1 represents an updated result compared to the value Z_x that appeared in the earlier discussion of the gradient-expanded exchange in section 2.3.

The LV form attempts to capture screened [137, 202, 208, 209] rather than pure exchange effects [202, 210]. It involves an evaluation of a $Z_x(q=0)$ response contribution. Figure 3 shows the corresponding diagrams. The '(a)' and '(b)' of $Z_{\rm ab}$ indicate that certain classes of diagrams, indicated in the figure labels, contribute [202, 209]. The third class of diagrams '(c)' can be identified as arising from nonlocal correlations and is not part of the screened exchange. The choice of not including these contributions in the internal functional motivates why only local correlations are included in the semilocal part of the xc energy of vdW-DF.

Standard GGA functionals have an enhancement factor $F_{\rm x}$ (52) that softens at larger s values compared to the aggressive quadratic enhancement factor within vdW-DF, see figure 11 for some examples. Such a quadratic form is chosen to make the vdW-DF construction as simple as feasible (the quadratic form is described by a single parameter), but also to ensure that very low density regions barely contribute to the nonlocal correlation energy. The aggressive enhancement factor acts as a cutoff because at low densities the scaled gradient s diverges, causing q_0 to diverge even more strongly. In turn, the effective dimensionless separation D diverges, thereby overwhelming the nonlocal correlation energy. This particular kind of cutoff mechanism observes the f-sum rule [72, 107], one of the constraints of vdW-DF.

Finally, we discuss the handling of screening in vdW-DF1. A common misconception is that because vdW-DF1 connects only two different density regions it lacks screening. However, $S_{\rm xc}$ is a semilocal approximation to the external field response. It has a screening account based on the density in its vicinity, much like in the ALL functional [44], that provides a good account of asymptotic vdW interactions. vdW-DF even includes gradient corrections and therefore reflects broader density variations. Related to this discussion is the fact that the evaluation of equation (53) and hence (44) can be viewed as the electrodynamical interaction between two semilocal xc holes $n_{\rm xc}^{\rm int}$. This is in line with the Rapcewicz and Ashcroft interpretation [43, 44, 109] of the fluctuation diagram that the second-order expansion of $E_c^{\rm nl}$ represents. We also point out that several applications of vdW-DF show that vdW-DF, to a large extent, captures screening effects such as image-plane and collective effects at typical binding separations [30, 76–78, 89, 90].

6.3. Self-consistency of vdW interactions

In the Kohn–Sham scheme of DFT [19], the interactions among electrons are accounted for by the sum of the mean-field electrostatic contributions and the xc potential $V_{\rm xc}[n](\mathbf{r}) = \delta E_{\rm xc}[n]/\delta n(\boldsymbol{r})$. This potential acts locally on each electron, and thus propagates these interactions only through its dependence on the density.

So far, the development of vdW-DF has focused on the xc energy functional $E_{\rm xc}[n]$ itself. The first implementations evaluated this functional in a post-processing manner: in the first step, the system in question is brought to full self-consistency with a standard functional—often PBE [27] or revPBE [182]—and the corresponding density is stored. In the second step, this static density is then used to evaluate $E_{\rm xc}[n]$ in a 'one-shot' calculation, performed by an independent code or inside the code that performed the first step. Clearly, this scheme is approximate as the vdW-DF is evaluated with a density that corresponds to a different functional and it was not until recently that an expression for the error made with such a non self-consistent evaluation was derived [79].

Self-consistency is important as it lays the foundation for the calculation of forces and the stress tensor, both essential for an efficient structural optimization [62, 211]. It is thus

crucial for efficient calculations of structure, energies, phase transitions, and elastic responses for bulk, layered, and molecular materials [108].

To make vdW-DF self-consistent, an expression for the nonlocal correlation potential $V_c^{\rm nl}(\mathbf{r})$ is required [62]. The vdW-DF xc energy consists of semilocal parts and a nonlocal part (37). The functional derivative of the semilocal part is well-established and we only focus on the derivative of the nonlocal energy functional:

$$V_c^{\rm nl}(\tilde{\mathbf{r}}) = \frac{\delta E_c^{\rm nl}[n]}{\delta n(\tilde{\mathbf{r}})} \,. \tag{56}$$

This functional derivative is straightforward but tedious to evaluate [62] and results in

$$V_c^{\rm nl}(\mathbf{r}) = \int {\rm d}^3 r'\, n(\mathbf{r}') \sum_{i=0}^{3} \alpha_i(\mathbf{r},\mathbf{r}')\, \Phi_i(\mathbf{r},\mathbf{r}') \,, \tag{57}$$

where the functions $\alpha_i(\mathbf{r}, \mathbf{r}')$ and $\Phi_i(\mathbf{r}, \mathbf{r}')$ are given by:

$$\alpha_0 = 1 \tag{58a}$$

$$\alpha_1 = \frac{1}{q_0(\mathbf{r})}\Big[\frac{Z_{ab}}{9}\nabla\cdot\mathbf{s}(\mathbf{r}) + \frac{7}{3}\frac{Z_{ab}}{9}s^2(\mathbf{r})k_{\rm F}(\mathbf{r}) \tag{58b}$$

$$-\frac{4\pi}{3}n(\mathbf{r})\varepsilon_{\rm xc}^{\rm LDA}(\mathbf{r})\Big] \tag{58b}$$

$$\alpha_2 = \frac{Z_{ab}}{9}\frac{\mathbf{s}(\mathbf{r})\cdot\nabla q_0(\mathbf{r})}{q_0(\mathbf{r})^2} \tag{58c}$$

$$\alpha_3 = \frac{Z_{ab}}{9}\hat{\mathbf{R}}_{\mathbf{r}\mathbf{r}'}\cdot\mathbf{s}(\mathbf{r}) \tag{58d}$$

and

$$\Phi_1 = d\phi_d(d,d') \tag{59a}$$

$$\Phi_2 = d^2\phi_{dd}(d,d') \tag{59b}$$

$$\Phi_3 = \phi_d(d,d') + d\phi_{dd}(d,d') + d'\phi_{dd'}(d,d') \,. \tag{59c}$$

Here, $\hat{\mathbf{R}}_{\mathbf{r}\mathbf{r}'}$ is a unit vector in the direction from $\mathbf{r}$ to $\mathbf{r}'$ and subscripts of d and d' denote the corresponding partial derivatives. The additional three kernel functions $\Phi_1(d, d')$ through $\Phi_3(d, d')$ are the analogues to the single kernel $\Phi_0(d, d')$ used for $E_c^{\rm nl}$. As pointed out earlier, $d = q_0(\mathbf{r})\,|\mathbf{r} - \mathbf{r}'|$ and $d' = q_0(\mathbf{r}')\,|\mathbf{r} - \mathbf{r}'|$.

Once it was developed, the self-consistent formulation was applied to a number of simple test cases including the Ar dimer. Figure 9 shows its interaction energy as a function of separation. The differences between the non self-consistent and the fully self-consistent results are minimal, at least at larger separations. The bottom panel shows that the forces calculated self-consistently for vdW-DF through the Hellmann–Feynman theorem agree well with the numerical derivative of the energy.

The self-consistent method can also be used to show how the density evolves under the influence of vdW interactions.

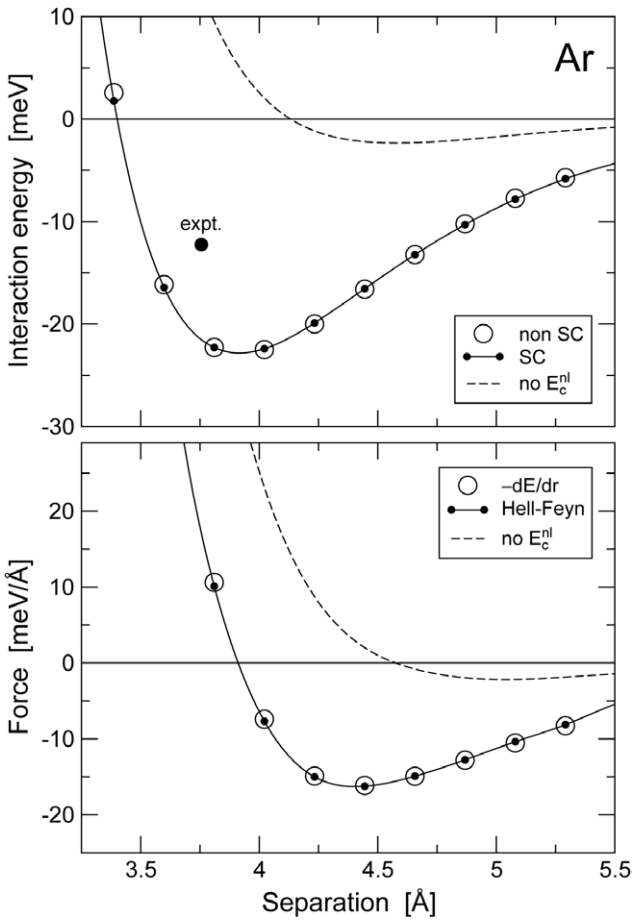

Figure 9. (top) Interaction energy of the Ar dimer as a function of separation for the self-consistent and non self-consistent approach. In addition, we show results where $E_c^{\rm nl}[n]$ has been neglected. (bottom) Forces calculated as the derivative of the energy ($-{\rm d}E/{\rm d}r$) and the Hellmann–Feynman forces. Reprinted with permission from [62], © 2007 American Physical Society.

The density change in the case of the Ar dimer is tiny (figure 10), but nonetheless responsible for the binding of the dimer by pulling charge in-between the nuclei. This captivating and illuminating picture quantitatively displays the nature of the vdW bond.

6.4. Efficient FFT implementation, algorithm of Román-Pérez and Soler

The evaluation of the nonlocal contribution to the exchange-correlation energy $E_c^{\rm nl}[n]$ requires solving a six-dimensional spatial integral; the evaluation of the corresponding potential $V_c^{\rm nl}(\mathbf{r})$ requires a three-dimensional integral for every point $\mathbf{r}$, see (44) and (57). A straightforward numerical evaluation of those integrals required for vdW-DF is much more time-consuming than for simple LDA or GGA functionals. As the vdW-DF kernel goes to zero for large separations, the first self-consistent implementations of vdW-DF used a spatial cutoff to limit the computational effort of evaluating those integrals. While such a spatial cut-off provides some form of 'linear-scaling', the prefactor still makes most simulations computationally very expensive.

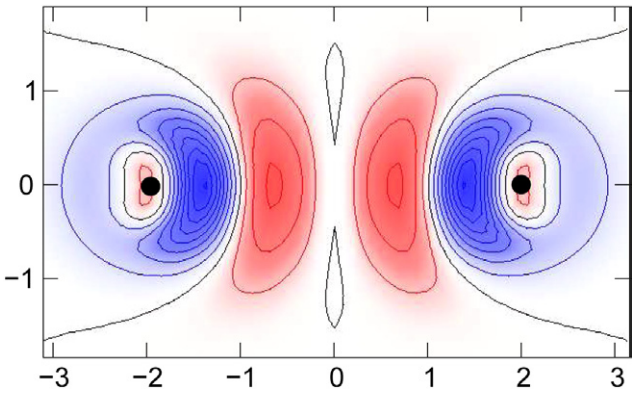

Figure 10. Bonding charge of the Ar dimer. Shown is the difference in induced electron density. The scale is in Å and the black dots mark the position of the nuclei. The zero level is marked by the black contour. Red areas represent areas of electron density gain when the nonlocal part is included; conversely, blue areas indicate loss of electron density. Increments between contour lines are 5×10^{-5} electrons Å^{-3}. Reprinted with permission from [62], © 2007 American Physical Society.

This bottle-neck was overcome by Román-Pérez and Soler, who rewrote $E_c^{\rm nl}[n]$ as an integral convolution using splines [212]. In this way, the dependence of the kernel on $\mathbf{r}$ and $\mathbf{r}'$ can be approximated as

$$\begin{aligned}\Phi_0(\mathbf{r},\mathbf{r}\,') &= \Phi_0(q_0(\mathbf{r}), q_0(\mathbf{r}\,'), |\,\mathbf{r}-\mathbf{r}\,'\,|)\\ &\approx \sum_{\alpha\beta} \Phi_0(q_\alpha, q_\beta, |\,\mathbf{r}-\mathbf{r}\,'\,|) p_\alpha(q_0(\mathbf{r})) p_\beta(q_0(\mathbf{r}\,')),\end{aligned} \tag{60}$$

where q_α are fixed values and p_α are cubic splines. It follows that the original nonlocal functional can be written as

$$\begin{aligned}E_c^{\rm nl}[n] &= \frac{1}{2}\sum_{\alpha\beta}\int \mathrm{d}^3r\,\mathrm{d}^3r'\,\theta_\alpha(\mathbf{r})\,\phi_{\alpha\beta}(|\,\mathbf{r}-\mathbf{r}'\,|)\,\theta_\beta(\mathbf{r}')\\ &= \frac{1}{2}\sum_{\alpha\beta}\int \mathrm{d}^3k\;\theta^*_\alpha(\mathbf{k})\,\phi_{\alpha\beta}(k)\,\theta_\beta(\mathbf{k})\,,\end{aligned} \tag{61}$$

where $\theta_\alpha(\mathbf{r}) = n(\mathbf{r})\; p_\alpha(q_0(\mathbf{r}))$ and $\theta_\alpha(\mathbf{k})$ is its Fourier transform. In the same sense, $\phi_{\alpha\beta}(k)$ is the Fourier transform of $\phi_{\alpha\beta}(r) \equiv \phi(q_\alpha, q_\beta, |\mathbf{r}-\mathbf{r}'|)$.

At first sight, the benefit of using equation (61) might seem minor—a six-dimensional integral has been traded for a three-dimensional one that contains Fourier transformed quantities. However, many of the implementations of vdW-DF have been in standard planewave DFT codes. As such, fast Fourier transforms are readily available and highly optimized. The overall computational speedup is dramatic and today vdW-DF calculations on large systems take barely any longer than standard GGA calculations.

6.5. Refinements of the first general-geometry vdW-DF version

Numerous applications have demonstrated that the first general-geometry vdW-DF version, vdW-DF1, is both robust and versatile. These qualities of vdW-DF will be illustrated in section 7 dedicated applications of vdW-DF. This success indicates just how potent vdW-DF1's underlying constraint-based construction

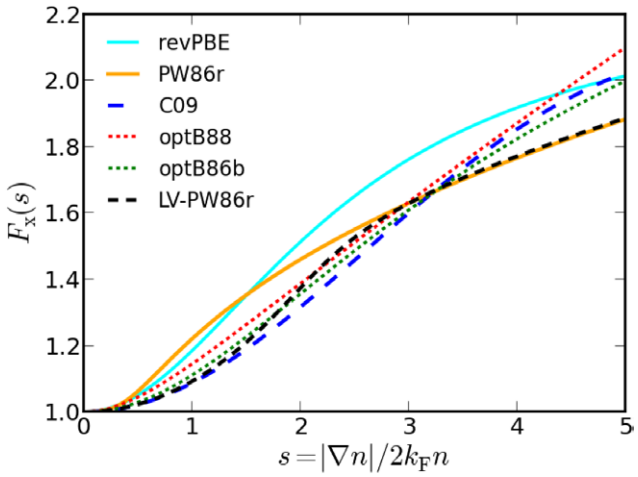

Figure 11. Enhancement factors $F_x(s)$ of exchange functionals suggested for vdW-DF1 and vdW-DF2 correlation.

is. It is only natural then that when designing new functionals, the original vdW-DF1 construction is often the starting point. There are several different aspects of vdW-DF1 one might want to improve, such as the typical overestimation of binding separations [106]; the account of binding energies, in particular for small molecules [63] and for hydrogen bonds strengths like those of water [196]; the description of covalently-bounded solids [197]; and consistency between exchange and correlation functionals [107]. Considering that vdW-DF is rooted in the electron gas tradition, we believe that it should be refined by carefully assessing constraints and first-principle input parameters. However, researchers outside the Rutgers–Chalmers program have attempted to improve the functionals by instead optimizing the functional based on selected reference data sets, that is, making semi-empirical variants of vdW-DF [196, 213].

The vdW-DF1 overestimation of binding separations was noted from the onset [59] and attributed to the choice of revPBE as exchange functional. Despite good reasons for starting out with revPBE, as discussed in section 5, there is no intrinsic reason why this specific exchange functional should be the only appropriate one for vdW-DF1. Several attempts to refine vdW-DF1 have therefore kept the correlation part fixed and focused on the exchange. For transparency, we encourage the use of a standard nomenclature vdW-DF-E_x; where E_x refers to the exchange functional. This has the added benefit of allowing one to specify different nonlocal correlation functions, e.g. vdW-DF versus vdW-DF2; while clearly identifying the form of exchange being employed.

Figure 11 shows several different exchange enhancement factors $F_x(s)$ suggested as partners for the vdW-DF1 and vdW-DF2 correlation. Here, $s = |\nabla\, n|/2k_{\rm F}n$ is the reduced gradient and the exchange energy is

$$E_{\rm x} = \int \mathrm{d}^3r\; n(\mathbf{r})\; \epsilon_{\rm x}^{\rm LDA}(n)\; F_x(s)\;. \tag{62}$$

The exchange functional C09 [106], suggested as an exchange partner for the vdW-DF1 correlation, is designed to counteract the overestimation of binding separations while also avoiding spurious exchange effects. This was achieved by using an enhancement factor $F_x(s)$ that interpolates between the

gradient expansion of the slowly-varying electron gas, as used in PW86 [143], at small reduced gradients s and the revPBE form at large s. This large-s form was also chosen to retain the good binding energies of vdW-DF. This functional (vdW-DF-C09) demonstrated that the issue of overestimation of separation distances in vdW-DF could be solved by assessing the constraints of the exchange functional.

A different approach was taken by Klimeš and co-workers [196] to design an exchange functional for vdW-DF1 correlation. They tuned the parameters of a set of familiar exchange functionals to optimize the binding energies of the S22 set of dimers. This is an example of what we call reference-system optimization, as distinguished from constraint-based functionals. In practice, the refitting reduces the overestimation of separations. Over time, the optB88 variant (vdW-DF-optB88) has revealed itself to provide an accurate account of many kinds of systems and thus has become widely used. In some codes, care must be taken when implementing this functional because its aggressive large-s behaviour makes it noise sensitive [92].

Murray and coworkers [207] also made an important exchange development by analysing what would be the most suited exchange functional for sparse matter at the GGA level. They found that the PW86 had the best agreement with Hartree–Fock interaction curves between many molecules, in particular beyond binding separations. This was attributed in part to the $s^{2/5}$ form of the enhancement factor $F_x(s)$ at large s. Others have reached similar conclusions [214]. This exponent form arises in the numerical GGA construction [143, 206], which is built around conservation of the exchange hole. Finally, PW86 was also refitted to update the small-s behaviour and to make the large-s evaluation of the numerical GGA construction exact (PW86r).

For some covalently-bound solids such as heavy transition metals, vdW-DF1's account can be inferior to that of standard GGAs. Motivated by this shortcoming, Klimeš and co-workers [197] designed an exchange functional for vdW-DF1 called optB86b. This functional is based on a 'minimalistic' one-parameter refitting of B86b [215] using a small-s form corresponding to the gradient expansion of the slowly-varying electron gas. This makes the small-s form similar to that of C09, yet the B86b form ensures that it crosses over to the $s^{2/5}$ form at large s, though with a quite different prefactor than PW86r or B86b. This functional (vdW-DF-optB86) performs well for many other kinds of systems and together with vdW-DF-optB88 it has played an important role in showing that vdW-DF can handle systems characterized by weak chemisorption.

Most recently, a formally appropriate exchange functional to pair with vdW-DF1 was derived [107]. This exchange functional is in part motivated by the fact that deviations between the outer and internal exchange form give rise to correction terms unaccounted for in the original derivation. It is also motivated by the robustness of vdW-DF1 for vdW-bonded systems. This robustness is linked to the success of the plasmon description underpinning the non-local part of the functional. The new exchange functional is therefore designed to resemble the internal functional of vdW-DF1 in as large of an s regime as feasible, while smoothly crossing over to the PW86r form at larger s (LV-PW86r). This exchange and correlation combination is referred to as vdW-DF-cx [107, 108], where cx stands for *consistent exchange*. In essence, the new exchange functional is quite similar to C09 and optB86b and thus partially validates their usage as well. Tests so far indicate that vdW-DF-cx has excellent performance, further supporting the quality of the plasmon model underpinning vdW-DF1.

Separate from the development of exchange functionals for vdW-DF1, a second version of vdW-DF for general geometries called vdW-DF2 was also developed [63] which updates both the exchange and correlation functional. For the nonlocal correlation, it was recognized that the small-s exchange parameter β of the B88 [216] functional would provide a more appropriate parametrization of the plasmon response of molecules than the slowly-varying electron-gas result underlying vdW-DF1. Indeed, this parameter is used in many successful functionals and can be derived from first principles using the large-N asymptote of neutral atoms [217]. For the exchange functional, the well-founded choice of PW86r [143] was made. Migrating from vdW-DF1 to vdW-DF2 simply entails setting $Z_{ab} = 1.887$ in the internal functional (52). The exchange and correlation of vdW-DF2 are reasonably consistent with each other because in the significant s regime beyond 0.1, the enhancement factor of PW86r agrees well with that of the internal exchange of vdW-DF2. The vdW-DF2 greatly improves both binding energies and separations for systems of small molecules, but has also been criticized for poorly describing the asymptotic interaction between molecules. However, in a fairly wide region beyond binding separation, vdW-DF2 does in fact predict interaction curves in good agreement with coupled cluster results for the S22 set of dimers [63].

While vdW-DF2 greatly improves the description of small molecules compared to vdW-DF1, issues with bulk matter and weakly chemisorbed systems remain. An alternative exchange functional for vdW-DF2 was very recently developed by Hamada [198]. Drawing on earlier experience with testing of the ad-hoc combination of vdW-DF2 correlation and C09 exchange, which works well for some systems [218], he reparameterized the enhancement factor of the B86b functional to better describe the small-s form of the slowly varying electron gas and approximately retain the large-s form of B86b [215], a functional designed for highly inhomogeneous systems. Initial benchmarking demonstrates that the combination of B86R and vdW-DF2, named rev-vdW-DF2 or vdW-DF2-B86R, results in good performance for small molecules as well as an improved description of bulk and weakly chemisorbed systems. With such promise, this functional deserves further benchmarking.

An almost opposite approach to how vdW-DF originally was developed is used in the 'BEEF–vdW model compromise' [219]. This is a reference-system optimized method taken to its extreme: the authors develop a methodology for semiempirical density functional optimization, using regularization and cross-validation methods from machine learning. The general idea is to minimize errors through a survey of a wide range of functionals through an understanding of the

expected error bars. To date, there have been a few examples demonstrating moderate success. It still remains to be seem as to whether or not computer driven optimization strategies will surpass scientific insight when designing better functionals.

6.6. The Vydrov and van Voorhis functionals

Remaining within the vdW-DF framework, Vydrov and van Voorhis designed a functional called vdW-DF-09 [213] by introducing reference-system optimization even for the nonlocal part. Even though they abandon vdW-DF's close connection to GGA, this method retains all the essential constraints of vdW-DF.

Closely following this work was the development of the two offspring of vdW-DF called VV09 [64] and VV10 [65]. These two functionals inherit many of the features of vdW-DF, but also include additional physical mechanisms at the cost of adhering to fewer exact constraints [201]. Using physical arguments to improve the account of long-range interactions between small molecules, they rely on reference-system optimization to parameterize one (VV09) or two (VV10) fixed parameters. Both functionals are designed for simplicity, VV10 radically so. The VV10 variant is also the most flexible and is more recently emphasized by the authors. The VV09 on the other hand is constructed in a manner most reminiscent of vdW-DF.

Both rely on a spatially varying gap $\omega_g(\mathbf{r})$ in the plasmon dispersion model that is given by [64, 220]

$$\omega_g^2(\mathbf{r}) = \frac{C}{m^2}\left|\frac{\nabla n}{n(\mathbf{r})}\right|^4 . \tag{63}$$

The parameter C was fit to optimize the C_6 coefficients, describing the long-range interaction between molecules.

Similar to vdW-DF, VV09 builds upon the plasmon propagator $S \approx S_{xc} = \ln(\epsilon)$ defined as

$$\tilde{S}_{\mathbf{q},\mathbf{q}'}(iu) = \int d\mathbf{r}\, e^{-i\mathbf{r}\cdot(\mathbf{q}-\mathbf{q}')}\frac{\omega_p^2(\mathbf{r})}{\omega_0^2(\mathbf{r})+u^2}F_{q,q'}(\mathbf{r}) , \tag{64}$$

with plasmon poles given by

$$\omega_0^2(\mathbf{r}) = \omega_g^2(\mathbf{r}) + \omega_p^2(\mathbf{r})/3 . \tag{65}$$

Here $\omega_p = \sqrt{4\pi n e^2/m}$ is the classical plasma frequency. Unlike vdW-DF, these poles do not shift as a function of wavevector; rather VV09 relies on damping factors $F_{q,q'} = \exp[-(q^2+q'^2)/(k_s^2\phi^2)]$ to reduce the weight of dispersive states [64]. Here k_s is the Thomas–Fermi wavevector and ϕ is the spin-scaling factor $\phi = [(1+\zeta)^{2/3} + (1-\zeta)^{2/3}]/2$.

This choice causes VV09 to break charge conservation, an essential constraint of vdW-DF [59, 201]. The 1/3 factor is motivated by the Clausius–Mossoti relation and the appropriate screening relation for jellium spheres [64].

Rather than attempting to approximate the exact ACF, the VV10 construction starts directly by assuming a universal kernel (44) given by a simple ansatz,

$$\Phi^{VV10}(\mathbf{r},\mathbf{r}',R=|\mathbf{r}-\mathbf{r}'|) = -\frac{3e^4}{2m^2\, gg'(g+g')} , \tag{66}$$

where $g = \omega_0(\mathbf{r})\, R^2 + \kappa(\mathbf{r})$ (similar for g') and $R = |\mathbf{r}-\mathbf{r}'|$. This kernel is designed to give the same asymptotic form as that of VV09. The κ function serves to dampen nonlocal-correlation energy contributions at shorter separations. It depends on a scaling parameter b which is fixed for a given semilocal partner by optimizing binding energies to the S22 benchmark [221]. In this respect, like the dispersion-corrected DFT methods, VV10 is reference-system optimized, though the number of input parameters is drastically reduced. In fact, in a separate development, the long-range account serves as input in such a method [177] (section 4.3). The evaluation of the non-local correlation energy in VV10 can also be sped up in a similar manner to that of vdW-DF [212] by introducing a small modification to the kernel [222].

VV10 has been tested for a range of problems including noble-gas and molecular systems, traditional bulk and layered vdW systems [165, 222–226]. It works particularly well for interactions between small molecules [65, 223, 227]. However, results for layered systems indicate that VV10's transferability across length scales may be inferior to that of vdW-DF [165, 224]. This shortcoming may be related to the crude mechanism used to account for the saturation of vdW forces at shorter separations, as it lacks the constraint-based mechanisms inherent to vdW-DF. On the other hand, the VV10 framework can readily be adapted to accurately describe special classes of systems. For instance, Björkman crafted a special purpose functional for layered systems [225] (VV10sol) that accurately describes the binding of layered systems. VV10 can also readily be paired up with hybrid functionals; thus producing the correct asymptotic exchange behaviour [65, 227, 228].

The overall success of VV09 and VV10 further illustrates the potency of using a density functional framework for including vdW forces. Being so closely related to vdW-DF, comparing their functionality to that of vdW-DF can be illuminating and may even trigger new developments.

7. Applications

After a decade of theory development and model calculations which culminated in the development of vdW-DF, a surge of computations on sparse matter has followed. An early review summarized the status in 2009 [66]. Since then the number and variety of applications have grown tremendously. A set of recent perspective papers [9, 10, 229] give a broader overview of the current situation methods and applications in the vdW computation arena. Being such a widely used method, it is impossible to cover every application in a single review. Here, we attempt to illustrate the depth and extent of modern applications of vdW-DF. This overview will necessarily have some bias towards work related to our own research. Several benchmark studies, such as that illustrated in figure 16, indicate that its accuracy has improved with more recent developments. Naturally, the race for higher accuracy functionals will continue. Additionally, since vdW forces are present in numerous systems such as organic, inorganic, polymeric and bio-organic systems, the

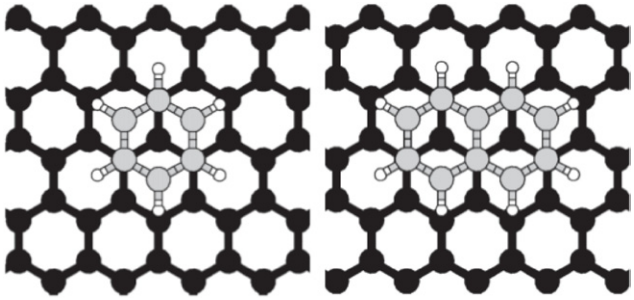

Figure 12. Binding geometries for benzene and naphthalene on graphene. Reprinted with permission from [80], © 2006 American Physical Society.

future will be full of interesting fundamental and applied studies.

7.1. Early applications

As seen in this review, early applications in the 90s focused on well-established vdW results at that time, namely asymptotic vdW interactions at large separations between fragments. To calculate, for instance, the C_6 coefficient of the vdW asymptote of two small fragments, the traditional method required quantum-mechanical calculations of numerous dipole matrix elements for each fragment. In this light, it might be understandable that figure 4 created almost euphoric feelings within the ALL collaboration; it did not only provide a simple formula for C_6 in terms of the electron density n, but also a 'milky way' (figure 4) that got narrower as the approach was successively improved.

The first application, including non-asymptotics was made for jellium [54, 56]. For this simple model system accurate calculations were available, and good agreement between these results and those with the early variant of vdW-DF0 showed promise. For a modern practitioner of vdW methods, the optimistic tone described in section 5 for graphite, using the year 2000 numbers [55], might seem surprising. However, one should keep in mind that in 2000 the leading DFT, namely the GGA, gave almost no binding at all and if so only at unphysically large separations. Later vdW-DF0 results were also found to be promising [29]. Figure 7 illustrates that this promise has been kept by further developments along the vdW-DF track, that is vdW-DF1, vdW-DF2 and vdW-DF-cx, the latter overlapping with results of accurate quantum Monte Carlo simulations.

An early pivotal application was on the adsorption of benzene and naphthalene on graphene [80]. Figure 12 depicts the corresponding binding geometries. This application provided a valuable comparison between theory and experiment because a far-sighted experimental group [194] had measured thermal desorption-energy values. vdW-DF1 predicts binding energies and separations that agree well with experiment. For the adsorption of benzene and naphthalene, figure 13 shows the binding curve and the experimental estimated ranges. The good agreement stimulated successive works with the vdW-DF as well as later theory development and numerous new applications of the functional. For instance, this work

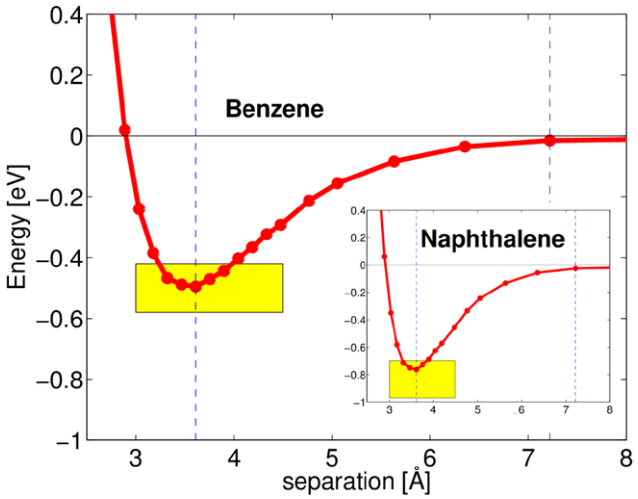

Figure 13. Binding curve for benzene (and naphthalene) on graphene, calculated with vdW-DF1 and compared to experimental estimates. Figure adapted from [80], © 2006 American Physical Society.

triggered many other early applications on adsorption of other molecules and on other surfaces [91]. A few years later, the general applicability of vdW-DF was further established with promising results for the adsorption of molecules on metallic surfaces, such as for benzene on coinage metals [99, 231].

Even on the molecular side, the benzene molecule provides the prototype. For the interaction between two benzene molecules, orientation must also be considered. An early vdW-DF study on a simple molecular dimer was on the benzene dimer, in the sandwich, slip-parallel, and T-shape configurations, detailed in [231]. In all cases, the vdW-DF1 curves were typically between the coupled cluster results at the CCSD(T) level and those of Møller–Plesset perturbation theory (MP2). It is gratifying that vdW-DF seems to improve upon the MP2 results which can overestimate the dispersion binding [221, 232].

The same is true when one hydrogen atom of a benzene ring is replaced by such groups as OH, CH_3, F, and CN [233]. These 'monosubstituted' benzene dimers are necessary precursors for applications of vdW-DF to the stacking of nucleobases and DNA base pairs reviewed in section 7.5. Just as with the benzene dimer [231], the monosubstituted benzene dimer [233], the benzene-water complex [234], and the methane-benzene system and related dimers [235] have been shown to give results that lie between CCSD(T) and MP2 for the binding energies as a function of separation.

Originally, van der Waals proposed his interaction to describe real gases, as distinguished from the ideal gas. In this spirit, replacing empirical force-field methods by vdW-DF is an interesting challenge. Such methods are widely used to determine the structure of molecular crystals and for larger disordered systems such as polymers. The prospect of using vdW-DF for such purposes was first investigated in a study of a solid polymer, polyethylene [95], in a low temperature, crystalline phase, for which experimental structures are available to compare with. The good agreement shown in figure 14 gave hope for using vdW-DF1 also in simulations on both ordered

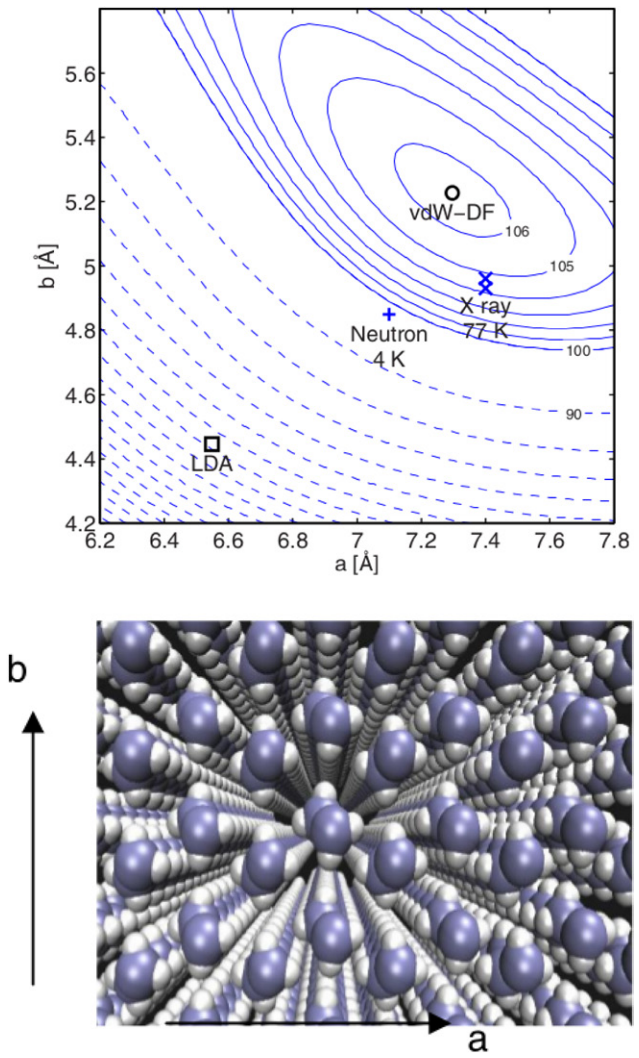

Figure 14. Binding energy contours for a polyethylene crystal compared with LDA and results from diffraction experiments. Reprinted with permission from [95], © 2007 American Physical Society.

and disordered systems with molecules interacting with vdW forces. This promise has continued to grow with many new successful applications on related systems such as nanotubes [76] and molecular crystals [77, 78].

The early findings eventually led to much further research, resulting in the release of vdW-DF2 and other variants and numerous applications, such as those highlighted in section 7, which are indicative of the present status.

7.2. Benchmark calculations

To assess the applicability of vdW-DF and other methods, we can rely on results from accurate theoretical and experimental methods. Common *theoretical* methods for this purpose are many-body quantum chemical methods such as coupled-cluster, e.g. CCSD(T), and perturbative methods, like MP2, which show high accuracy, in particular for relatively small systems. Early benchmark calculations of this kind are mentioned in section 7.1. From *experiment* carefully determined quantities describing structural and binding properties are often used (refer to section 4.2). The literature is full of comparative assessments of the performance of various sparse-matter methods.

For the vdW-DF method there are both virtues and vices. Already from the beginning [59] the rare-gas dimers were perturbing examples of the latter: vdW-DF1 was applied to the 'rare-gas dimers, where it is shown to give a realistic description'. The 'moderate successes' are quantified by results for C_6 coefficients of rare-gas dimers and binding-energy curves of Ar_2 and Kr_2 [59]. This is certainly progress compared to GGA results, but its limitations are obvious and partly analysed in further functional developments. The rare-gas systems are the prototypical vdW systems, where the dispersion interactions are the only source of attraction between atoms and for which highly accurate *ab initio* or empirical results are available. The rare-gas dimers, accounted for in this review, have been used numerous times for the testing of functionals for weak interactions.

Small atomic and molecular dimers traditionally serve as benchmarks or stepping stones for larger applications. The classic cases of noble-gas dimers were originally treated with the vdW-DF1 method and signaled problems with the lighter atoms, while for the Ar and Kr dimers the binding energies get reasonable values, though binding distances are overestimated by a few percent [59]. Recently [223, 236], several variants of the vdW functionals have been tested on rare-gas dimers (from He_2 to Kr_2) and solids (Ne, Ar, and Kr) and their accuracy was compared to standard semilocal approximations, supplemented by an atom-pairwise dispersion correction [49]. As depicted in figure 15, in general modern variants such as vdW-DF-optB88 [196], vdW-DF2 [63], vdW-DF-C09 [106] (see erratum: [236]), and related functionals like rVV10 [222], exhibit significant improvements in their treatment of noble-gas dimers with respect to binding separation distances, albeit not at the desired chemical accuracy for binding energies. Nevertheless, it is important to note that the noble-gas dimers are not systems one would expect the vdW-DF method to perform well as its emphasis on electron-gas many-body physics makes it ideally suited for systems with extended states, not for strongly localized ones. The later developed vdW-DF2 has a design that makes it better suited for smaller molecules.

Another popular theoretical benchmark, the so-called S22 data set [221], comprised of CCSD(T) calculations of 22 molecular duplexes including H-bonded, dispersion dominated, and mixed systems, has been extensively studied to assess how techniques for including dispersion interactions perform. vdW-DF calculations have been performed on all duplexes in the S22 data set and results are presented in [63, 79, 106, 107, 196, 197, 237]. Figure 16 presents an overview of the performance of vdW-DF versions developed by us for the three kinds of systems. This figure and the publications listed highlight how the performance of vdW-DF has improved over time, either through rederivation of the nonlocal correlation term or through the development of exchange functionals, as discussed in section 6.5. In all cases, the mean absolute deviation (MAD) has been reduced from 65 meV for the original functional to 10–20 meV, i.e. to within chemical

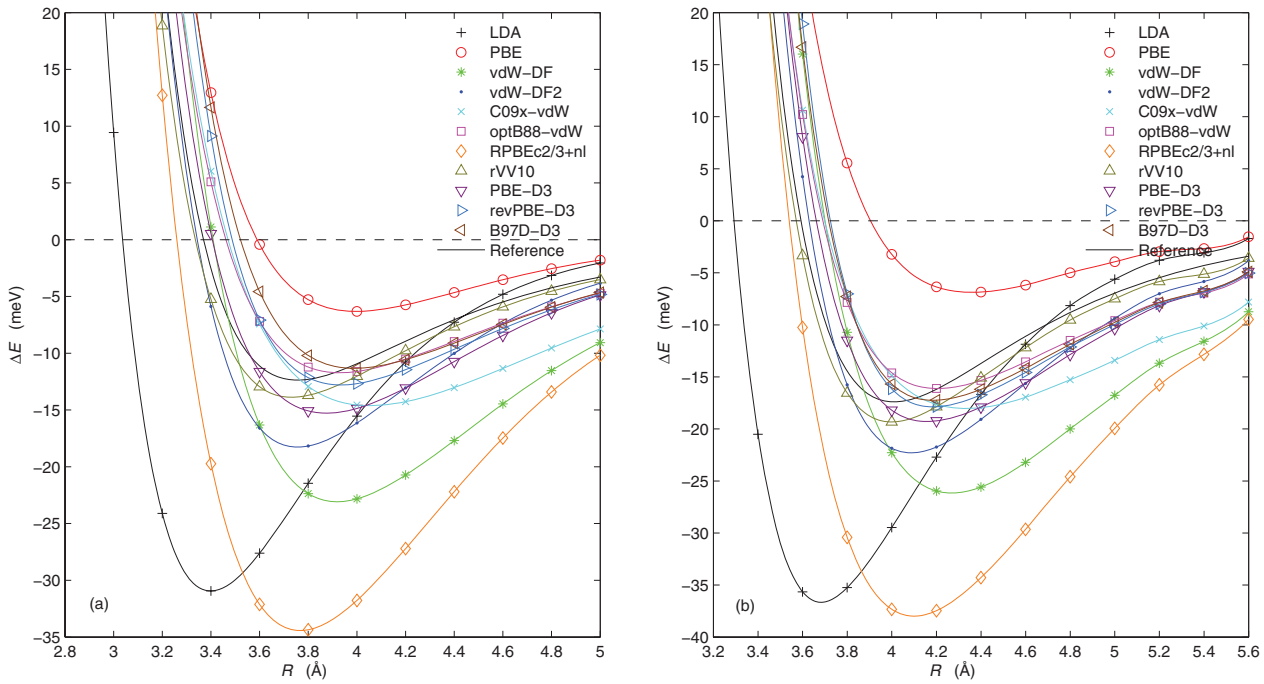

Figure 15. Interaction energy curves for (*a*) (left) Ar_2 and (right) Kr_2 obtained from various functionals and compared to reference results (black line without symbols). (N.B. the curves for vdW-DF-C09 in figure 15 and the data for this functional were updated in an erratum [236]; now showing much better agreement with other functionals like vdW-DF-optB88). Adapted with permission from [223], © 2013 American Institute of Physics.

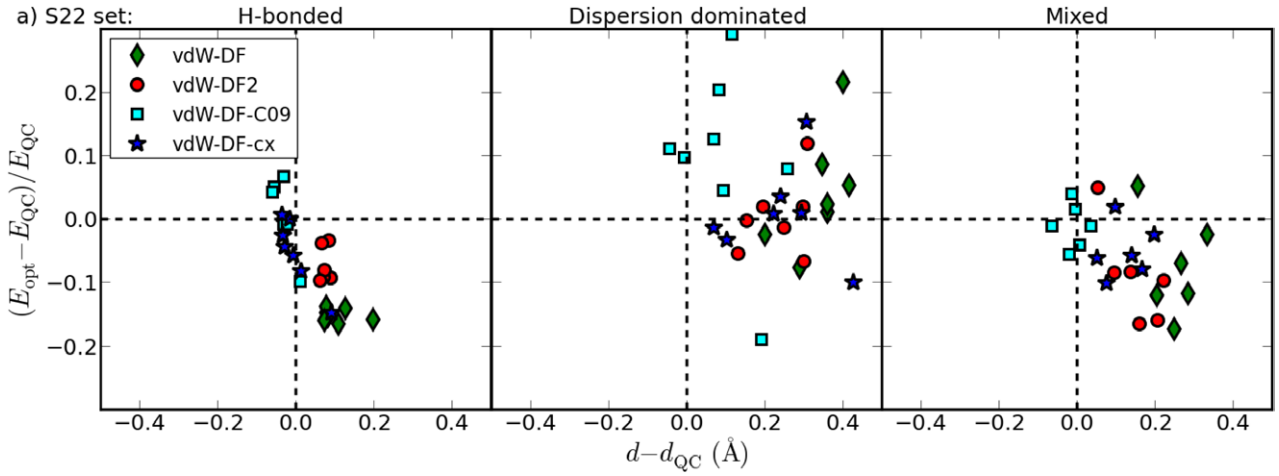

Figure 16. Comparison of vdW-DF versions for the S22 data set. vdW-DF-C09, vdW-DF2, and vdW-DF-cx represent an improved overall performance compared to vdW-DF1, in particular the overestimation of separations is reduced. Reprinted with permission from [108], © 2014 American Institute of Physics.

accuracy. Similar improvements in accuracy have also been observed for vdW-DF-optB86 [197] as well as the recent vdW-DF2-B86R functional [198] and with reference-optimized functionals like vdW-DF-optB88 [196]. We note that there certainly exists limits for what can be gained from reference-system optimization and from benchmarking against such datasets. For example, reference systems like the S22 and rare-gas dimer sets tell very little about contributions arising from the *d*-electrons.

Comparisons with experiment also give new insights into how well vdW-DF performs both qualitatively and quantitatively as the many examples of this chapter will illustrate. Additionally, some experimental results provide particularly accurate data and therefore constitute accurate benchmarks.

Crystalline solids stand out as excellent case studies for how well a method can predict structures, because x-ray and neutron scattering can precisely determine the atomic positions in such materials. The good results for polymer crystals mentioned in section 7.1 were therefore encouraging during the early testing phase of vdW-DF. Similarly, molecular crystals serve as particularly good benchmarks for vdW-DF because they are held together by non-covalent forces. An early such comparison for the high-symmetry molecular crystals hexamine, dodecahedrane, cubane, and C_{60} [77, 78]

showed that vdW-DF describes the structure, cohesive energies, and bulk moduli of these molecular crystals well, though vdW-DF1 consistently overestimates the crystal cell volume. Similar conclusions have been drawn in other studies on molecular crystals [9, 211, 238–240].

Surface adsorption studies also provide a unique avenue for benchmarking. For example, the adsorption of molecules on metal surfaces, which are closer to jellium surfaces, can be insightful in testing and designing functionals with dispersion interactions. Section 4.2 exemplifies this with a case study on the adsorption of H_2 on copper. It is shown that vdW-DF2, in particular, gives potential-energy curves for different Cu facets that agree well with experiment [89, 90]. This is a feat, which techniques that employ pairwise corrections are unable to reproduce, presumably due to the inability of such potentials in distinguishing between bulk and surface density regions.

The performance of vdW-DF has also been benchmarked against QMC results for molecular-hydrogen phases [241] and for bulk water [242]. The studies test the vdW-DF method as a description of a full potential-energy variation for molecular dynamics, sharing a benchmarking philosophy with our H_2 physiosorption studies [89, 90]. The molecular-hydrogen and water studies compare QMC and vdW-DF calculations for a rich set of configurations both within and among different phases and allow for flexible molecular configurations. The vdW-DF1 and vdW-DF2 versions are found to have very good transferability across length scales, tending to overestimate the binding separation but being reliable on the total-energy variation.

The positive feedback from benchmarks as well as from quantitative and qualitative comparison between theory and experiment signals a new era for nonlocal functionals in which they can be used to understand the role that dispersion interactions play in real materials. Many such applications are mentioned next.

7.3. Adsorption

The adsorption of molecules to surfaces and within porous media is a defining feature of numerous industrial, chemical, and energy relevant processes. For example, the self-assembly of organic molecules and catalytic reactivity are mediated by molecular chemisorption to surfaces. Similarly, carbon sequestration and H_2 storage in carbon-based structures are driven by the dispersion-dominated physisorption of guest molecules. In addition, the charging and discharging of lithium ion batteries depend on the movement of metal ions between weakly bound planes of a graphitic anode. These examples highlight the need for a method that can cross the traditional boundary of chemisorption to weaker physisorption. In this regard, vdW-DF has been proven to be both sufficiently accurate and computationally efficient for simulating the intricate details of dispersion interactions at surfaces and within porous materials.

7.3.1. On surfaces. The physisorption of molecules to graphite and two-dimensional surfaces, including graphene, metal dichalcogenides like MoS_2, and PAHs, has been a long-standing focus of vdW-DF calculations [30, 80, 82, 84–87, 91, 243–248]. These surfaces often allow for meaningful comparisons with quantum-chemical calculations. For instance, a comparison of the adsorption energy of H_2 interacting with PAHs shows excellent agreement with previous MP2 calculations—with only small deviations at large separation distances [246]. This is in dramatic contrast to the behaviour of GGA functionals that show little to no binding, or even LDA functionals which overbind molecules to graphene.

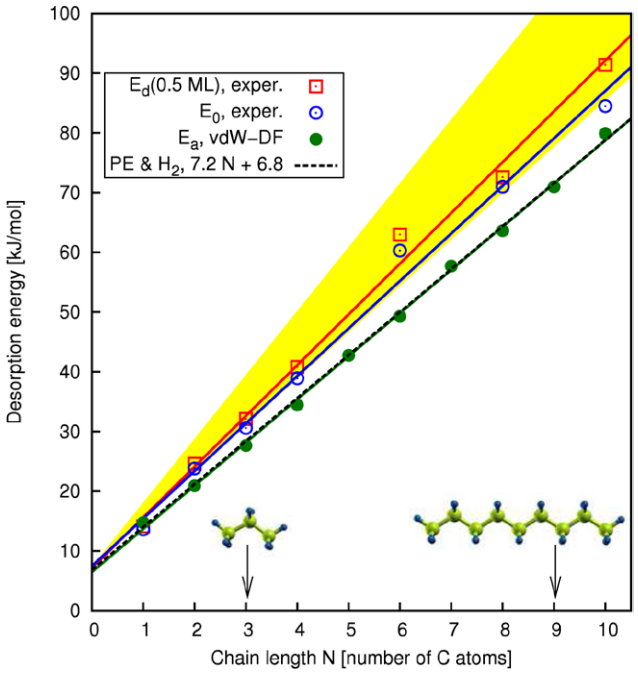

Figure 17. Adsorption energies of *n*-alkane chains on graphene. Solid points are vdW-DF1 results, open points are from the TPD measurements by Tait *et al* [249]. Linear fits for the three sets of data points are also shown. Study detailed in [243].

Figure 17 compares experimental data on *n*-alkane adsorption on C(0001) deposited on Pt(1 1 1) with vdW-DF1 results [243]. Experimentally it is found that the adsorption energy varies linearly with N the number of units in the alkane for several different surfaces, but with a small offset at $N = 0$. This result might be puzzling in a naive picture of vdW contributions to binding. However, the calculations of Londero *et al* [243] show that this trend and offset is well reproduced in vdW-DF. This shift can be attributed to the role of the end groups of the alkane chains. In fact, they find that the offset of 6.44 kJ mol^{-1} in vdW-DF agrees well with the calculated adsorption energy of an H_2 molecule of 6.48 kJ mol^{-1}. Similar comparisons between vdW-DF and experimental data [250] have also been performed for *n*-butane on Cu, Au, and Pt surfaces. Only a small part of the polymer chain can contribute significantly to the binding. This is related to the fact that low-density regions dominate the nonlocal correlation energy [207].

Adsorption systems, such as the above examples, are well suited for analysing the properties of vdW-DF. A study in this vein [30] compares the adsorption of benzene and C_{60} on graphene and hexagonal-BN (*h*-BN). C_{60} is bigger but its interface

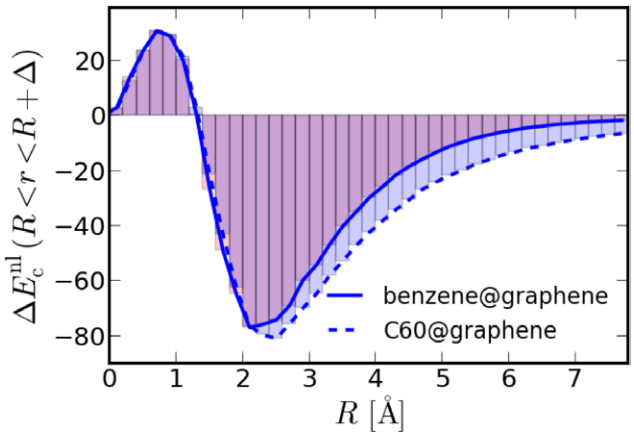

Figure 18. The nonlocal correlation energy contributions [equation (44)] to the adsorption energy for different separations between density regions $R = |r - r'|$. The two curves compare this analysis for benzene and C_{60} on graphene at the same molecule-to-graphene separation. Reprinted with permission from [30], © 2013 American Physical Society.

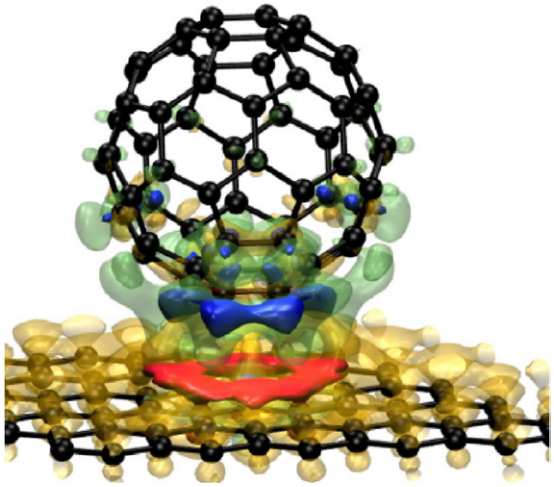

Figure 19. Charge transfer isosurfaces for C_{60} on graphene. Blue isosurfaces indicate loss of charge. Red isosurfaces indicate gain in charge. Reprinted with permission from [30], © 2013 American Physical Society.

with graphene is similar to benzene. This comparison casts light on how different separation distances contribute to the nonlocal correlation energy. At a fixed molecule–graphene distance, vdW-DF1 shows (figures 18 and 19) that the binding contributions of benzene and C_{60} are almost identical at short separations but different at larger separations. The repulsive contributions for short separations reflect the oscillatory shape of the vdW-DF kernel in figure 8. At asymptotic separations the vdW-DF description of C_{60} has shortcomings as discussed in section 3.4. In spite of this, vdW-DF provides a good description of the binding energy of C_{60}, relative to benzene. The vdW-DF1 values, of 0.49 for benzene and 0.85 eV for C_{60}, agree with experiment. The higher binding energy of C_{60} comes primarily from the larger vdW attraction of the bigger C_{60} molecule; yet, a small contribution also comes from a charge transfer induced dipole (figure 19). The presence of such a dipole suggests that C_{60} can act as a contact to graphene in molecular electronics [86].

Understanding metal-organic interfaces is important for the development of organic-light emitting diodes and molecular electronics. The nature of such interfaces is determined by the combination of different physical effects. For flat aromatic molecules on (1 1 1) metal surfaces the type of adsorption can range from weak (dominated by vdW forces but softened by a small amount of charge transfer, typical for coinage metals) to strong chemical binding (typical for transition metals), with vdW forces significantly contributing to the binding [101, 251]. Capturing the fine balance between attractive and repulsive contributions to the binding is challenging for theory. Early calculations for benzene on coinage metals gave promising binding energies with vdW-DF1 [99, 230]. However, comparisons with experimental vacuum-level shifts for benzene [230] and bigger molecules [252–254] indicate that vdW-DF1 overestimates the separation by as much as 0.4–0.8 Å, more than twice of what is typical for vdW-DF1. Normal incidence x-ray standing wave experiments for the PTCDA molecule adsorbed on Ag(1 1 1) provide further evidence for this overestimation, with vdW-DF1 predicting 3.6 Å [50, 108] compared to an experimental value of 2.86 Å [255]. Aromatic molecules on coinage metals were one kind of system where improvements were sorely needed. Work by Hamada and Tsukada [256] and by us [90] showed that this issue can be resolved by updating the exchange choice. However, the excellent capabilities of vdW-DF were only recently established with a string of extensive studies combining vdW-DF1 correlation with optB88 and optB86b exchange, providing accurate results for binding separations and energies both for the weaker adsorption on coinage metals and the stronger adsorption on transition metals [251, 257–260]. New studies also indicate that vdW-DF-cx [108] and vdW-DF2-B86R [260] are well suited for describing these kinds of systems.

Callsen and coworkers compared the results of a combined GGA and DFT-D calculation with those of vdW-DF1 for the weak-chemisorption of thiophene on Cu(1 1 1) [261]. The nonlocal-correlation energy density, derived as the spatially-resolved contribution to the vdW-DF1 (44) is determined. Using this approach, the binding is shown to arise from a wide region that exists between the adsorbate and the substrate.

The finding is fully corroborated by an analysis of the nonlocal-correlation binding presented (by other means) in [30, 109]. The saddle-point or trough-like regions between interacting fragments are important to this and related effects. This insight and the realization that these regions correspond to low-to-moderate values of the scaled-density gradient were instrumental in the design of the recent consistent-exchange functional in vdW-DF-cx [107–109].

7.3.2. In porous materials. Adsorption on surfaces builds the foundation for exploring the adsorption within porous materials. Nanoporous materials have seen a surge in interest over the past few decades. A driving force is their potential for wide applicability in practical devices ranging from sensing to gas separation and storage. Of particular interest are applications for hydrogen storage and carbon capture, where relevant

materials challenge first-principles materials modelling: the adsorbate typically binds to the host via physisorption, making vdW interactions important. On the other hand, the host material itself is typically an extended system of considerable size. As such, methods are needed that can treat extended systems and vdW interactions on the same footing—a perfect application for vdW-DF.

The first studies of vdW-DF on porous materials investigated the binding energy of H_2 in metal organic framework (MOF) materials [262, 263]. MOFs consist of metal clusters connected by organic linkers, typically creating networks of cavities or channels inside. Due to the vast number of choices for both the metals and the linkers, the number of MOFs that can be synthesized is beyond counting. In the recent past, due to size limitations, quantum-chemical calculations have focused on understanding how molecules such as hydrogen interact with the linker fragments as a gauge of how a particular MOF would perform. Similar considerations can be applied to other porous materials, such as clathrates and nanoporous carbons. vdW-DF calculations have shown that the binding in the true porous structure is significantly enhanced beyond that predicted by simple arguments based on linker fragments.

Furthermore, vdW-DF calculations show remarkable agreement with experimental signatures such as infrared (IR) frequency and nuclear-magnetic resonance signal shifts and heats of adsorption [264–271]; for a short review on the integration of experiment and vdW-DF calculations see [272, 273]. The ability to monitor changes in IR spectra *in situ*, combined with vdW-DF calculations can be crucial for developing a complete atomistic understanding of the dynamics of molecules such as H_2, CO_2, and H_2O within porous media [274]. Understanding these mechanisms can be powerful tools for designing MOFs with new functionalities or preventing degradation. For example, based on knowledge of how water molecules interact with the framework, a new class of MOF, called F-MOF, was designed to overcome this problem by fluorinating the inside of its cavity [275]. Fluoride ligands repel water molecules, which then start to form small water clusters in the MOF cavity rather than causing the MOF to degrade. Another study related to the hydrogen storage capacity of MOFs [276] investigated the filling of such MOFs with $(H_2)_4CH_4$, a vdW crystal itself. $(H_2)_4CH_4$ has the highest hydrogen mass-storage density of all materials, except pure hydrogen itself, but is unfortunately not stable under practical conditions. The results of the study showed that these MOFs can be used to significantly improve the stability window of $(H_2)_4CH_4$ by providing external pressure to such clusters in its cavity.

Clathrates, another class of porous materials, are similar to MOFs with large cages which can be used for gas storage. They are formed under low temperatures or high pressures and are found at the bottom of the ocean in huge deposits around the globe. Naturally occurring clathrates typically have CH_4 trapped inside, which is believed to be responsible for their stability. A first study of the binding and diffusion of CH_4, CO_2, and H_2 in the clathrate structures SI and SH is reported in [277]. The authors show that the adsorption

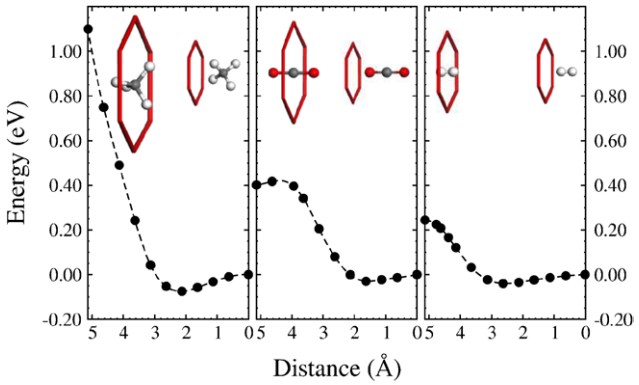

Figure 20. Diffusion barriers for (left) CH_4, (middle) CO_2, and (right) H_2 molecules through a clathrate cage. All energies are reported with respect to the adsorption energy of the molecule at the centre of the clathrate cage. The relaxation of the framework (shown in the inset, not to scale) is essential for obtaining accurate barriers for diffusion. Reprinted with permission from [277] © 2010 American Physical Society.

energy is dominated by vdW, interactions and that without them, gas hydrates would not be stable. The authors further find that the calculated maximum adsorption capacities as well as the maximum hydrocarbon size that can be adsorbed are in good agreement with experiment. One particularly interesting discovery is that the relaxation of the host lattice is crucial for an accurate description of molecule diffusion, as the framework deforms significantly when molecules diffuse from one cage to another (see figure 20). A follow-up study [278] expands the same ideas to rotational barriers of molecules in various types of cages and also includes the structure SII—which is particularly challenging to model, as its unit cell contains 408 atoms—demonstrating the efficient scaling of vdW-DF.

Adsorption in nanoporous carbons brings a new challenge to theory and computation. Unlike clathrates and MOFs, these do not contain regularly sized pores. In fact, depending on starting materials and synthesis conditions they can have varied distributions of pores. Modern approaches, particularly neutron scattering, have been developed to probe the microstructure of pores [279]. Using vdW-DF combined with an efficient continuum model it was shown that adsorption capacities and heats of adsorption could be predicted for a wide range of carbons and for both H_2 and methane, with knowledge of only the pore distribution [280, 281]. This method can also be used to define the optimal pore size range that enhances adsorption [281]. This study further provides insight into why carbons that seem similar adsorb very different amounts of a particular molecule. The approach mentioned here could be the foundation for rapid screening for the design of highly adsorbing nanoporous materials.

7.3.3. Strong versus weak adsorption. The adsorption of molecules to metal and semiconducting surfaces is of tremendous practical importance for catalysis, self-assembly, and the formation of molecule-metal junctions or templates for the growth of porous materials. In many cases, these involve interactions that span the range of strong chemisorption bonds

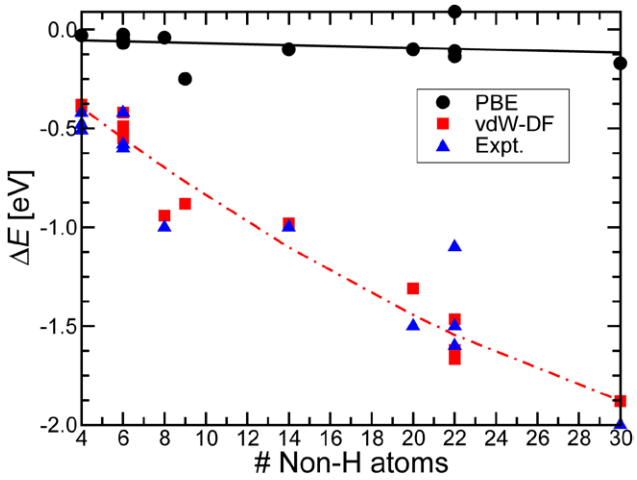

Figure 21. Interaction energy as a function of non-hydrogen atoms for a range of organic molecules on metal surfaces. Black circles, red squares, and blue triangles represent PBE, vdW-DF, and experimental data, respectively. The solid black line and red dashed lines are fits to the data.

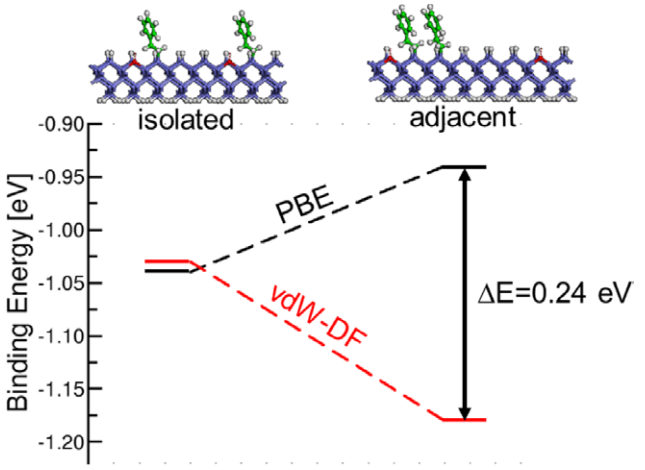

Figure 22. Interaction energies for monomers and dimers adsorbed on the H-terminated Si surface. The fact that the difference in energy between PBE and vdW-DF for the dimers is roughly equal to that of gas-phase dimers demonstrates the crucial role that dispersion interactions play in the self-assembly of styrene wires on these surfaces.

to what has been thought of as weakly physisorbed states. Traditionally, it was thought that the strongly chemisorbed states could be adequately represented by standard GGA-type functionals and that dispersion interactions would only play a small role in physisorbed states. Recent work however using vdW-DF has illustrated that dispersion interactions play important roles in both regimes. For example, many studies have explored the physisorption of organic molecules to different noble metal surfaces (i.e. Ag, Cu, Au and Pt) [83, 97, 99–101, 230, 250, 252–254, 257, 282–284]. These papers find that vdW-DF brings the adsorption energies of these molecules into the correct order of magnitude as compared with experiment, a vast improvement over GGA. A survey of adsorption energies demonstrates that they depend strongly on the size of the molecule. Figure 21 illustrates this trend, relating binding energy to molecular size ($\sim N - N^2$). This simple trend arises even if the molecules all have different structures—some chains, some with connected six-membered rings, some with and some without additional atoms such as N and O—and it is irrespective of the surface being considered. This contrasts PBE results that show very little binding and no dependence on molecular size.

Furthermore, some adsorption studies highlight the importance of atomic relaxations. Results for melanine, PTCDA, and NTCDA adsorption show that the difference in binding energy between fully relaxed and non self-consistent calculations, or calculations with static molecule and surface geometries, may be as large as 20% [282]. Adsorption studies also provide an understanding of the organization of overlayers of organic molecules [97, 99, 100, 250, 285, 286] and water [287, 288] as well as their spectroscopic signatures [230, 253, 254].

Some of the earlier studies on adsorption employed vdW-DF1 and therefore overestimate molecule-surface separation distances. This overestimation can be larger for adsorption on some metals than what would be typically expected for other systems [9, 108, 230].

The chemisorption of molecules on surfaces is also affected by dispersion interactions. In some cases, the adsorption of a molecule can be dramatically stabilized, allowing the molecule to stick to the surface. For example, the adsorption of Alq_3 on the Mg(0 0 1) surface [285] requires a delicate balance between structural deformations and weaker surface adsorption. PBE predicts that these molecules would be weakly bound, whereas vdW-DF calculations stabilize the binding by up to 900 meV over the PBE energies. In other cases, this interaction can stabilize a particular adsorption configuration. For instance, traditional DFT calculations predict that for benzene adsorbed to the silicon surface the tight-bridge configuration is the most stable. In contrast, vdW-DF, in spite of predicting a binding energy that differs merely by ∼0.2 eV from the PBE result, shows a preference for the butterfly configuration, in agreement with MP2 calculations and experiment [81]. This change in interaction energy is primarily due to molecule-surface interactions mediated by dispersion forces [91]. In addition to the interaction between the molecule and surface, interactions between molecules on a surface can significantly affect how molecules arrange themselves [85]. For instance, vdW interactions between styrene molecules drive their self-assembly on H-terminated Si [286]. Figure 22 depicts the interaction energies for isolated styrene molecules and dimers chemisorbed on the Si surface obtained with PBE and vdW-DF. As can be seen from the plot, vdW interactions stabilize the dimer configuration over the isolated monomers. Here, the energy difference of 0.24 eV between PBE and the vdW-DF calculations for the dimer configuration is roughly equal to the difference in binding energy for a gas-phase dimer (≈0.21 eV) between the two functionals. vdW interactions also play a key role in the self-assembly of aromatic molecules on surfaces with low corrugation, such as coinage metal surfaces, where the competition with surface-mediated interactions [97, 99, 100]—which has an even longer range than vdW forces—ultimately controls adsorption geometries and energies.

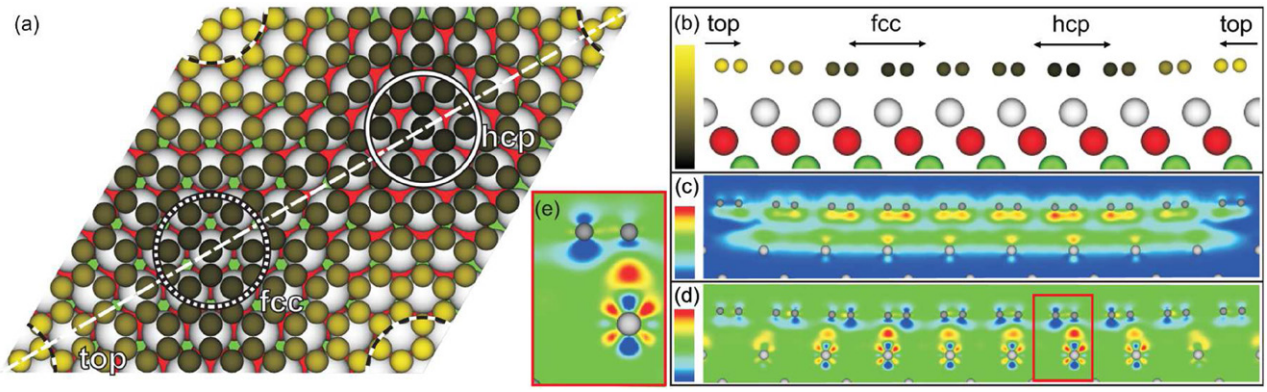

Figure 23. (*a*) Top view and (*b*) side view (cut along the dashed line in (*a*)) of the relaxed structure of graphene/Ir(1 1 1) obtained by vdW-DF. Regions of high-symmetry stacking (fcc, hcp, top) are marked by circles (*a*) or arrows (*b*)–(*d*). (*c*) Visualization of the nonlocal-correlation binding-energy density caused by adsorption. (*d*) Charge transfer upon adsorption. A negative value indicates loss of electron density. (*e*) Magnified view of red box in (*d*). Reprinted with permission from [289], © 2011 American Physical Society.

Such interplay between strong and weak interactions are even more evident when considering the crossover from molecules to graphene adsorbed on metal surfaces. In a concerted effort of experiment (standing-wave x-ray diffraction) and theory (vdW-DF), epitaxy has been studied in Ir(1 1 1) [289]. In fact, epitaxial growth on metals is a key method for producing high-quality graphene on large scales. In the interface region the strength of the C–C bonds varies. Large incommensurate or weakly commensurate superstructures are found for lattice-mismatched systems. In the case of graphene on Ir(1 1 1), precise agreement between calculated (3.41 Å of the C atom; DFT-GGA calculations give 3.9 Å) and measured (3.38 Å) values for the mean height has been obtained. This allows for the interpretation that the bonding of graphene to Ir(1 1 1) is due to vdW interactions with an additional antibonding average contribution arising from chemical interactions [289]. Despite its globally repulsive character, in certain areas of the large graphene moiré unit cell, charge accumulation between the Ir substrate and graphene C atoms is observed, indicating the formation of a weak covalent bond. In other words, graphene on Ir(1 1 1) can be described as physisorption with chemical modulation. Thanks to the vdW-DF analysis this can be clearly illustrated, as in figure 23. Here, the variation over the unit cell of the nonlocal-correlation energy density and charge transfer caused by adsorption is depicted. This example emphasizes the fact that dispersion interactions are essential in weakly bound systems, while having significant contributions to the binding in systems that are chemically bound to a surface. These interactions thus play an important role in many processes at surfaces that are fundamental to many modern applications such as catalysis and molecular self-assembly. Therefore, this result provides a useful benchmark for the applicability of the nonlocal functional. [289] shows also another important aspect, namely that the vdW-DF is a handy tool in the everyday collaboration with experimentalists.

A final poignant example is that of the so-called CO-adsorption puzzle [290]. For CO chemisorption on metals, GGAs almost always favours a hollow site, whereas experiments reveal that top-site adsorption is typical, for example, on Pt, Rh, Cu. This failure of GGAs was particularly surprising given the fact that CO bonds to a metal surface should be covalent in character and should thus be adequately described by GGAs. In this regard, Lazić and co-workers reported an important early demonstration of vdW-DF, showing that the inclusion of vdW interactions offered a promising solution to this long standing issue [291]. Appearing in parallel were demonstrations that RPA also corrects GGA errors in finding a top-site CO-adsorption preference on Cu(1 1 1) [159, 292], further indicating the importance of nonlocal correlations. The behaviour of RPA was anticipated by [291]. The CO-adsorption progress was important to development efforts as it gave early indications that vdW-DF could serve as a general-purpose functional [57, 108, 109, 293]. Thus emphasizing the the aim of the vdW-DF method to work both for sparse matter (where GGA fails) as well as for dense matter (where GGA often but not always succeeds).

We note that the vdW-DF method and its variants are gaining acceptance as a first-principle method that can be trusted to predict properties of a wide array of materials. For example, Kokott and coworkers used vdW-DF-optB86b to provide first-principle predictions of the impact of nonmetallic substrates on the bandstructure of silicene overlayers [294]. They demonstrate that a cleaved CaF_2 surface will leave the electron dynamics in the silicene overlayer unchanged from that of a buckled free standing film and suggest intensive experimental studies based on their first-principles vdW-DF exploration. Also, Sun and coworkers have combined both vdW-DF1 and vdW-DF-optPBE with the DFT + U formalism to map out the hydrogenation of Pu and Pu-oxides [295]. Here, the vdW-DF + U description is used in an *ab initio* molecular dynamics exploration of how H_2 molecules penetrate various Pu-oxide surfaces. Generally, When experiments are scarce, trust in the overall results seems to now be built on the fact that vdW-DF represents a parameter-free approach.

In general, the extensive use and benchmarking of vdW-DF suggests that it is indeed capable of accounting for dispersion interactions involved in the adhesion of molecules (and materials) to surfaces and within pores. These results give promise for extending the method to examining the

properties of densely packed materials and large molecular systems.

7.4. Solids and liquids

In organic crystals, physical and chemical properties are strongly influenced by the structure of the material. The structure depends on mutual forces between the participating atoms and often on growth conditions, which lead to differences in crystal packing. In such a thermal process weak forces also play a role, for instance in the arrangement of hydrogen bonds and π–π stackings within the crystal. This often makes it hard to consistently produce high quality samples. Knowledge of which polymorphs can form and their respective properties is therefore of great importance for both the synthesis and application of organic crystals.

Given the number of different crystal structures that can form and how close their corresponding cohesive energies are to the ground-state structure, theoretical crystal structure prediction is a daunting task. This challenge is even more dramatic for liquids, where there are no periodic structures and innumerable different configurations can form. As such, the study of vdW bonded solids and liquids is yet another good application for vdW-DF.

Perhaps the prototypical class of a vdW bonded solid are layered materials such as graphite, hexagonal boron nitride (*h*-BN), and metal dichalcogenides like MoS_2. Here, covalently bonded 2D layers are attracted to each other via interplanar dispersion interactions. In fact, initial attempts at developing vdW-DF were mostly focused on the interactions between layered materials [29, 58], as discussed in section 5. Successive improvements of vdW-DF have led to an even better description of the binding of graphite, as seen in figure 7, thus setting vdW-DF up for extensive studies of other vdW bonded layered materials [107, 165, 224, 296], such as V_2O_5 [74, 92] and graphane [75].

Luo and co-workers used vdW-DF-C09 to examine the atomic, electronic, and thermoelectric properties of Bi_2Se_3 and Bi_2Te_3 [297]. They showed that by including vdW interactions they were able to obtain much better agreement with the experiment for the structural properties of the two materials. Furthermore, using this structural model their band structures gave equally good qualitative agreement with photoemission spectra. Even more interestingly, they demonstrated that strain could be used to tune the thermoelectric properties, with the *n*-type Seebeck coefficient of Bi_2Te_3 increasing under compressive inplane strain and Bi_2Se_3 increasing under tensile strain.

The ability to accurately model the interactions between planes opens up the potential for studying real world applications such as the intercalation of ions between graphene sheets [73, 108], which is relevant to battery technology, and understanding the pore size dependent adsorption of neutral non-polar molecules [280, 281], such as H_2 and CH_4, which is critical for alternative energy technologies. The spintronics of a ferromagnet/graphene junction, Co(0001) with graphene, was studied in [298]. This system is another example in which there is strong charge rearrangement at short distances but the binding comes from nonlocal correlation.

Complementary to the 2D layered materials, crystal structures comprised of carbon nanotubes and long-chain hydrocarbons have also been studied using vdW-DF [76, 93–96]. These studies were discussed in more detail in a previous review [66]. It is interesting to note, however, that the intertube interaction energy was determined to be on the order of that found in graphite.

Due to the many possible molecules, a huge number of potential molecular crystals are believed to exist, out of which only a comparatively few have been synthesized. The inability to predict molecular crystal structures is one of the most notorious failures of traditional DFT methods. With this in mind, vdW-DF has been applied to the study of organic crystal structures, exhibiting significant predictive capabilities [9, 239, 299].

In addition, vdW-DF has been used to explore the physical properties of functional materials. For instance, a ferroelectric organic crystal comprised of phenazine and chloranilic acid [240] and boron based hydrogen-storage materials, such as ammonia borane (NH_3BH_3) [300] and magnesium borohydride ($Mg(BH_4)_2$) [301], have been studied. In the case of $Mg(BH_4)_2$ it is not obvious that dispersion interactions would play a role in defining the crystal structure. It has long been assumed that covalent interactions dominate and are responsible for its structure. However, the results of [301] show that the inclusion of vdW interactions between the BH_4 units is crucial for getting the correct ground-state structure. The application of vdW-DF led—for the first time—to good agreement with experiment, favouring the α-$Mg(BH_4)_2$ phase (P6122) and a closely related $Mn(BH_4)_2$-prototype phase (P3112) over a large set of polymorphs at low temperatures. This study thus demonstrates the need to go beyond semilocal density functional approximations for a reliable description of crystalline high valent metal borohydrides.

A particularly interesting non-standard dimer that forms a molecular crystal is presented in [302], i.e. the phenalenyl dimer and closed-shell analogues. Phenalenyl—an open-shell neutral radical that can form both π-stacked dimers and conducting molecular crystals—has gained attention for its interesting and potentially useful electrical and magnetic properties. The results indicate that vdW-DF is capable of qualitatively describing the interaction between two neutral radicals in the π-stacked configuration, giving binding distances that are significantly below the sum of the vdW radii, in agreement with experiment.

A recent derivation of the appropriate formalism for calculating stress in vdW-DF can be a useful tool in many studies of systems at finite pressure. For instance, the pressure-dependent phase transitions of amino acid crystals have been explored [211].

Bulk water itself has long been a particularly difficult material to model. Results of vastly overestimated LDA and GGA freezing temperatures of water triggered the first applications of vdW-DF to small water clusters. The smallest water system, i.e. the water dimer, is part of the S22 data set and its vdW-DF results have been reported as part of the benchmark

calculations [63, 106, 107, 196]. Further exploratory studies have focused on the energetic, structural, and vibrational properties of small water clusters $(H_2O)_n$ with $n \leqslant 6$ and standard ice I_h [303–305]. In addition, while vdW-DF shows significant improvements with regards to the structure and binding energies over LDA and GGA, a remarkable improvement is also found for the vibrational frequencies. In-depth analyses shed light on why LDA and GGA fail in describing water.

The improvements of vdW-DF for small water clusters gives hope that the freezing temperature of bulk water predicted with DFT calculations might also be improved. Indeed, recent vdW-DF simulations show remarkable differences in the predicted structure of water [105, 306], again better aligned with experiment.

Finally, it should be noted that vdW-DF is also capable of describing traditional densely packed solids. Whereas the vdW-DF1 and vdW-DF2 descriptions predict somewhat too large volumes for some inorganic crystals, other modern vdW-DF variants actually perform better than a standard semilocal functional like PBE [107–109, 197].

7.5. Biological molecules

Soft matter is fundamental for all life. Not only do dispersion forces play a critical role in defining form and function of genetic material, but they are crucial in the interactions of organic molecules with the genetic material and thus critical for our understanding of how to treat many diseases.

For a review on molecular simulations of biomaterials, see [307]. Indeed, initial vdW-DF studies focused on examining the interactions between and within DNA base pairs [102, 308] and between base pairs and anti-cancer drugs [103]. Even with the systematic overestimation of separation distances typical of vdW-DF1, the importance of including dispersion interactions was evident. For instance, the twist and rise of DNA clearly emerge as a result of nonlocal interactions, with unprecedented agreement with x-ray crystallography data and computationally costly quantum-chemical calculations. A more detailed summary of our early studies can be found in [66]. Recently, a Harris-type scheme [79] has been explored for speeding up vdW-DF calculations of large sparse matter system, such as the interactions between strands of DNA [104]. The results demonstrate the ability to scale such calculations to large numbers of atoms with limited effects on accuracy.

There has been recent interest in using DNA molecules as molecular wires. This involves the adsorption and interaction of nucleobases with metal surfaces and other substrates such as graphene. In theoretical studies, graphene is also used as a model for carbon nanotubes, which can be used in applications in medicine and as sensors. The adsorption of nucleobases and other biological molecules on graphene provides a venue for studying the complicated interactions between nucleobases in biological matter and thus casts light on processes such as molecular recognition and self assembly. As a first step, the adsorption of adenine on graphene was studied and compared with the two-dimensional crystal forming in the denser phase [85]. This work was later followed by studies of all five nucleobases [88].

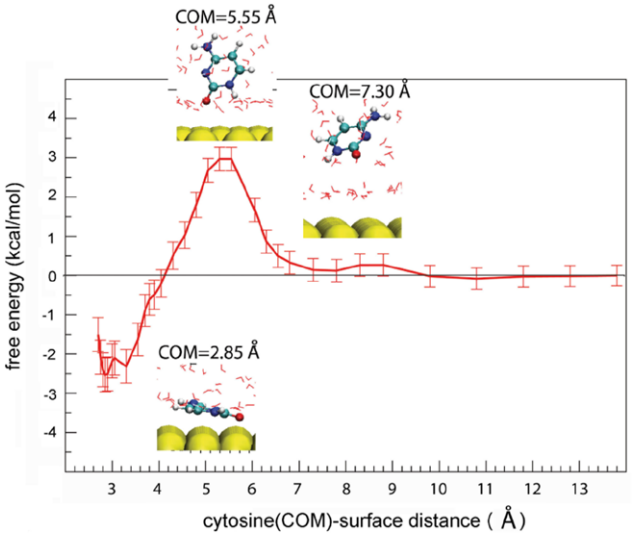

Figure 24. Potential energy surface for the adsorption of cytosine to the Au(1 1 1) surface obtained with the GolDNA-AMBER force field derived from vdW-DF calculations. Adapted with permission from [309], © 2014 American Chemical Society.

It is often necessary to study biomolecules in solution, possibly including the effect of entropy. To this end, classical molecular dynamics atomistic simulations are used, utilizing force fields to describe the atomic interactions. An example where vdW-DF calculations were used to tune parts of such a force field is the study of DNA bases in aqueous solution adsorbed on Au(1 1 1), defining the new GolDNA-AMBER force field [309]. Using this vdW-DF derived potential they were able to map out the potential energy surface for the adsorption/desorption of DNA bases from the Au(1 1 1) surface (see figure 24).

Naturally, given the societal benefits of understanding the interactions of biomolecules, either from a biological or technological perspective, it is expected that applications in this arena will surely increase in years to come. This is especially true, given advances in computers and algorithms that will allow for the study of materials on biologically relevant scales.

Dispersion interactions are ubiquitous and our understanding of them is still developing. As demonstrated in many recent applications, these forces are necessary not only for prototypical weakly bound systems, but also play a vital role in materials where they were traditionally thought of as negligible. As new methods, algorithms, and computational resources continue to develop and evolve, we expect to see methods that include these interactions becoming even more widely used.

8. Conclusions and outlook

Today's emphasis in computational materials science has shifted from semiconductors and metals to nanomaterials and biological materials. With this new emphasis, the standard tools of the past—LDA- and GGA-based DFT—often fall short because of the many low-density regions, i.e. vdW regions. Several pictures of vdW forces have been touched upon in this review, starting with the London picture and later

continuing with the vdW-DF method which unifies these different pictures of vdW forces within a DFT framework derived from the coupling-constant integration of the adiabatic connection formula. The efforts to develop vdW-DF have been driven by the need for general purpose theoretical tools that can describe molecules, bulk materials, and surfaces on equal footing. To do so, we need to describe both dense and sparse electron systems.

For ground-state properties DFT has been used for half a century, yet only within the most recent decade has its applicability to sparse, and hence general matter, been significantly improved. There are many examples of systems where such methods are needed, far beyond those indicated in this review. With the aim of designing general-purpose methods, non-empirical criteria are preferable. vdW-DF is such a method, delivering simple yet accurate and robust functionals.

Initial vdW-DF developments focused on the nonlocal correlation. Contact had to be made with available vdW results at that time; typically the asymptotic behaviours of simple model systems. The ALL and related descriptions gave the correct R^{-6}, z^{-3}, and d^{-2} forms for model systems and simple formulas for the vdW parameters. These led to promising quantitative results. The later-developed vdW-DF0 and vdW-DF1 functionals further advanced the field with significant improvements in the description of vdW-bonded regions. The vdW-DF1, usually called vdW-DF, is in common use and has given many valuable results, especially for adsorbed molecules and bulk materials. Physically motivated by issues of overestimation of separations and underestimation of H-bond energies of small molecule and molecule-molecule interactions, vdW-DF2, with its update to the exchange energy and the nonlocal correlation energy, brought further enhancements.

More recently, the focus has switched to exchange with the purpose of improving performance and for internal consistency reasons. Issues related to the overestimation of separation distances were solved with new exchange variants paired with vdW-DF1. Modern variants to the exchange also provide a good account of systems beyond the vdW regime, such as covalent solids and systems with a mix of different binding characteristics, giving interaction energies that now approach chemical accuracy. For internal consistency, one could also use an exchange functional derived from the same plasmon-based model from which the nonlocal correlation energy was derived. The recent functional vdW-DF-cx stands out in its attempt to do so.

A major advance on the computational side was the move from slow, non self-consistent, in-house codes to stable, efficient, FFT-based codes implemented in mainstream DFT packages. Now, the many diverse and successful applications of the vdW-DF method have helped to paint a modern picture of vdW forces, where they play an essential role, even in systems traditionally thought to be dominated by ionic or covalent bonding.

The excellent performance for bulk systems for modern variants makes vdW-DF a contender for a spot in the standard repertoire of the contemporary materials scientist. There are phenomena and processes where the flexibility of DFT is called for: for instance, when the extended nature of the polarized electrons really matters, like for molecules on metal surfaces where the characteristics of the bulk and surface are drastically different; or for charge transfer and screening at, for example, grain boundaries. Catalytic processes on surfaces and in sparse matter, such as MOFs is yet another example.

As for the future of vdW-DF, a good starting point is to consider its weaknesses, as we see them. To begin with, current variants of vdW-DF lack spin and the explicit exchange mechanisms typical of hybrid functionals. Other issues include low accuracy for noble-gas dimers, incorrect asymptotic power laws of low-dimensional structures and metals, and *d*- and *f*-electron effects.

Spin properties can be introduced by extending the treatment through first-principle arguments. Like in the local spin density approximation, this means that up and down spins will be described by different potentials. Such a development will make it possible to describe, for instance, ionization potentials of atoms and molecules, and magnetic materials, which in fact are often bound by vdW forces.

The lack of hybrid features might be solved by attempting to apply arguments used to extend GGA. Hybrid functionals often only change the exchange. The fact that PW86r was chosen for vdW-DF2 because it mimics Hartree–Fock could be helpful in making such an extension.

For the future, higher accuracy will likely be obtainable for many physical effects. A possible solution for the problem of dealing with noble gases could be to carefully design a gap mechanism, like that in dielectric semiconductor models, and then possibly learn from the VV functionals. For the asymptotic behaviour of low-dimensional structures and metals possible solutions require updating the plasmon model to capture sophisticated many-particle effects.

The ultimate solution would be to generalize the theory underlying the unified treatment in [53], involving an explicit solution of the electrodynamics to smaller separations and to solve it efficiently. In fact, the vdW-DF0 attempts to do such a generalization, but for the very restrictred layered geometry and with an inaccurate plasmon model. Ultimately, strong connections with these earlier models would be extremely beneficial for the future development of vdW-DFs.

As more and more systems are revealed to be affected by vdW forces, we believe that vdW-DF could replace GGA. On the other hand, methods such as RPA and developments in that direction might replace vdW-DF for smaller-to-medium sized vdW bonded systems. However, bigger systems and time-dependent calculations will still require DFT-based methods. Nevertheless, new functionals within the vdW-DF family are expected to be derived or present variants may be extended (as mentioned, spin is currently being developed). It is also likely that vdW-DF will continue to inspire the development of other nonlocal correlation functionals that might capture additional physical effects or be specialized for particular kinds of systems.

If we dare to speculate, we believe that nonlocal correlation functionals will replace dispersion-corrected DFT in practical use. Nonlocal correlation functionals rest on firmer physical foundations, are more flexible, can be as fast as local and semi-local functionals and are available in all major codes.

For systems outside the reach of DFT, force field methods will still have its place.

In conclusion, dispersion interactions are ubiquitous and our understanding of them is still developing. As demonstrated in many recent applications, these forces are necessary not only for prototypical weakly bound systems, but also play a vital role in materials where they were traditionally thought of as negligible. New systems for applying the vdW-DF method are probably bigger, more extensive, and sparser than today's materials and more often involve time-dependent phenomena. Disordered systems, liquids, systems with several length scales, systems with several kinds of competing interactions, and biological systems are cases of such systems. The vdW-DF method adheres to important conservation rules—a feature that has good potential for transferability and lays the foundation for broader conclusions about the capacity of the method. With positive results in test cases that can be seen as difficult and that cover a range of problems where interactions compete [108], there is also potential for good performance for general problems. The vdW-DF method so far provides competitive density functionals for sparse matter and its robust and flexible formulation offers a promise for further improvements [66, 108]. As new methods, algorithms, and computational resources continue to develop and evolve, we expect to see methods that include these interactions becoming even more widely used. That said, there is truly an open playground ready to be explored—where dispersion interactions are no longer an afterthought, but a key interaction that must be understood.

Acknowledgments

Our late colleague D Langreth was first invited by Reports on Progress in Physics (RoPP) to review our vdW-DF method. Sadly, David barely got time to start it. We owe him a lot and therefore dedicate this review to him. We thank K Z Soliman for the careful checking of the references. We also thank M Kuisma and T L Einstein for comments and discussions. Work by KB, ES, and PH was supported by the Swedish Research Council (VR) under grants VR-2011-4052 and VR-2010-4149 and by the Chalmers Area of Advance, Materials. TT acknowledges support from US NSF Grant No. DMR-1145968. VRC was supported by the US Department of Energy Office of Science, Basic Energy Sciences, Materials Sciences and Engineering Division. KL was supported by the US Department of Energy, Office of Basic Energy Sciences, Division of Chemical Sciences, Geosciences, and Biosciences under award DE-FG02-12ER16362.

References

[1] Lundqvist B I, Andersson Y, Shao H, Chan S and Langreth D C 1995 Density functional theory including van der Waals forces *Int. J. Quantum Chem.* **56** 247–55

[2] Grimme S 2011 Density functional theory with London dispersion corrections *WIREs: Comput. Mol. Sci.* **1** 211–28

[3] Tkatchenko A, Romaner L, Hofmann O T, Zojer E, Ambrosch-Draxl C and Scheffler M 2010 van der Waals interactions between organic adsorbates and at organic/inorganic interfaces *MRS Bull.* **35** 435–42

[4] Johnson E R, Mackie I D and DiLabio G A 2009 Dispersion interactions in density-functional theory *J. Phys. Org. Chem.* **22** 1127–35

[5] Burns L A, Vázquez-Mayagoitia Á, Sumpter B G and Sherrill C D 2011 Density-functional approaches to noncovalent interactions: a comparison of dispersion corrections (DFT-D), exchange-hole dipole moment (XDM) theory, and specialized functionals *J. Chem. Phys.* **134** 084107

[6] Gräfenstein J and Cremer D 2009 An efficient algorithm for the density-functional theory treatment of dispersion interactions *J. Chem. Phys.* **130** 124105

[7] Vydrov O A and Van Voorhis T 2012 Nonlocal van der Waals density functionals based on local response models *Fundamentals of Time-Dependent Density Functional Theory* ed M A L Marques *et al* (Berlin: Springer) p 443

[8] Cooper V R, Kong L and Langreth D C 2010 Computing dispersion interactions in density functional theory *Phys. Proc.* **3** 1417

[9] Klimeš J and Michaelides A 2012 Perspective: advances and challenges in treating van der Waals dispersion forces in density functional theory *J. Chem. Phys.* **137** 120901

[10] Becke A D 2014 Perspective: 50 years of density-functional theory in chemical physics *J. Chem. Phys.* **140** 18A301

[11] van der Waals J D 1873 Over de continuiteit van den Gas- en Vloeistoftoestand (on the continuity of the gas and liquid state) *PhD Thesis* University of Leiden, Leiden, The Netherlands

[12] Margenau H and Kestner N R 1969 *Theory of Interatomic Forces* 2nd edn (Oxford: Pergamon Press)

[13] Eisenshitz R and London F 1930 Über das Verhältnis der van der Waalsschen Kräfte zu den homöopolaren Bindungskräften *Z. Phys.* **60** 491–527

[14] London F 1937 The general theory of molecular forces *Z. Physik. Chemie* **33** 8–26
Hettema H 2000 English translations *Quantum Chemistry, Classic Scientific Papers* (Singapore: World Scientific)
London F 1937 *Trans. Faraday Soc.* **33** 8

[15] London F 1930 Zur Theorie und Systematik der Molekularkräfte *Z. Phys.* **63** 245–79

[16] Lennard-Jones J E 1932 Processes of adsorption and diffusion on solid surfaces *Trans. Faraday Soc.* **28** 333–59

[17] Persson M and Andersson S 2008 Physisorption dynamics at metal surfaces *Handbook of Surface Science* 3 ed E Hasselbrink and B I Lundqvist (Amsterdam: Elsevier) p 95 chapter 4

[18] Hohenberg P and Kohn W 1964 Inhomogeneous electron gas *Phys. Rev.* **136** B864

[19] Kohn W and Sham L J 1965 Self-consistent equations including exchange and correlation effects *Phys. Rev.* **140** A1133–8

[20] Jones R O and Gunnarsson O 1989 The density functional formalism, its applications and prospects *Rev. Mod. Phys.* **61** 689–746

[21] Burke K and Wagner L O 2013 DFT in a nutshell *Int. J. Quantum Chem.* **113** 96–101

[22] Hedin L and Lundqvist B I 1971 Explicit local exchange-correlation potentials *J. Phys.* C **4** 2064

[23] von Barth U and Hedin L 1972 A local exchange-correlation potential for the spin polarized case: I *J. Phys.* C **5** 1629

[24] Gunnarsson O and Lundqvist B I 1976 Exchange and correlation in atoms, molecules, and solids by the spin-density-functional formalism *Phys. Rev.* B **13** 4274–98

[25] Langreth D C and Mehl M J 1981 Easily implementable nonlocal exchange-correlation energy functional *Phys. Rev. Lett.* **47** 446–50

[26] Perdew J P, Chevary J A, Vosko S H, Jackson K A, Pederson M R, Singh D J and Fiolhais C 1992 Atoms, molecules, solids, and surfaces: applications of the generalized gradient approximation for exchange and correlation *Phys. Rev.* B **46** 6671–87

[27] Perdew J P, Burke K and Ernzerhof M 1996 Generalized gradient approximation made simple *Phys. Rev. Lett.* **77** 3865–8

[28] Zhang P, Crespi V H, Chang E, Louie S G and Cohen M L 2001 Computational design of direct-bandgap semiconductors that lattice-match silicon *Nature* **409** 69–71

[29] Rydberg H, Jacobson N, Hyldgaard P, Simak S I, Lundqvist B I and Langreth D C 2003 Hard numbers on soft matter *Surf. Sci.* **532–5** 606–10

[30] Berland K and Hyldgaard P 2013 Analysis of van der Waals density functional components: binding and corrugation of benzene and C_{60} on boron nitride and graphene *Phys. Rev.* B **87** 205421

[31] de Boer J H 1936 The influence of van der Waals' forces and primary bonds on binding energy, strength and orientation, with special reference to some artificial resins *Trans. Faraday Soc.* **32** 10–37

[32] Hamaker H C 1937 The London–van der Waals attraction between spherical particles *Physica* **4** 1058–72

[33] Reinganum M 1912 Kräfte elektrischer Doppelpunkte nach der statistischen Mechanik und Anwendung auf molekulare und Ionenwirkungen *Ann. Phys.* **343** 649–68

[34] Wang S C 1927 The mutual energy of two hydrogen atoms *Phys. Z.* **28** 663

[35] Lifshitz E M 1955 The theory of molecular attractive forces between solids *Zh. Eksp. Teor. Fiz.* **29** 94
Lifshitz E M 1956 *Sov. Phys. JETP* **2** 73

[36] Dzyaloshinskii I E, Lifshitz E M and Pitaevskii L P 1961 The general theory of van der Waals forces *Adv. Phys.* **10** 165–209

[37] Bohr N and Lindhard J 1954 Electron capture and loss by heavy ions penetrating through matter *Dan. Mat. Fys. Medd.* **28** 1–30

[38] Lindhard J 1954 On the properties of a gas of charged particles *Dan. Mat. Fys. Medd.* **28** 1–30

[39] Nozières P and Pines D 1958 Correlation energy of a free electron gas *Phys. Rev.* **111** 442–54

[40] Mahan G D 1990 *Many-Particle Physics* 2nd edn (New York: Plenum)

[41] Langreth D C and Perdew J P 1975 The exchange-correlation energy of a metallic surface *Solid State Commun.* **17** 1425–9

[42] Langreth D C and Perdew J P 1977 Exchange-correlation energy of a metallic surface: wave-vector analysis *Phys. Rev.* B **15** 2884–901

[43] Rapcewicz K and Ashcroft N W 1991 Fluctuation attraction in condensed matter: a nonlocal functional approach *Phys. Rev.* B **44** 4032–5

[44] Andersson Y, Langreth D C and Lundqvist B I 1996 van der Waals interactions in density-functional theory *Phys. Rev. Lett.* **76** 102–5

[45] Wu X, Vargas M C, Nayak S, Lotrich V and Scoles G 2001 Towards extending the applicability of density functional theory to weakly bound systems *J. Chem. Phys.* **115** 8748–57

[46] Grimme S 2004 Accurate description of van der Waals complexes by density functional theory including empirical corrections *J. Comput. Chem.* **25** 1463–73

[47] Grimme S 2006 Semiempirical hybrid density functional with perturbative second-order correlation *J. Chem. Phys.* **124** 034108

[48] Tkatchenko A and Scheffler M 2009 Accurate molecular van der Waals interactions from ground-state electron density and free-atom reference data *Phys. Rev. Lett.* **102** 073005

[49] Grimme S, Antony J, Ehrlich S and Krieg H 2010 A consistent and accurate *ab initio* parametrization of density functional dispersion correction (DFT-D) for the 94 elements H–Pu *J. Chem. Phys.* **132** 154104

[50] Ruiz V G, Liu W, Zojer E, Scheffler M and Tkatchenko A 2012 Density-functional theory with screened van der Waals interactions for the modeling of hybrid inorganic-organic systems *Phys. Rev. Lett.* **108** 146103

[51] Tkatchenko A, DiStasio R A, Car R and Scheffler M 2012 Accurate and efficient method for many-body van der Waals interactions *Phys. Rev. Lett.* **108** 236402

[52] Hult E, Andersson Y, Lundqvist B I and Langreth D C 1996 Density functional for van der Waals forces at surfaces *Phys. Rev. Lett.* **77** 2029–32

[53] Hult E, Rydberg H, Lundqvist B I and Langreth D C 1999 Unified treatment of asymptotic van der Waals forces *Phys. Rev.* B **59** 4708–13

[54] Rydberg H, Lundqvist B I, Langreth D C and Dion M 2000 Tractable nonlocal correlation density functionals for flat surfaces and slabs *Phys. Rev.* B **62** 6997–7006

[55] Lundqvist B I *et al* 2001 Density-functional bridge between surfaces and interfaces *Surf. Sci.* **493** 253–70

[56] Rydberg H 2001 Nonlocal correlations in density functional theory *PhD Thesis* Department of Applied Physics, Chalmers University of Technology, Göteborg, Sweden http://bitmath.se/rydberg/Thesis

[57] Rydberg H 2001 Nonlocal correlations in density functional theory *PhD Thesis* Department of Applied Physics, Chalmers University of Technology, Göteborg, Sweden (paper number 6) http://bitmath.se/rydberg/Thesis/PaperVI.pdf

[58] Rydberg H, Dion M, Jacobson N, Schröder E, Hyldgaard P, Simak S I, Langreth D C and Lundqvist B I 2003 van der Waals density functional for layered structures *Phys. Rev. Lett.* **91** 126402

[59] Dion M, Rydberg H, Schröder E, Langreth D C and Lundqvist B I 2004 van der Waals density functional for general geometries *Phys. Rev. Lett.* **92** 246401

[60] Dion M, Rydberg H, Schröder E, Langreth D C, Lundqvist B I 2004 van der Waals density functional for general geometries *Phys. Rev. Lett.* **92** 246401
Dion M, Rydberg H, Schröder E, Langreth D C and Lundqvist B I 2005 *Phys. Rev. Lett.* **95** 109902 (erratum)

[61] Langreth D C, Dion M, Rydberg H, Schröder E, Hyldgaard P and Lundqvist B I 2005 van der Waals density functional theory with applications *Int. J. Quantum Chem.* **101** 599–610

[62] Thonhauser T, Cooper V R, Li S, Puzder A, Hyldgaard P and Langreth D C 2007 van der Waals density functional: self-consistent potential and the nature of the van der Waals bond *Phys. Rev.* B **76** 125112

[63] Lee K, Murray È D, Kong L, Lundqvist B I and Langreth D C 2010 Higher-accuracy van der Waals density functional *Phys. Rev.* B **82** 081101

[64] Vydrov O A and Van Voorhis T 2009 Nonlocal van der Waals density functional made simple *Phys. Rev. Lett.* **103** 063004

[65] Vydrov O A and Van Voorhis T 2010 Nonlocal van der Waals density functional: the simpler the better *J. Chem. Phys.* **133** 244103

[66] Langreth D C *et al* 2009 A density functional for sparse matter *J. Phys.: Condens. Matter* **21** 084203

[67] Gunnarsson O, Jonson M and Lundqvist B I 1979 Descriptions of exchange and correlation effects in inhomogeneous electron systems *Phys. Rev.* B **20** 3136–64

[68] Andersson Y, Hult E, Rydberg H, Apell P, Lundqvist B I and Langreth D C 1997 van der Waals interactions in density functional theory *Electronic Density Functional Theory: Recent Progress and New Directions* ed J F Dobson *et al* (Berlin: Plenum)

[69] Andersson Y and Rydberg H 1999 Dispersion coefficients for van der Waals complexes, including C_{60}–C_{60} *Phys. Scr.* **60** 211

[70] Andersson Y, Hult E, Apell P, Langreth D C and Lundqvist B I 1998 Density-functional account of van der Waals forces between parallel surfaces *Solid State Commun.* **106** 235–8

[71] Hult E, Hyldgaard P, Rossmeisl J and Lundqvist B I 2001 Density-functional calculation of van der Waals forces for free-electron-like surfaces *Phys. Rev.* B **64** 195414

[72] Dion M 2004 van der Waals forces in density functional theory *PhD Thesis* Rutgers University, Piscataway, NC, USA

[73] Ziambaras E, Kleis J, Schröder E and Hyldgaard P 2007 Potassium intercalation in graphite: a van der Waals density-functional study *Phys. Rev.* B **76** 155425

[74] Londero E and Schröder E 2010 Role of van der Waals bonding in the layered oxide V_2O_5 : first-principles density-functional calculations *Phys. Rev.* B **82** 054116

[75] Rohrer J and Hyldgaard P 2011 Stacking and band structure of van der Waals bonded graphane multilayers *Phys. Rev.* B **83** 165423

[76] Kleis J, Schröder E and Hyldgaard P 2008 Nature and strength of bonding in a crystal of semiconducting nanotubes: van der Waals density functional calculations and analytical results *Phys. Rev.* B **77** 205422

[77] Berland K and Hyldgaard P 2010 Structure and binding in crystals of cagelike molecules: hexamine and platonic hydrocarbons *J. Chem. Phys.* **132** 134705

[78] Berland K, Borck Ø and Hyldgaard P 2011 van der Waals density functional calculations of binding in molecular crystals *Comput. Phys. Commun.* **182** 1800–4

[79] Berland K, Londero E, Schröder E and Hyldgaard P 2013 Harris-type van der Waals density functional scheme *Phys. Rev.* B **88** 045431

[80] Chakarova-Käck S D, Schröder E, Lundqvist B I and Langreth D C 2006 Application of van der Waals density functional to an extended system: adsorption of benzene and naphthalene on graphite *Phys. Rev. Lett.* **96** 146107

[81] Johnston K, Kleis J, Lundqvist B I and Nieminen R M 2008 Influence of van der Waals forces on the adsorption structure of benzene on silicon studied using density functional theory *Phys. Rev.* B **77** 121404

[82] Moses P G, Mortensen J J, Lundqvist B I and Nørskov J K 2009 Density functional study of the adsorption and van der Waals binding of aromatic and conjugated compounds on the basal plane of MoS_2 *J. Chem. Phys.* **130** 104709

[83] Wellendorff J, Kelkkanen A, Mortensen J, Lundqvist B I and Bligaard T 2010 RPBE-vdW description of benzene adsorption on Au(1 1 1) *Top. Catal.* **53** 378–83

[84] Chakarova-Käck S D, Vojvodic A, Kleis J, Hyldgaard P and Schröder E 2010 Binding of polycyclic aromatic hydrocarbons and graphene dimers in density functional theory *New J. Phys.* **12** 013017

[85] Berland K, Chakarova-Käck S D, Cooper V R, Langreth D C and Schröder E 2011 A van der Waals density functional study of adenine on graphene: single-molecular adsorption and overlayer binding *J. Phys.: Condens. Matter* **23** 135001

[86] Bergvall A, Berland K, Hyldgaard P, Kubatkin S and Löfwander T 2011 Graphene nanogap for gate-tunable quantum-coherent single-molecule electronics *Phys. Rev.* B **84** 155451

[87] Åkesson J, Sundborg O, Wahlström O and Schröder E 2012 A van der Waals density functional study of chloroform and other trihalomethanes on graphene *J. Chem. Phys.* **137** 174702

[88] Le D, Kara A, Schröder E, Hyldgaard P and Rahman T S 2012 Physisorption of nucleobases on graphene: a comparative van der Waals study *J. Phys.: Condens. Matter* **24** 424210

[89] Lee K, Kelkkanen A K, Berland K, Andersson S, Langreth D C, Schröder E, Lundqvist B I and Hyldgaard P 2011 Evaluation of a density functional with account of van der Waals forces using experimental data of H_2 physisorption on Cu(1 1 1) *Phys. Rev.* B **84** 193408

[90] Lee K, Berland K, Yoon M, Andersson S, Schröder E, Hyldgaard P and Lundqvist B I 2012 Benchmarking van der Waals density functionals with experimental data: potential-energy curves for H_2 molecules on Cu(1 1 1), (1 0 0), and (1 1 0) surfaces *J. Phys.: Condens. Matter* **24** 424213

[91] Chakarova-Käck S D, Borck Ø, Schröder E and Lundqvist B I 2006 Adsorption of phenol on graphite (0001) and α-Al_2O_3 (0 0 0 1): nature of van der Waals bonds from first-principles calculations *Phys. Rev.* B **74** 155402

[92] Londero E and Schröder E 2011 Vanadium pentoxide (V_2O_5): a van der Waals density functional study *Comput. Phys. Commun.* **182** 1805–9

[93] Kleis J and Schröder E 2005 van der Waals interaction of simple, parallel polymers *J. Chem. Phys.* **122** 164902

[94] Kleis J, Hyldgaard P and Schröder E 2005 van der Waals interaction of parallel polymers and nanotubes *Comput. Mater. Sci.* **33** 192–9

[95] Kleis J, Lundqvist B I, Langreth D C and Schröder E 2007 Towards a working density-functional theory for polymers: first-principles determination of the polyethylene crystal structure *Phys. Rev.* B **76** 100201

[96] Schröder E and Hyldgaard P 2003 van der Waals interactions of parallel and concentric nanotubes *Mater. Sci. Eng.* C **23** 721–5

[97] Wyrick J *et al* 2011 Do two-dimensional 'Noble gas atoms' produce molecular honeycombs at a metal surface? *Nano Lett.* **11** 2944–8

[98] Schröder E and Hyldgaard P 2003 The van der Waals interactions of concentric nanotubes *Surf. Sci.* **532–5** 880–5

[99] Berland K, Einstein T L and Hyldgaard P 2009 Rings sliding on a honeycomb network: adsorption contours, interactions, and assembly of benzene on Cu(1 1 1) *Phys. Rev.* B **80** 155431

[100] Sun D *et al* 2010 Effective elastic properties of a van der Waals molecular monolayer at a metal surface *Phys. Rev.* B **82** 201410

[101] Kelkkanen A K, Lundqvist B I and Nørskov J K 2011 van der Waals effect in weak adsorption affecting trends in adsorption, reactivity, and the view of substrate nobility *Phys. Rev.* B **83** 113401

[102] Cooper V R, Thonhauser T, Puzder A, Schröder E, Lundqvist B I and Langreth D C 2008 Stacking interactions and the twist of DNA *J. Am. Chem. Soc.* **130** 1304–8

[103] Li S, Cooper V R, Thonhauser T, Lundqvist B I and Langreth D C 2009 Stacking interactions and DNA intercalation *J. Phys. Chem.* B **113** 11166–72

[104] Londero E, Hyldgaard P and Schröder E 2013 A van der Waals density functional mapping of attraction in DNA dimers arXiv:1304.1936

[105] Møgelhøj A, Kelkkanen A K, Wikfeldt K T, Schiøtz J, Mortensen J J, Pettersson L G M, Lundqvist B I, Jacobsen K W, Nilsson A and Nørskov J K 2011 *Ab initio* van der Waals interactions in simulations of water alter structure from mainly tetrahedral to high-density-like *J. Phys. Chem.* B **115** 14149–60

[106] Cooper V R 2010 van der Waals density functional: an appropriate exchange functional *Phys. Rev.* B **81** 161104

[107] Berland K and Hyldgaard P 2014 Exchange functional that tests the robustness of the plasmon description of the van der Waals density functional *Phys. Rev.* B **89** 035412

[108] Berland K, Arter C A, Cooper V R, Lee K, Lundqvist B I, Schröder E, Thonhauser T and Hyldgaard P 2014 van der Waals density functionals built upon the electron-gas tradition: facing the challenge of competing interactions *J. Chem. Phys.* **140** 18A539

[109] Hyldgaard P, Berland K and Schröder E 2014 Interpretation of van der Waals density functionals *Phys. Rev.* B **90** 075148

[110] Boato G, Cantini P and Tatarek R 1977 Diffraction of molecular beams from a low temperature metal surface *Proc. of the 7th Int. Vacuum Congress and the 3rd Int. Conf. on Solid Surfaces* (*Congress Centre Hofburg, Vienna, Austria, 12–16 September* 1977) ed F Berger *et al* (Vienna: Dobrozemsky) p 1377

[111] Moran-Lopez J L and Bosch A T 1977 Changes in work function due to charge transfer in chemisorbed layers *Surf. Sci.* **68** 377–84

[112] Zaremba E and Kohn W 1976 van der Waals interaction between an atom and a solid surface *Phys. Rev.* B **13** 2270–85

[113] Zaremba E and Kohn W 1977 Theory of helium adsorption on simple and noble-metal surfaces *Phys. Rev.* B **15** 1769–81

[114] Nordlander P and Harris J 1984 The interaction of helium with smooth metal surfaces *J. Phys. C* **17** 1141

[115] Liebsch A 1986 Density-functional calculation of the dynamic image plane at a metal surface: reference-plane position of He- and H_2-metal van der Waals interaction *Phys. Rev.* B **33** 7249–51

[116] Andersson S and Persson M 1993 Sticking in the physisorption well: influence of surface structure *Phys. Rev. Lett.* **70** 202–5

[117] Andersson S and Persson M 1993 Crystal-face dependence of physisorption potentials *Phys. Rev.* B **48** 5685–8

[118] Schönhammer K and Gunnarsson O 1980 Sticking probability on metal surfaces: contribution from electron-hole-pair excitations *Phys. Rev.* B **22** 1629–37

[119] Brenig W 1987 Dynamics and kinetics of gas-surface interaction: sticking, desorption and inelastic scattering *Phys. Scr.* **35** 329

[120] Harris J and Liebsch A 1982 Interaction of helium with a metal surface *J. Phys.* C **15** 2275

[121] Andersson S, Persson M and Harris J 1996 Physisorption energies: influence of surface structure *Surf. Sci.* **360** L499–504

[122] Esbjerg N and Nørskov J K 1980 Dependence of the He-scattering potential at surfaces on the surface-electron-density profile *Phys. Rev. Lett.* **45** 807–10

[123] Smoluchowski R 1941 Anisotropy of the electronic work function of metals *Phys. Rev.* **60** 661–74

[124] Jacobsen K W, Nørskov J K and Puska M J 1987 Interatomic interactions in the effective-medium theory *Phys. Rev.* B **35** 7423–42

[125] Roy R J L 1976 Determining potential energy constants for atom- and molecule-surface interactions *Surf. Sci.* **59** 541–53

[126] Perreau J and Lapujoulade J 1982 Selective adsorption of He, H_2 on copper surfaces *Surf. Sci.* **122** 341–54

[127] Yu C-f, Whaley K B, Hogg C S and Sibener S J 1985 Investigation of the spatially isotropic component of the laterally averaged molecular hydrogen/Ag(1 1 1) physisorption potential *J. Chem. Phys.* **83** 4217–34

[128] Chiesa M, Mattera L, Musenich R and Salvo C 1985 Energy level splitting in the study of H_2–Ag(1 1 0) surface selective adsorption *Surf. Sci. Lett.* **151** L145 –52

[129] Harten U, Toennies J P and Wöll C 1986 Molecular beam translational spectroscopy of physisorption bound states of molecules on metal surfaces. I. HD on Cu(1 1 1) and Au(1 1 1) single crystal surfaces *J. Chem. Phys.* **85** 2249–58

[130] Andersson S, Wilzén L and Persson M 1988 Physisorption interaction of H_2 with noble-metal surfaces: a new H_2–Cu potential *Phys. Rev.* B **38** 2967–73

[131] Lindhard J and Scharff M 1953 Energy loss in matter by fast particles of low charge *Dan. Mat. Fys. Medd.* **27** 15

[132] Brandt W and Lundqvist S 1963 Atomic response function *Phys. Rev.* **132** 2135–43

[133] Hedin L and Lundqvist S 1969 Effects of electron–phonon interactions on the one-electron states of solids *Solid State Physics* vol 23, ed F Seitz (New York: Academic) p 1

[134] Lundqvist B I 1967 Single-particle spectrum of degenerate electron gas. I. Structure of spectral weight function *Phys. Kond. Mat.* **6** 193

[135] Carbotte J P, LeBlanc J P F and Nicol E J 2012 Emergence of plasmaronic structure in the near-field optical response of graphene *Phys. Rev.* B **85** 201411

[136] Maggs A C and Ashcroft N W 1987 Electronic fluctuation and cohesion in metals *Phys. Rev. Lett.* **59** 113–6

[137] Langreth D C and Vosko S H 1987 Exact electron-gas response functions at high density *Phys. Rev. Lett.* **59** 497–500

[138] Lundqvist S and Sjölander A 1964 On polarization waves in van der Waals crystals *Ark. Fys.* **26** 17

[139] Mahan G D 1965 van der Waals forces in solids *J. Chem. Phys.* **43** 1569–74

[140] Ma S and Brueckner K 1968 Correlation energy of an electron gas with a slowly varying high density *Phys. Rev.* **165** 18–31

[141] Barash Y S, Ginzburg V L 1984 Some problems in the theory of van der Waals forces *Usp. Fiz. Nauk.* **143** 345
Barash Y S and Ginzburg V L 1984 *Sov. Phys.—Usp.* **27** 467

[142] Gunnarsson O and Jones R O 1980 Density functional calculations for atoms, molecules and clusters *Phys. Scr.* **21** 394

[143] Perdew J P and Wang Y 1986 Accurate and simple density functional for the electronic exchange energy: generalized gradient approximation *Phys. Rev.* B **33** 8800

[144] Mavroyannis C and Stephen M J 1962 Dispersion forces *Mol. Phys.* **5** 629–38

[145] Andersson Y 1996 van der Waals density functionals *PhD Thesis* Department of Applied Physics, Chalmers University of Technology, Göteborg, Sweden

[146] Dobson J F and Dinte B P 1996 Constraint satisfaction in local and gradient susceptibility approximations: application to a van der Waals density functional *Phys. Rev. Lett.* **76** 1780–3

[147] Pérez-Jordá J M and Becke A D 1995 A density-functional study of van der Waals forces: rare gas diatomics *Chem. Phys. Lett.* **233** 134–7

[148] Hult E and Kiejna A 1997 Trends in atom/molecule-surface van der Waals interactions *Surf. Sci.* **383** 88–94

[149] Ruzsinszky A, Perdew J P, Tao J, Csonka G I and Pitarke J M 2012 van der Waals coefficients for nanostructures: fullerenes defy conventional wisdom *Phys. Rev. Lett.* **109** 233203

[150] Perdew J P, Ruzsinszky A, Sun J, Glindmeyer S and Csonka G I 2012 van der Waals interaction as a summable asymptotic series *Phys. Rev.* A **86** 062714

[151] Elstner M, Hobza P, Frauenheim T, Suhai S and Kaxiras E 2001 Hydrogen bonding and stacking interactions of nucleic acid base pairs: a density-functional-theory based treatment *J. Chem. Phys.* **114** 5149–55

[152] Wu Q and Yang W 2002 Empirical correction to density functional theory for van der Waals interactions *J. Chem. Phys.* **116** 515

[153] Gianturco F A and Paesani F 2000 The He-OCS van der Waals potential from model calculations: bound states, stable structures, and vibrational couplings *J. Chem. Phys.* **113** 3011

[154] Meijer E J and Sprik M 1996 A density-functional study of the intermolecular interactions of benzene *J. Chem. Phys.* **105** 8684–9

[155] Grimme S, Antony J, Schwabe T and Muck-Lichtenfeld C 2007 Density functional theory with dispersion corrections for supramolecular structures, aggregates, and complexes of (bio)organic molecules *Org. Biomol. Chem.* **5** 741–58

[156] Brooks F C 1952 Convergence of intermolecular force series *Phys. Rev.* **86** 92–7

[157] von Lilienfeld O A and Tkatchenko A 2010 Two- and three-body interatomic dispersion energy contributions to binding in molecules and solids *J. Chem. Phys.* **132** 234109

[158] Kaltak M, Klimeš J and Kresse G 2014 Cubic scaling algorithm for the random phase approximation: self-interstitials and vacancies in Si *Phys. Rev.* B **90** 054115

[159] Harl J and Kresse G 2009 Accurate bulk properties from approximate many-body techniques *Phys. Rev. Lett.* **103** 056401

[160] Eshuis H, Bates J E and Furche F 2012 Electron correlation methods based on the random phase approximation *Theor. Chem. Acc.* **131** 1084

[161] Ren X, Tkatchenko A, Rinke P and Scheffler M 2011 Beyond the random-phase approximation for the electron correlation energy: the importance of single excitations *Phys. Rev. Lett.* **106** 153003

[162] Harl J, Schimka L and Kresse G 2010 Assessing the quality of the random phase approximation for lattice constants and atomization energies of solids *Phys. Rev.* B **81** 115126

[163] Eshuis H and Furche F 2011 A parameter-free density functional that works for noncovalent interactions *J. Phys. Chem. Lett.* **2** 983–9

[164] Schimka L, Harl J, Stroppa A, Grüneis A, Marsman M, Mittendorfer F and Kresse G 2010 Accurate surface and adsorption energies from many-body perturbation theory *Nat. Mater.* **9** 741–4

[165] Björkman T, Gulans A, Krasheninnikov A V and Nieminen R M 2012 van der Waals bonding in layered compounds from advanced density-functional first-principles calculations *Phys. Rev. Lett.* **108** 235502

[166] Kurth S and Perdew J P 1999 Density-functional correction of random-phase-approximation correlation with results for jellium surface energies *Phys. Rev.* B **59** 10461

[167] Fuchs M and Gonze X 2002 Accurate density functionals: approaches using the adiabatic-connection fluctuation-dissipation theorem *Phys. Rev.* B **65** 235109

[168] Sato T, Tsuneda T and Hirao K 2005 A density-functional study on π-aromatic interaction: benzene dimer and naphthalene dimer *J. Chem. Phys.* **123** 104307

[169] Sato T, Tsuneda T and Hirao K 2007 Long-range corrected density functional study on weakly bound systems: balanced descriptions of various types of molecular interactions *J. Chem. Phys.* **126** 234114

[170] Iikura H, Tsuneda T, Yanai T and Hirao K 2001 A long-range correction scheme for generalized-gradient-approximation exchange functionals *J. Chem. Phys.* **115** 3540

[171] Silvestrelli P L 2008 van der Waals interactions in DFT made easy by Wannier functions *Phys. Rev. Lett.* **100** 053002

[172] Marzari N and Vanderbilt D 1997 Maximally localized generalized Wannier functions for composite energy bands *Phys. Rev.* B **56** 12847

[173] Silvestrelli P L, Marzari N, Vanderbilt D and Parinello M 1998 Maximally-localized Wannier functions for disordered systems: application to amorphous silicon *Solid State Commun.* **107** 7–11

[174] Silvestrelli P L 2009 van der Waals interactions in density functional theory using Wannier functions *J. Phys. Chem.* A **113** 5224–34

[175] Andrinopoulos L, Hine N D M and Mostofi A A 2011 Calculating dispersion interactions using maximally localized Wannier functions *J. Chem. Phys.* **135** 154105

[176] Ambrosetti A and Silvestrelli P L 2012 van der Waals interactions in density functional theory using Wannier functions: improved C_6 and C_3 coefficients by a different approach *Phys. Rev.* B **85** 073101

[177] Vydrov O A and Van Voorhis T 2010 Dispersion interactions from a local polarizability model *Phys. Rev.* A **81** 062708

[178] Becke A D and Johnson E R 2005 A density-functional model of the dispersion interaction *J. Chem. Phys.* **123** 154101

[179] Becke A D and Johnson E R 2007 Exchange-hole dipole moment and the dispersion interaction revisited *J. Chem. Phys.* **127** 154108

[180] Perdew J P and Wang Y 1992 Pair-distribution function and its coupling-constant average for the spin-polarized electron gas *Phys. Rev.* B **46** 12947–54

[181] Dobson J F and Wang J 1999 Successful test of a seamless van der Waals density functional *Phys. Rev. Lett.* **82** 2123–6

[182] Zhang Y and Yang W 1998 Comment on generalized gradient approximation made simple *Phys. Rev. Lett.* **80** 890

[183] Perdew J P 1991 Unified theory of exchange and correlation beyond the local density approximation *Electronic Structure of Solids* vol 91, ed P Ziesche and H Eschrig (Berlin: Akademie)

[184] Benedict L X, Chopra N G, Cohen M L, Zettl A, Louie S G and Crespi V H 1998 Microscopic determination of the interlayer binding energy in graphite *Chem. Phys. Lett.* **286** 490–6

[185] Yin M T and Cohen M L 1984 Structural theory of graphite and graphitic silicon *Phys. Rev.* B **29** 6996–8

[186] Schabel M C and Martins J L 1992 Energetics of interplanar binding in graphite *Phys. Rev.* B **46** 7185–8

[187] Furthmüller J, Hafner J and Kresse G 1994 *Ab initio* calculation of the structural and electronic properties of carbon and boron nitride using ultrasoft pseudopotentials *Phys. Rev.* B **50** 15606–22

[188] Charlier J-C, Gonze X and Michenaud J-P 1994 Graphite interplanar bonding: electronic delocalization and van der Waals interaction *Europhys. Lett.* **28** 403

[189] Charlier J-C, Gonze X and Michenaud J-P 1995 First-principles study of carbon nanotube solid-state packings *Europhys. Lett.* **29** 43

[190] Lebégue S, Harl J, Gould T, Ángyán J G, Kresse G and Dobson J F 2010 Cohesive properties and asymptotics of the dispersion interaction in graphite by the random phase approximation *Phys. Rev. Lett.* **105** 196401

[191] Spanu L, Sorella S and Galli G 2009 Nature and strength of interlayer binding in graphite *Phys. Rev. Lett.* **103** 196401

[192] Chakarova S D and Schröder E 2005 van der Waals interactions of the benzene dimer: towards treatment of polycyclic aromatic hydrocarbon dimers *Mater. Sci. Eng.* C **25** 787–92

[193] Chakarova S D and Schröder E 2005 van der Waals interactions of polycyclic aromatic hydrocarbon dimers *J. Chem. Phys.* **122** 054102

[194] Zacharia R, Ulbricht H and Hertel T 2004 Interlayer cohesive energy of graphite from thermal desorption of polyaromatic hydrocarbons *Phys. Rev.* B **69** 155406

[195] Langreth D C 1970 Singularities in the x-ray spectra of metals *Phys. Rev.* B **1** 471–7

[196] Klimeš J, Bowler D R and Michaelides A 2010 Chemical accuracy for the van der Waals density functional *J. Phys.: Condens. Matter* **22** 022201

[197] Klimeš J, Bowler D R and Michaelides A 2011 van der Waals density functionals applied to solids *Phys. Rev.* B **83** 195131

[198] Hamada I 2014 van der Waals density functional made accurate *Phys. Rev.* B **89** 121103

[199] Baym G and Kadanoff L P 1961 Conservation laws and correlation functions *Phys. Rev.* **124** 287–99

[200] Berland K 2012 Connected by voids: interactions and screening in sparse matter *PhD Thesis* Department of Microtechnology, Nanoscience: MC2, Chalmers University of Technology, Göteborg, Sweden

[201] Langreth D C and Lundqvist B I 2010 Comment on 'nonlocal van der Waals density functional made simple' *Phys. Rev. Lett.* **104** 099303

[202] Langreth D C and Vosko S H 1990 Response functions and non-local functionals *Adv. Quantum Chem.* **21** 175–99

[203] Barash Y S 1988 van der Waals interactions between thin conducting layers *Fiz. Tverd. Tela* **30** 2738
Barash Y S 1988 *Sov. Phys. Solid State* **30** 1578

[204] Sernelius B E and Björk P 1998 Interaction energy for a pair of quantum wells *Phys. Rev.* B **57** 6592

[205] Dobson J F, Gould T and Vignale G 2014 How many-body effects modify the van der Waals interaction between graphene sheets *Phys. Rev.* X **4** 021040

[206] Perdew J P, Burke K and Wang Y 1996 Generalized gradient approximation for the exchange-correlation hole of a many-electron system *Phys. Rev.* B **54** 16533–9

[207] Murray É D, Lee K and Langreth D C 2009 Investigation of exchange energy density functional accuracy for interacting molecules *J. Chem. Theory Comput.* **5** 2754–62

[208] Langreth D C and Perdew J P 1980 Theory of nonuniform electronic systems. I. Analysis of the gradient approximation and a generalization that works *Phys. Rev.* B **21** 5469

[209] Rasolt M and Geldart D J W 1975 Gradient corrections in the exchange and correlation energy of an inhomogeneous electron gas *Phys. Rev. Lett.* **35** 1234–7

[210] Kleinman L and Lee S 1988 Gradient expansion of the exchange-energy density functional: effect of taking limits in the wrong order *Phys. Rev.* B **37** 4634–6

[211] Sabatini R, Küçükbenli E, Kolb B, Thonhauser T and de Gironcoli S 2012 Structural evolution of amino acid crystals under stress from a non-empirical density functional *J. Phys.: Condens. Matter* **24** 424209

[212] Román-Pérez G and Soler J M 2009 Efficient implementation of a van der Waals density functional: application to double-wall carbon nanotubes *Phys. Rev. Lett.* **103** 096102

[213] Vydrov O A and Van Voorhis T 2009 Improving the accuracy of the nonlocal van der Waals density functional with minimal empiricism *J. Chem. Phys.* **130** 104105

[214] Kannemann F O and Becke A D 2009 van der Waals interactions in density-functional theory: rare-gas diatomics *J. Chem. Theory Comput.* **5** 719–27

[215] Becke A D 1986 On the large-gradient behavior of the density functional exchange energy *J. Chem. Phys.* **85** 7184–7

[216] Becke A D 1988 Density-functional exchange-energy approximation with correct asymptotic behavior *Phys. Rev.* A **38** 3098–100

[217] Schwinger J 1981 Thomas–Fermi model: the second correction *Phys. Rev.* A **24** 2353–61

[218] Hamada I and Otani M 2010 Comparative van der Waals density-functional study of graphene on metal surfaces *Phys. Rev.* B **82** 153412

[219] Wellendorff J, Lundgaard K T, Møgelhøj A, Petzold V, Landis D D, Nørskov J K, Bligaard T and Jacobsen K W 2012 Density functionals for surface science: exchange-correlation model development with Bayesian error estimation *Phys. Rev.* B **85** 235149

[220] Gutle C, Savin A, Krieger J B and Chen J 1999 Correlation energy contributions from low-lying states to density functionals based on an electron gas with a gap *Int. J. Quantum Chem.* **75** 885–8

[221] Jurecka P, Sponer J, Cerny J and Hobza P 2006 Benchmark database of accurate (MP2 andCCSD(T) complete basis set limit) interaction energies of small model complexes, DNA base pairs, and amino acid pairs *Phys. Chem. Chem. Phys.* **8** 1985–93

[222] Sabatini R, Gorni T and de Gironcoli S 2013 Nonlocal van der Waals density functional made simple and efficient *Phys. Rev.* B **87** 041108

[223] Tran F and Hutter J 2013 Nonlocal van der Waals functionals: the case of rare-gas dimers and solids *J. Chem. Phys.* **138** 204103

[224] Björkman T, Gulans A, Krasheninnikov A V and Nieminen R M 2012 Are we van der Waals ready? *J. Phys.: Condens. Matter* **24** 424218

[225] Björkman T 2012 van der Waals density functional for solids *Phys. Rev.* B **86** 165109

[226] Björkman T 2014 Testing several recent van der Waals density functionals for layered structures *J. Chem. Phys.* **141** 074708

[227] Vydrov O A and Van Voorhis T 2012 Benchmark assessment of the accuracy of several van der Waals density functionals *J. Chem. Theory Comput.* **8** 1929–34

[228] Hujo W and Grimme S 2011 Performance of the van der Waals density functional VV10 and (hybrid)GGA variants for thermochemistry and noncovalent interactions *J. Chem. Theory Comput.* **7** 3866–71

[229] Burke K 2012 Perspective on density functional theory *J. Chem. Phys.* **136** 150901

[230] Toyoda K, Nakano Y, Hamada I, Lee K, Yanagisawa S and Morikawa Y 2009 First-principles study of benzene on noble metal surfaces: adsorption states and vacuum level shifts *Surf. Sci.* **603** 2912–22

[231] Puzder A, Dion M and Langreth D C 2006 Binding energies in benzene dimers: nonlocal density functional calculations *J. Chem. Phys.* **124** 164105

[232] Cybulski S M and Lytle M L 2007 The origin of deficiency of the supermolecule second-order Møller–Plesset approach for evaluating interaction energies *J. Chem. Phys.* **127** 141102

[233] Thonhauser T, Puzder A and Langreth D C 2006 Interaction energies of monosubstituted benzene dimers via nonlocal density functional theory *J. Chem. Phys.* **124** 164106

[234] Li S, Cooper V R, Thonhauser T, Puzder A and Langreth D C 2008 A density functional theory study of the benzene–water complex *J. Phys. Chem.* A **112** 9031–6

[235] Hooper J, Cooper V R, Thonhauser T, Romero N A, Zerilli F and Langreth D C 2008 Predicting C–H/π interactions with nonlocal density functional theory *ChemPhysChem* **9** 891–5

[236] Tran F and Hutter J 2013 Nonlocal van der Waals functionals: the case of rare-gas dimers and solids *J. Chem. Phys.* **138** 204103
Tran F and Hutter J 2013 *J. Chem. Phys.* **139** 039903 (erratum)

[237] Gulans A, Puska M J and Nieminen R M 2009 Linear-scaling self-consistent implementation of the van der Waals density functional *Phys. Rev.* B **79** 201105

[238] Otero-de-la-Roza A and Johnson E R 2012 A benchmark for non-covalent interactions in solids *J. Chem. Phys.* **137** 054103

[239] Nabok D, Puschnig P and Ambrosch-Draxl C 2008 Cohesive and surface energies of π-conjugated organic molecular crystals: a first-principles study *Phys. Rev.* B **77** 245316

[240] Lee K, Kolb B, Thonhauser T, Vanderbilt D and Langreth D C 2012 Structure and energetics of a ferroelectric organic crystal of phenazine and chloranilic acid *Phys. Rev.* B **86** 104102

[241] Clay R C III , McMinis J, McMahon J M, Pierleoni C, Ceperley D M and Morales M A 2014 Benchmarking exchange-correlation functionals for hydrogen at high pressures using quantum Monte Carlo *Phys. Rev.* B **89** 184106

[242] Morales M A, Gergely J R, McMinis J, McMahon J M, Kim J and Ceperley D M 2014 Quantum Monte Carlo benchmark of exchange-correlation functionals for bulk water *J. Chem. Theory Comput.* **10** 2355

[243] Londero E, Karlson E K, Landahl M, Ostrovskii D, Rydberg J D and Schröder E 2012 Desorption of n-alkanes from graphene: a van der Waals density functional study *J. Phys.: Condens. Matter* **24** 424212

[244] Schröder E 2013 Methanol adsorption on graphene *J. Nanomater.* **2013** 871706

[245] Jiang D-E, Cooper V R and Dai S 2009 Porous graphene as the ultimate membrane for gas separation *Nano Lett.* **9** 4019–24

[246] Cooper V R, Ihm Y and Morris J R 2012 Hydrogen adsorption at the graphene surface: a vdW-DF perspective *Phys. Proc.* **34** 34–8

[247] Björk J, Hanke F, Palma C-A, Samori P, Cecchini M and Persson M 2010 Adsorption of aromatic and anti-aromatic systems on graphene through π–π stacking *J. Phys. Chem. Lett.* **1** 3407–12

[248] Amft M, Lebégue S, Eriksson O and Skorodumova N V 2011 Adsorption of Cu, Ag, and Au atoms on graphene including van der Waals interactions *J. Phys.: Condens. Matter* **23** 395001

[249] Tait S L, Dohnálek Z, Campbell C T and Kay B D 2006 n-alkanes on Pt(1 1 1) and on C(0 0 0 1)/Pt(1 1 1): chain length dependence of kinetic desorption parameters *J. Chem. Phys.* **125** 234308

[250] Lee K, Morikawa Y and Langreth D C 2010 Adsorption of n-butane on Cu(1 0 0), Cu(1 1 1), Au(1 1 1), and Pt(1 1 1): van der Waals density-functional study *Phys. Rev.* B **82** 155461

[251] Liu W, Carrasco J, Santra B, Michaelides A, Scheffler M and Tkatchenko A 2012 Benzene adsorbed on metals: concerted effect of covalency and van der Waals bonding *Phys. Rev.* B **86** 245405

[252] Romaner L, Nabok D, Puschnig P, Zojer E and Ambrosch-Draxl C 2009 Theoretical study of PTCDA adsorbed on the coinage metal surfaces, Ag(1 1 1), Au(1 1 1), and Cu(1 1 1) *New J. Phys.* **11** 053010

[253] Toyoda K, Nakano Y, Hamada I, Lee K, Yanagisawa S and Morikawa Y 2009 First-principles study of the pentacene/Cu(1 1 1) interface: adsorption states and vacuum level shifts *J. Electron Spectrosc. Relat. Phenom.* **174** 78–84

[254] Toyoda K, Hamada I, Lee K, Yanagisawa S and Morikawa Y 2010 Density functional theoretical study of pentacene/noble metal interfaces with van der Waals corrections: vacuum level shifts and electronic structures *J. Chem. Phys.* **132** 134703

[255] Hauschild A, Temirov R, Soubatch S, Bauer O, Schöll A, Cowie B C C, Lee T-L, Tautz F S and Sokolowski M 2010 Normal-incidence x-ray standing-wave determination of the adsorption geometry of PTCDA on Ag(1 1 1): comparison of the ordered room-temperature and disordered low-temperature phases *Phys. Rev.* B **81** 125432

[256] Hamada I and Tsukada M 2011 Adsorption of C_{60} on Au(1 1 1) revisited: a van der Waals density functional study *Phys. Rev.* B **83** 245437

[257] Yildirim H, Greber T and Kara A 2013 Trends in adsorption characteristics of benzene on transition metal surfaces: role of surface chemistry and van der Waals interactions *J. Phys. Chem.* C **117** 20572–83

[258] Yildirim H and Kara A 2013 Effect of van der Waals interactions on the adsorption of olympicene radical on Cu(1 1 1): characteristics of weak physisorption versus strong chemisorption *J. Phys. Chem.* C **117** 2893–902

[259] Carrasco J, Liu W, Michaelides A and Tkatchenko A 2014 Insight into the description of van der Waals forces for benzene adsorption on transition metal (1 1 1) surfaces *J. Chem. Phys.* **140** 084704

[260] Björk J and Stafström S 2014 Adsorption of large hydrocarbons on coinage metals: a van der Waals density functional study *Chem. Phys. Chem.* **15** 2851

[261] Callsen M, Atodiresei N, Caciuc V and Blügel S 2012 Semiempirical van der Waals interactions versus *ab initio* nonlocal correlation effects in the thiophene-Cu(1 1 1) system *Phys. Rev.* B **86** 085439

[262] Kong L, Cooper V R, Nijem N, Li K, Li J, Chabal Y J and Langreth D C 2009 Theoretical and experimental analysis of H_2 binding in a prototypical metal-organic framework material *Phys. Rev.* B **79** 081407

[263] Lan A *et al* 2009 RPM3 : a multifunctional microporous MOF with recyclable framework and high H_2 binding energy *J. Inorg. Chem.* **48** 7165–73

[264] Nijem N, Veyan J-F, Kong L, Wu H, Zhao Y, Li J, Langreth D C and Chabal Y J 2010 Molecular hydrogen 'pairing' interaction in a metal organic framework system with unsaturated metal centers (MOF-74) *J. Am. Chem. Soc.* **132** 14834–48

[265] Lopez M G, Canepa P and Thonhauser T 2013 NMR study of small molecule adsorption in MOF-74-Mg *J. Chem. Phys.* **138** 154704

[266] Nijem N, Canepa P, Kong L, Wu H, Li J, Thonhauser T and Chabal Y J 2012 Spectroscopic characterization of van der Waals interactions in a metal organic framework with unsaturated metal centers: MOF-74-Mg *J. Phys.: Condens. Matter* **24** 424203

[267] Yao Y, Nijem N, Li J, Chabal Y J, Langreth D C and Thonhauser T 2012 Analyzing the frequency shift of physiadsorbed CO_2 in metal organic framework materials *Phys. Rev.* B **85** 064302

[268] Tan K, Nijem N, Canepa P, Gong Q, Li J, Thonhauser T and Chabal Y J 2012 Stability and hydrolyzation of metal organic frameworks with paddle-wheel SBUs upon hydration *Chem. Mater.* **24** 3153–67

[269] Poloni R, Smit B and Neaton J B 2012 CO_2 capture by metal organic frameworks with van der Waals density functionals *J. Phys. Chem.* A **116** 4957–64

[270] Poloni R, Smit B and Neaton J B 2012 Ligand-assisted enhancement of CO_2 capture in metal organic frameworks *J. Am. Chem. Soc.* **134** 6714–9

[271] Poloni R, Lee K, Berger R F, Smit B and Neaton J B 2014 Understanding trends in CO_2 adsorption in metal organic frameworks with open-metal sites *J. Phys. Chem. Lett.* **5** 861–5

[272] Nijem N, Wu H, Canepa P, Marti A, Balkus K J, Thonhauser T, Li J and Chabal Y J 2012 Tuning the gate opening pressure of metal-organic frameworks (MOFs) for the selective separation of hydrocarbons *J. Am. Chem. Soc.* **134** 15201–4

[273] Zuluaga S, Canepa P, Tan K, Chabal Y J and Thonhauser T 2014 Study of van der Waals bonding and interactions in metal organic framework materials *J. Phys.: Condens. Matter* **26** 133002

[274] Canepa P, Nijem N, Chabal Y J and Thonhauser T 2013 Diffusion of small molecules in metal organic framework materials *Phys. Rev. Lett.* **110** 026102

[275] Nijem N *et al* 2013 Water cluster confinement and methane adsorption in the hydrophobic cavities of a fluorinated metal-organic framework *J. Am. Chem. Soc.* **135** 12615–26

[276] Li Q and Thonhauser T 2012 A theoretical study of the hydrogen-storage potential of $(H_2)_4$ CH_4 in metal organic framework materials and carbon nanotubes *J. Phys.: Condens. Matter* **24** 424204

[277] Román-Pérez G, Moaied M, Soler J M and Yndurain F 2010 Stability, adsorption, and diffusion of CH_4, CO_2, and H_2 in clathrate hydrates *Phys. Rev. Lett.* **105** 145901

[278] Li Q, Kolb B, Román-Pérez G, Soler J M, Yndurain F, Kong L, Langreth D C and Thonhauser T 2011 *Ab initio* energetics and kinetics study of H_2 and CH_4 in the SI clathrate hydrate *Phys. Rev.* B **84** 153103

[279] Morris J R *et al* 2013 Modern approaches to studying gas adsorption in nanoporous carbons *J. Mater. Chem.* A **1** 9341–50

[280] Ihm Y, Cooper V R, Gallego N C, Contescu C I and Morris J R 2014 Microstructure-dependent gas adsorption: accurate predictions of methane uptake in nanoporous carbons *J. Chem. Theory Comput.* **10** 1–4

[281] Ihm Y, Cooper V R, Peng L and Morris J R 2012 The influence of dispersion interactions on the hydrogen adsorption properties of expanded graphite *J. Phys.: Condens. Matter* **24** 424205

[282] Mura M, Gulans A, Thonhauser T and Kantorovich L 2010 Role of van der Waals interaction in forming molecule-metal junctions: flat organic molecules on the Au(1 1 1) surface *Phys. Chem. Chem. Phys.* **12** 4759–67

[283] Li G, Tamblyn I, Cooper V R, Gao H-J and Neaton J B 2012 Molecular adsorption on metal surfaces with van der Waals density functionals *Phys. Rev.* B **85** 121409

[284] Morikawa Y, Toyoda K, Hamada I, Yanagisawa S and Lee K 2012 First-principles theoretical study of organic/metal interfaces: vacuum level shifts and interface dipoles *Curr. Appl. Phys.* **12** S2–9

[285] Yanagisawa S, Hamada I, Lee K, Langreth D C and Morikawa Y 2011 Adsorption of Alq_3 on Mg(0 0 1) surface: role of chemical bonding, molecular distortion, and van der Waals interaction *Phys. Rev.* B **83** 235412

[286] Li G, Cooper V R, Cho J-H, Du S, Gao H-J and Zhang Z 2011 Self-assembly of molecular wires on H-terminated Si(1 0 0) surfaces driven by London dispersion forces *Phys. Rev.* B **84** 241406

[287] Hamada I, Lee K and Morikawa Y 2010 Interaction of water with a metal surface: importance of van der Waals forces *Phys. Rev.* B **81** 115452

[288] Carrasco J, Santra B, Klimeš J and Michaelides A 2011 To wet or not to wet? Dispersion forces tip the balance for water ice on metals *Phys. Rev. Lett.* **106** 026101

[289] Busse C *et al* 2011 Graphene on Ir(1 1 1): physisorption with chemical modulation *Phys. Rev. Lett.* **107** 036101

[290] Feibelman P J, Hammer B, Nørskov J K, Wagner F, Scheffler M, Stumpf R, Watwe R and Dumesic J 2001 The CO/Pt(1 1 1) puzzle *J. Phys. Chem.* B **105** 4018–25

[291] Lazić P, Alaei M, Atodiresei N, Caciuc V, Brako R and Blügel S 2010 Density functional theory with nonlocal correlation: a key to the solution of the CO adsorption puzzle *Phys. Rev.* B **81** 045401

[292] Ren X, Rinke P and Scheffler M 2009 Exploring the random phase approximation: application to CO adsorbed on Cu(1 1 1) *Phys. Rev.* B **80** 045402

[293] Lazić P, Atodiresei N, Caciuc V, Brako R, Gumhalter B and Blügel S 2012 Rationale for switching to nonlocal functionals in density functional theory *J. Phys.: Condens. Matter* **24** 424215

[294] Kokott S, Pflugradt P, Matthes L and Bechstedt F 2014 Nonmetallic substrates for growth of silicene: an *ab initio* prediction *J. Phys.: Condens. Matter* **26** 185002

[295] Sun B, Liu H, Song H, Zhang G, Zheng H, Zhao X-G and Zhang P 2014 The different roles of Pu-oxide overlayers in the hydrogenation of Pu-metal: an *ab initio* molecular dynamics study based on van der Waals density functional (vdW-DF) + U *J. Chem. Phys.* **140** 164709

[296] Graziano G, Klimeš J, Fernandez-Alonso F and Michaelides A 2012 Improved description of soft layered materials with van der Waals density functional theory *J. Phys.: Condens. Matter* **24** 424216

[297] Luo X, Sullivan M B and Quek S Y 2012 First-principles investigations of the atomic, electronic, and thermoelectric properties of equilibrium and strained Bi_2 Se_3 and Bi_2 Te_3 including van der Waals interactions *Phys. Rev.* B **86** 184111

[298] Sipahi G M, Žutić I, Atodiresei N, Kawakami R K and Lazić P 2014 Spin polarization of Co(0 0 0 1)/graphene junctions from first principles *J. Phys.: Condens. Matter* **26** 104204

[299] Ambrosch-Draxl C, Nabok D, Puschnig P and Meisenbichler C 2009 The role of polymorphism in organic thin films: oligoacenes investigated from first principles *New J. Phys.* **11** 125010

[300] Lin Y, Ma H, Matthews C W, Kolb B, Sinogeikin S, Thonhauser T and Mao W L 2012 Experimental and theoretical studies on a high pressure monoclinic phase of ammonia borane *J. Phys. Chem.* C **116** 2172–8

[301] Bil A, Kolb B, Atkinson R, Pettifor D G, Thonhauser T and Kolmogorov A N 2011 van der Waals interactions in the ground state of $Mg(BH_4)_2$ from density functional theory *Phys. Rev.* B **83** 224103

[302] Kolb B, Kertesz M and Thonhauser T 2013 Binding interactions in dimers of phenalenyl and closed-shell analogues *J. Phys. Chem.* A **117** 3642–9

[303] Kelkkanen A K, Lundqvist B I and Nørskov J K 2009 Density functional for van der Waals forces accounts for hydrogen bond in benchmark set of water hexamers *J. Chem. Phys.* **131** 046102

[304] Hamada I 2010 A van der Waals density functional study of ice I_h *J. Chem. Phys.* **133** 214503

[305] Kolb B and Thonhauser T 2011 van der Waals density functional study of energetic, structural, and vibrational properties of small water clusters and ice I_h *Phys. Rev.* B **84** 045116

[306] Wang J, Román-Pérez G, Soler J M, Artacho E and Fernandez-Serra M-V 2011 Density, structure, and dynamics of water: the effect of van der Waals interactions *J. Chem. Phys.* **134** 024516

[307] Kolb B and Thonhauser T 2012 Molecular biology at the quantum level: can modern density functional theory forge the path? *Nano LIFE* **2** 1230006

[308] Cooper V R, Thonhauser T and Langreth D C 2008 An application of the van der Waals density functional: hydrogen bonding and stacking interactions between nucleobases *J. Chem. Phys.* **128** 204102

[309] Rosa M, Corni S and Felice R D 2014 Enthalpy-entropy tuning in the adsorption of nucleobases at the Au(1 1 1) surface *J. Chem. Theory Comput.* **10** 1707–16